THE
PHYSICAL REVIEW
A Journal of Experimental and Theoretical Physics Established by E. L. Nichols in 1893
VOL. 58, NO. 10 NOVEMBER 15, 1940 SECOND SERIES

The Disintegration of N^{14} and N^{15} by Deuterons

M. G. HOLLOWAY AND B. L. MOORE
Cornell University, Ithaca, New York
(Received September 19, 1940)

A mixture of N^{14} and N^{15} gas has been bombarded with deuterons of 1 Mev and the disintegration particles observed at right angles to the direction of the deuteron beam. The ranges of the disintegration particles were measured by means of a shallow ionization chamber and pulse amplifier. The shortest measurable range was 2.1 cm (15°C, 760 mm Hg). The reaction $N^{15}(d, \alpha)C^{13}$ gave rise to one group of alpha-particles at 5.25 cm range with a Q value of 7.54 Mev. Three groups of alpha-particles (11.97 cm, 6.54 cm and 3.47 cm range) were observed arising from the reaction $N^{14}(d, \alpha)C^{12}$. The Q values corresponding to these three groups are 13.39 Mev, 9.02 Mev and 5.77 Mev, respectively. From the reaction $N^{14}(d, p)N^{15}$ two valid groups of protons were observed having ranges of 90.5 cm and 21.02 cm with Q values of 8.51 Mev and 3.15 Mev. The ranges given above are from a single measurement and the Q values are the average of the results of several measurements. A group at 66 cm previously reported due to this reaction was found to be due to boron contamination. No proton groups were found which could be attributed to the reaction $N^{15}(d, p)N^{16}$, although a radioactivity of half-life 9.5±1.0 sec. was found to result from deuteron bombardment of the mixture of N^{14} and N^{15}. This radioactivity was not found when N^{14} alone was bombarded. A method of range measurement is described which allows accurate corrections to be made for the effect of chamber depth and of the bias on the grid of the counting thyratron on the output of the pulse amplifier.

INTRODUCTION

SINCE the careful work of Cockcroft and Lewis (1936)[1] very little work has been done on the measurement of the energy of the heavy particles emitted when nitrogen, carbon and oxygen are bombarded with high energy deuterons. Such heavy particle measurements are of particular interest in that they can give very accurate information about energy levels in the residual nuclei, although selection rules quite often prevent this method from giving information about all of the energy levels that one could on energy considerations expect to be involved. The present investigation is limited to a study of the (d, p) and (d, α) reactions with N^{15} and N^{14} as the target nuclei. The results given in this report are based on more measurements with better corrections than those reported previously[2,3] and are believed to be more accurate.

EXPERIMENTAL ARRANGEMENTS

The source of the high energy ions used in this experiment was the Cornell cyclotron. The beam of ions could be directed outside the cyclotron chamber to a position 14 to 30 cm from the chamber wall. As is shown in Fig. 1 the target cell is bolted to the exit port of the cyclotron. The deuterons enter the target cavity through an aluminum foil at the end of the foil tube.

[1] J. D. Cockcroft and W. B. Lewis, Proc. Roy. Soc. **154**, 261 (1936).

[2] M. G. Holloway and B. L. Moore, Phys. Rev. **56**, 705 (1939).

[3] M. G. Holloway, Phys. Rev. **57**, 347 (1940).

The foil is attached to the supporting gridwork with Glyptal. The target gas is admitted to the target cell through the tube at the left and the pressure of the gas is measured by means of a Bourdon type vacuum gauge which is not shown in the drawing. Such a gauge can be used in this experiment since the gas pressure in the target cell is usually less than 7 cm of Hg and errors in this measurement amount to only several hundredths of a millimeter range.

The disintegration particles to be observed pass out through the mica foil at the side of the target cell. The direction of these particles is generally at 90° to the direction of the deuteron beam, but no collimation is introduced at this point. After passing through the foil the disintegration particles traverse the range cell in which the pressure of dry air can be varied by means of an external system. This pressure is measured by a mercury manometer. The temperatures of the target cell, range cell, and ionization chamber are measured with three thermometers in copper tubes soldered to the respective parts. The particles enter the ionization chamber through a collimating head which supports an aluminum foil, which is one electrode of the parallel plane ionization chamber.

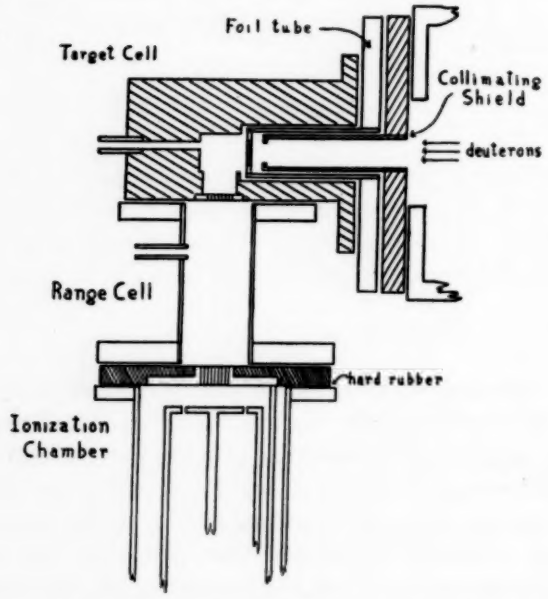

FIG. 1. Sketch of the assembly of target cell, range cell and ionization chamber used in measuring the ranges of the particles emitted in a direction 90° to the direction of the deuteron beam. The gaskets and screws which hold the components together are not shown.

The collecting electrode and its guard ring can be moved parallel to its axis on threads of 1-mm pitch turned on the guard ring cyclinder. The physical depth of the ionization chamber is measured by moving the collecting electrode forward until it makes electrical contact with the collimating head and foil, then the guard ring cylinder is screwed back. The number of revolutions of this cylinder determines the physical depth of the ionization chamber. In some cases the ionization chamber was modified, but these modifications will be mentioned in connection with the particular experiment.

The collimating head on the ionization chamber allows a maximum angle of 5.4° with the direction of the axis of the range cell and ionization chamber. It is necessary to have such a collimator because for some of the short range measurements the physical separation of the two foils bounding the range cell was only 1.4 cm and the obliquity correction in this case was 0.5 percent and less in all other cases. All three gridworks were drilled from the same pattern and have a ratio of open to total area of 0.54.

The collecting electrode of the ionization chamber is connected directly to the grid of the first amplifier tube of the 6-stage linear pulse amplifier described previously.[4] The output of this amplifier is connected to the grid of a discriminating thyratron which operated a mechanical counter. This grid is biased so that the output voltage pulse must be above a certain value before the thyratron will flash. With no signal on the grid, the thyratron will flash at -15 volts grid bias, so for any negative bias, V, greater than 15 volts, the pulse height required to flash the tube is $V-15$ volts. It will be shown in a later section that the method of range measurement used in these experiments makes it necessary that the amplifier be linear in its response to voltage pulses. For this reason it was necessary to make frequent measurements of the response of the amplifier. This was done with the thyratron oscillator described in reference 4, p. 24.

It was necessary to use a current integrator because the deuteron beam was somewhat unsteady. This integrator is similar to the type

[4] M. G. Holloway and M. S. Livingston, Phys. Rev. 54, 18 (1938).

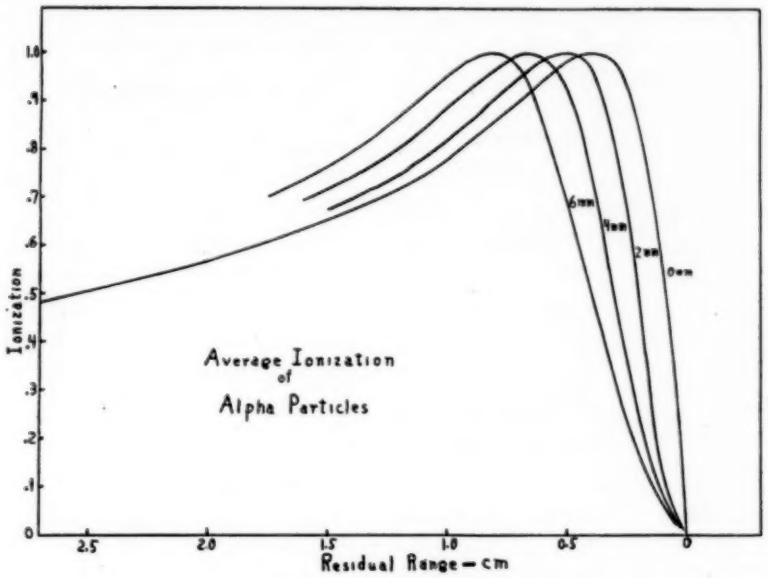

FIG. 2. The average ionization produced by alpha-particles in ionization chambers of different depths.

described by Herb, Kerst and McKibben[5] and has been found to be very satisfactory, although in the summer months precautions must be taken to prevent surface leakage across insulators. In Fig. 1 it can be seen that the grounded collimating shield prevents the beam from striking any part of the foil tube but the foil and supporting gridwork. Such a precaution is necessary, for if the beam shifts in position then a part of it will strike the solid edges of the supporting gridwork or the walls of the foil tube and no fraction of this current can reach the target gas although it will be measured by the integrator. However, with the beam restricted to the gridwork it is certain that 54 percent of the measured beam does get to the target gas.

For some of the longer range groups it would have been impractical because of intensity considerations to obtain sufficient absorber thickness by removing the ionization chamber a large distance from the target cell and consequently mica absorbers were used. A set of mica foils was made from *one* large piece of mica. The air equivalents of two thin pieces of this lot were measured with a collimated beam of polonium alphas; these foils were placed in the alpha-particle beam so that the average energy of the alphas in the mica corresponded to a residual range of 3 cm of air. The areas and masses of the two pieces were measured and from these measurements the mass/cm²/cm air was found to be 1.44 mg/cm²/cm air and 1.41 mg/cm²/cm air; the average of these is 1.425 mg/cm²/cm air and this value was taken as the stopping power for that sample of mica for alphas of 3-cm residual range. From the mass/cm² of the thicker pieces their thickness in air centimeters could be obtained. However, some correction had to be made to the thicknesses so obtained because the factor 1.425 mg/cm²/cm air was obtained at a residual range of 3 cm and all of the thicker absorbers were used at much higher ranges. Livingston and Bethe[6] have given a table of the stopping power relative to air of aluminum for various velocities of alpha-particles and protons. The correction for mica was taken as half the correction for aluminum. For velocities above 1.5×10^9 cm/sec. alpha-particles and protons have almost the same range. While these corrections are somewhat uncertain they are of second order in the range measurement and errors in the corrections are not too serious. The corrections for the one platinum foil used

[5] R. G. Herb, D. W. Kerst and J. L. McKibben, Phys. Rev. **51**, 691 (1937).

[6] M. S. Livingston and H. A. Bethe, Rev. Mod. Phys. **9**, 272 (1937).

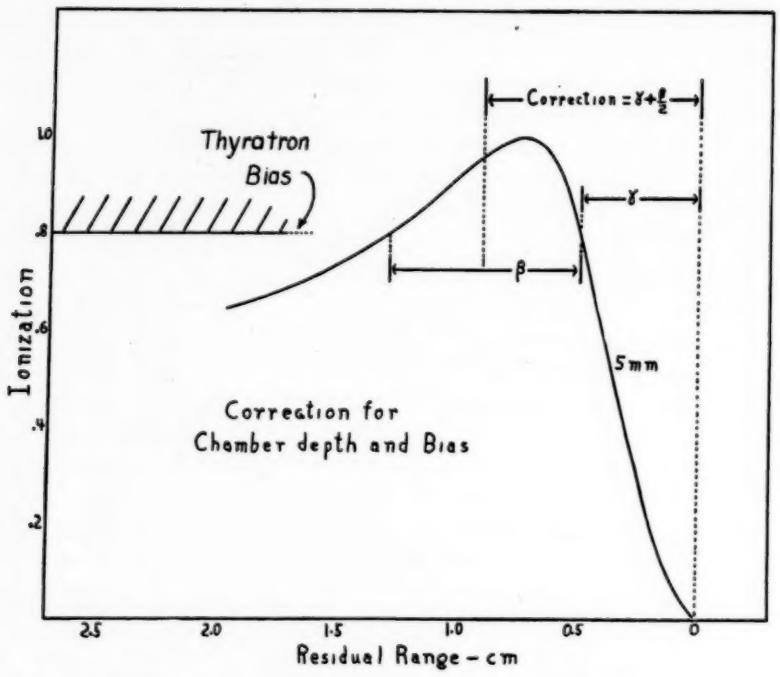

FIG. 3. Diagram showing the quantities involved in the correction to the range for ionization chamber depth and thyratron bias.

in these experiments were made with the curve for gold.

METHOD OF RANGE MEASUREMENT

The determination of the "range" in an absorber of a group of heavy particles is in most cases the problem of measuring the range of the group in such a manner that the average initial energy of the particles in the group can be determined; that is, a knowledge of the actual length of the path of a particle is useful only in that it is a means of obtaining the kinetic energy of the particle at some particular point. It is the purpose of this section to describe the method used in these experiments in obtaining the energy of the particle groups by means of range measurements. All ranges given in this paper are for dry air at 15°C and 760 mm of Hg.

Each alpha-particle or proton as it moves through a gas produces ion pairs along its path. The number of ion pairs per cm path length $dI(x)/dx$ is not constant for any one particle, but is a decided function of the velocity of the particle. In air the dependence of $dI(x)/dx$ upon velocity is such that $dI(x)/dx$ has a maximum several millimeters from the end of its path. This end of path is defined as that point along the path at which the particle has so little energy (<33 ev) that it cannot produce even one ion pair. In Fig. 2 is shown the ionization collected in parallel plate ionization chambers of different depths as a function of the distance of the face of the ionization chamber from the end of the path of an average alpha-particle. The differential specific ionization $dI(x)/dx$ is given by the curve (0 mm) for zero chamber depth.[7] The chamber depth for each curve is indicated by the number to the right of the curve. These curves for chambers of finite depth are obtained from the differential specific ionization curve by taking the integral

$$\int_{x-\delta}^{x} \frac{dI(c)}{dc} dc,$$

where δ is the chamber depth, and then normalizing the ordinate so that the maximum of the curve for each chamber depth is 1.0.[8]

[7] Reference 4, p. 29.

[8] From the work of I. Curie and F. Béhounek (J. de phys. et rad. 7, 125 (1926) and Ann. de physique 3, 299 (1925)) it can be deduced that the ion pairs corresponding to the maximum of the differential specific ionization curve

In Fig. 3 is shown a curve giving the ionization collected in a 5-mm chamber as a function of the distance of the face of the chamber from the end of the range of the alphas in the group having the mean range of the group. Since under rather wide operating conditions the voltage pulse on the grid of the first amplifier tube is proportional to the ionization produced by the individual alpha-particle in the chamber, the ordinate of the curve in Fig. 3 will also represent the voltage pulse on the discriminating thyratron as a function of the ion chamber position. This last is true only if the amplifier is linear in its response to voltage pulses. The drawing indicates a bias on the discriminating thyratron which would correspond to a pulse height 0.8 of the maximum average obtainable with the 5-mm chamber. With such a bias the chamber face could be at any position within β and the alpha-particle would still be counted by the discriminating thyratron. If the ion chamber face is anywhere outside of β the alpha would not be counted. If the range straggling is of the form $\exp[-x^2/\alpha^2]$ it can be shown easily that the peak of the curve connecting number of counts with the position of the chamber face will be at the center of β or displaced by $\gamma+\frac{1}{2}\beta$ from the mean range. β and γ are both functions of δ, the chamber depth, and of P, the pulse height below which the discriminating thyratron will not flash.

For a very high bias corresponding to ionization pulses in the near neighborhood of 1.0, $\beta(\delta, P)$ is very small and $\gamma(\delta, P)$ is very nearly equal to the distance of the position of maximum ionization from the end of range. In this case the peak of the counting (high bias number-distance) curve will occur at the same position as that of the maximum of the ionization curve for that particular chamber depth.

It is very easy to realize experimentally these last conditions. The procedure is to take a number-distance curve and use a bias known from experience to be slightly higher than the mean pulse height at the maximum of the ionization curve. The peak of this number-distance curve will be very near the position of the peak of the ionization curve; the accuracy of this being limited by the rather poor statistics coming from the few counts at high bias. The ion chamber is then placed at the position of maximum counting rate and a number bias curve taken (see Fig. 8, reference 4). At this position of the chamber the bias for half-maximum counting rate is then the bias corresponding to the mean of the ionization pulses arising from particles having their maximum ionization in the ion chamber. The bias of the discriminating thyratron is set at this bias which corresponds to ionization pulses of height 1.0 in Fig. 3. One must remember that the curve in this figure represents the ionization pulse such that half the particles in the group produce larger and half smaller pulses than that given by the ordinate of the curve. The number distance curve is then repeated with the bias corresponding to ionization pulse height 1.0. The true mean range of the group of particles is the sum of the distance between source and the position of the peak in the counting rate curve and of $\gamma(\delta, 1.0)$ for the particular chamber depth used. If the bias is for a pulse height less than 1.0 then the correction is not $\gamma(\delta, 1.0)$ but $\gamma(\delta, P)$ $+\frac{1}{2}\beta(\delta, P)$ appropriate for the particular bias. The reason for using a bias for pulse height as near 1.0 as possible is that this bias gives a larger ratio of maximum to half-width of the

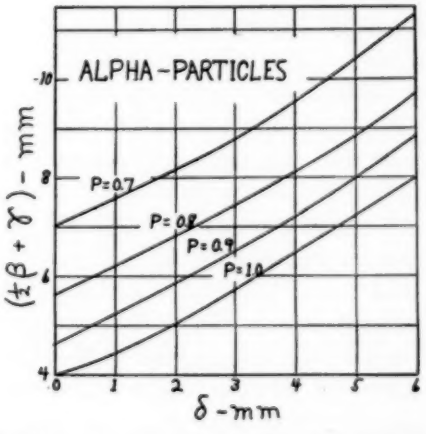

FIG. 4. The correction to the range of alpha-particles for thyratron bias and ionization chamber depth as a function of the chamber depth for different pulse heights (different thyratron biases).

is 6760 ion pairs/mm. With this value, the maxima of the curves for finite chamber depth are: 2 mm, 13,480; 4 mm, 26,400; 5 mm, 32,450; 6 mm, 38,400 ion pairs/mm. The numbers give the number of ion pairs produced in the chamber when the face of the chamber is set at the position of the maximum of the curve.

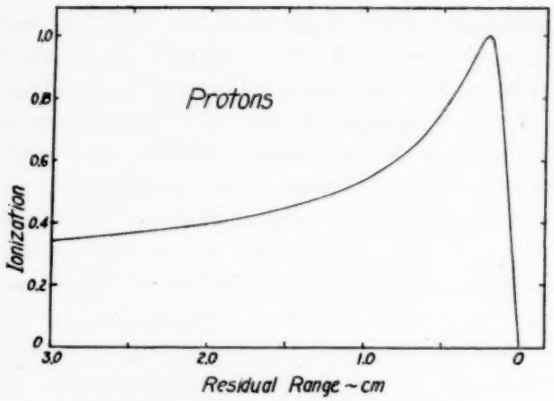

FIG. 5. The average differential specific ionization produced by a proton.

counting rate *vs.* position curve than any other bias.

From the set of curves in Fig. 2 the correction $(\gamma+\frac{1}{2}\beta)$ for different depths δ and pulse height P can be obtained. Figure 4 gives this correction as a function of δ for different P's for alpha-particles. Again it should be mentioned that for most experiments $P \geqq 1.0$ and the range correction for bias and chamber depth is $\frac{1}{2}\beta(\delta, 1.0) + \gamma(\delta, 1.0)$; for $P<1.0$, the correction is $\frac{1}{2}\beta(\delta, P) + \gamma(\delta, P)$.

In order to check this method of range measurement the mean range of polonium alphas was measured with a 2-mm chamber and with a 4-mm chamber. The 2-mm chamber measurement gave 3.84_5 cm and the measurement with the 4-mm chamber gave 3.85_5 and 3.85_0 in two measurements. Since we have taken 3.842 ± 0.006 cm as the standard range of the polonium alpha-group it would appear that this method of measurement gives the correct range to an accuracy limited by errors in measurement of the dimensions of the apparatus. The range and energy of the polonium alpha-group gives a point on the range-energy relation and thus, if the mean range of some new group of alpha-particles were measured by the method described above and found to be 3.84 cm one would be certain that the mean energy of the group is 5.29_8 Mev. Similar points betweeen 2 Mev[9] and 10.5 Mev[10] based on measurements of the range and energy of alphas from naturally radioactive sources make the method reliable in this region. The theoretical extension of the range energy relation to energies higher than 10 Mev is straightforward and is quite accurate. The curve in the region below 2 Mev is obtained by integrating the differential specific ionization curve and fitting the integrated curve to the experimental curve at about 4 Mev; this may be in error because of a possible variation in energy loss per ion pair in the low energy region.

The measurement of the range of protons is a problem similar to that for alpha-particles. However, the differential specific ionization for an average proton of a group is not as well known as that of the alpha-particle. Parkinson, Herb, Bellamy and Hudson[11] in their work on the range of protons in air used a very shallow (0.04 cm) ionization chamber and obtained curves of ion current *vs.* energy (for a fixed air path) showing the familiar specific ionization curve for heavy particles. These curves of specific ionization *vs.* energy can be transformed into curves of specific ionization *vs.* range. In particular, curve VI, Fig. 5, reference 11, was so transformed. The transformed curve is a "Bragg" curve for a proton group having in this case a very small straggling. The effect of the finite chamber depth and range straggling is to put a small tail at the foot of the curve and to decrease the slope of the face of the specific ionization curve (this is discussed in reference 4). Initially it was assumed that the true differential specific ionization curve was the same as curve VI, Fig. 5, reference 11, except that the linear face of the specific ionization curves was extended directly to the axis, i.e., no tail. To this curve was then applied a straggling of 0.5 mm (more than would be expected from the Wisconsin high voltage generator) and a new curve computed. There was no appreciable change in the curve except that a tail was added to the foot and the curve displaced by about 1 mm. The effect of the finite chamber depth of 0.4 mm was also to add a tail and decrease the slope by about 15 percent. The differential specific ionization curve of the average proton of the group was then taken as curve VI, Fig. 5,

[9] G. Mano, Ann. de physique **1**, 407 (1934); G. H. Briggs, Proc. Roy. Soc. **114**, 341 (1927).

[10] W. B. Lewis and B. V. Bowden, Proc. Roy. Soc. **145**, 235 (1934); S. Rosenblum and G. Dupouy, J. de phys. et rad. **4**, 262 (1933).

[11] D. B. Parkinson, R. G. Herb, J. C. Bellamy and C. M. Hudson, Phys. Rev. **52**, 75 (1937).

reference 11, with the linear face extrapolated to the axis and a 15 percent increase in slope of the face. This curve is shown in Fig. 5. In measuring ranges the same procedure as for alpha-particles is followed and the correction $\frac{1}{2}\beta(\delta, P)+\gamma(\delta, P)$ for protons is given in Fig. 6. Because the curves for $P=0.9$, 0.8 and 0.7 are so near the curve for $P=1.0$, only the correction for $P=1.0$ is given. In as much as the proton produces only about a third the maximum ionization per millimeter as an alpha-particle it is very easy to distinguish between the two types of particles by the height of the voltage pulse which they produce in the output of the amplifier.[12]

The range-energy relation for protons was taken from the work of Parkinson, Herb, Bellamy and Hudson with some corrections to their data to get mean ranges and mean energies. Above 1.95 Mev the relation was obtained by transforming the alpha-particle range-energy relation by means of the relations

$$R_H(v)=(M_H/M_\alpha)(Z_\alpha/Z_H)^2R_\alpha(v)-c$$

and

$$E_H(v)=(M_H/M_\alpha)E_\alpha(v).$$

The constant c takes care of the difference in the capture and loss effect between proton and alpha-particles, and is equal to 0.3 ± 0.06 cm.

Measurement of the Deuteron Energy

It was necessary to determine as accurately as possible the energy of the deuterons from the cyclotron, since the energy of the bombarding particle enters into the calculation of the disintegration energy of a nuclear reaction. Theoretically the energy can be calculated from the frequency of the oscillating "dee" voltage and the geometry of the cyclotron chamber. However, uncertainties in the determination of the radius of curvature of the last half-circular path make this method unsatisfactory for accurate work. A more direct method is to measure the range of the particles, but because of the large beam intensity a pulse amplifier could not be used to count the individual particles and as a result the correction for chamber depth could not be made accurately. This inaccuracy in the determination of the range of the very short range deuterons was too large to allow the use of this method.

A third method, which was the one adopted in the present work, is to use some nuclear reaction. The one chosen here was the reaction $H^2(d, p)H^3$. If the Q value of this reaction and the energy of the emitted proton (say at 90°) is known the energy of the bombarding particle can be computed. However, by measuring the energy of the protons emitted in the forward direction and at 90° to the deuteron beam it is possible to determine both the Q value and the energy of the incident deuterons. Once the Q value is known it is necessary to measure the proton range only in the 90° direction in order to obtain the deuteron energy.

The experimental arrangement for measuring the protons in the 90° direction was the same as that previously described with a 19.2-cm range cell. For the measurement at 0° a 33-cm range cell and a target cell with a foil on the forward end was used. The depth of the target cell was 1.1 cm. Since the energy of the deuterons incident on the target gas was about 1 Mev and

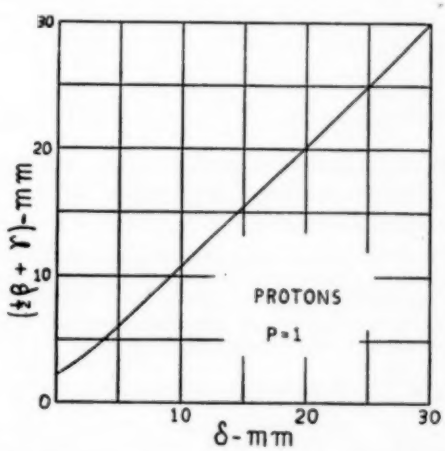

FIG. 6. The correction to the range of protons for ionization chamber depth for a thyratron bias corresponding to $P=1.0$.

[12] For alpha-particles and protons of energies greater than 1 Mev and 0.1 Mev, respectively, the loss and gain of charge is negligible, and for alphas and protons of the same velocity the ratio of the differential specific ionization of the alpha-particle to that of the proton should be in the ratio of the square of their charges, namely 4/1. Comparison of the differential specific ionization curves of the alpha-particle and the proton in the region of 3-cm residual range gives an absolute ordinate for the proton curve such that the maximum corresponds to 2320 ion pairs/mm. If a very deep chamber is used it is necessary to extend the differential specific ionization curve to greater residual ranges. This can be done by using Eq. (749), reference 6.

the air equivalent of the gas was about 0.1 cm there was left about 1.4 cm of the deuteron range to be stopped in the exit foil. At this bombarding energy there is a group of protons from aluminum of about 35-cm range which might have interfered with the measurement of the group from the deuterium. In order to eliminate this the last foil was made up of a platinum foil of 1.1 cm air equivalent and an aluminum foil of 0.46 cm air equivalent. This last foil was not entirely made of platinum because the correction of the stopping power of platinum for different velocities is not very well known, and it was desirable to keep this correction as small as possible. The excitation function for the aluminum reaction becomes very small for 0.4-Mev deuterons and no protons from the small thickness of aluminum were observed in the region of 33-cm range.

Equations (1) and (2) relate the Q value and the deuteron energy E_1, with the energies of the protons emitted in the forward and 90° directions.[13]

$$E_1=\frac{(M_2+M_3)^2}{4M_1M_2}\frac{(E_2^0-E_2^{90})^2}{E_2^0}, \tag{1}$$

$$Q=\frac{M_2+M_3}{M_3}\left[E_2^{90}-\frac{(M_3-M_1)(M_3+M_2)}{4M_1M_2}\times\frac{(E_2^0-E_2^{90})^2}{E_2^0}\right]. \tag{2}$$

The following notation is used: The subscript 0, 1, 2 and 3 refer to the initial nucleus, incident particle, emitted particle and residual nucleus, respectively. The superscript 0 will refer to the measurement in the 0° direction and 90 to the 90° direction. The cyclotron was not shut down during the change of target cells so that conditions in the cyclotron would be the same for the two measurements. The mean range of the protons in the forward direction was 30.63 cm corresponding to an energy of 4.71$_5$ Mev; in the 90° direction the range and energy was 15.94 cm and 3.22 Mev, respectively. Using these values of E_2^0 and E_2^{90} in Eqs. (1) and (2) one is led to the value 0.95 Mev for the energy of the deuterons in the center of the gas in the target cell and 3.98 Mev for the Q value for the reaction $H^2(d, p)H^3$.[14] Since the air equivalent of the aluminum foil through which the deuterons passed into the target cell was 0.80 cm the energy of the deuterons incident on the foil was 1.27 Mev. From this energy value and the frequency of the cyclotron oscillator the radius of the last circle in the cyclotron can be computed and used for future determinations of the deuteron energy. However, this must be checked frequently because adjustments of the cyclotron can very easily change the geometry enough to require a new calibration of the beam energy.

In order to see how errors in E_2^0 and E_2^{90} affect E_1 and Q we take the differentials of Eqs. (1) and (2).

$$\delta E_1=\frac{(M_2+M_3)^2}{4M_1M_2}\left[\frac{2(E_2^0-E_2^{90})}{E_2^0}\delta(E_2^0-E_2^{90})-\left(\frac{E_2^0-E_2^{90}}{E_2^0}\right)^2\delta E_2^0\right], \tag{3}$$

$$\delta Q=\frac{M_2+M_3}{M_3}\delta E_2^{90}-\frac{(M_3-M_1)}{M_3}\delta E_1. \tag{4}$$

The first item in (3) involves inaccuracies in the *difference* $(E_2^0-E_2^{90})$ and the second term inaccuracies in E_2^0 alone, and since the errors in the two terms are approximately independent of each other the two terms must be added as the square root of the sum of their squares.

In the case of the measurement of the beam energy by the method of observing the emitted protons in two directions from the disintegration

[13] From conservation of mass and energy $Q=E_2+E_3-E_1$ and from the conservation of momentum

$$M_3E_3=M_1E_1+M_2E_2-2(M_1M_2E_1E_2)^{\frac{1}{2}}\cos\theta,$$

where θ is the angle between the direction of the incident and emitted particles. Measurements of the energy of the protons emitted in the forward direction and in the 90° direction allow the use of two independent equations involving the unknown quantities Q and E_1.

(a) $$Q=\frac{M_2+M_3}{M_3}E_2^{90}-\frac{M_3-M_1}{M_3}E_1 \text{ at } 90°,$$

(b) $$Q=E_2^0+\frac{[(M_1E_1)^{\frac{1}{2}}-(M_2E_2^0)^{\frac{1}{2}}]^2}{M_3}-E_1 \text{ at } 0°.$$

From these two equations can be obtained the Eqs. (1) and (2) above.

[14] M. L. E. Oliphant, A. R. Kempton and Lord Rutherford, Proc. Roy. Soc. **149**, 406 (1935), give 3.98±0.02 Mev and F. E. Myers, R. D. Huntoon, C. G. Shull and C. M. Crenshaw, Phys. Rev. **56**, 1104 (1939), give 3.93±0.10 Mev.

of deuterium, the peak of the counting curve could be determined to about 2 mm of Hg pressure and the temperature to about 0.5°C. The estimated error in the measurement of the length of the 19.2 cm long range cell was about 0.01 cm. These errors give together a total error in the air equivalent of the range cell of 0.06 cm of air. There are two foils whose air equivalents are known to about 0.01 cm. The combined error in the chamber depth measurement and the chamber depth corrections to the range is about 0.02 cm. These constitute the experimental errors in the range of the 15.94-cm protons (90°) and total about 0.065 cm error for the 19.2-cm range cell. The longer range cell of length 33.0 cm has a somewhat larger error amounting in all to 0.08 cm in the 30.63-cm group observed at 0°. The difference $(E_2^0-E_2^{90})$ does not involve the inaccuracy in one foil or the error in the chamber depth and its corrections, and consequently the error in this difference is 0.094 cm rather than 0.103 cm as would be expected from adding the errors in the two ranges. The above errors are all the result of inaccuracies in measuring physical quantities in the course of the experiment.

The proton range-energy relation of Parkinson, Herb, Bellamy and Hudson includes the region up to about 2 Mev and is accurate to about 1 percent in range and energy. As was mentioned previously the range-energy relation for protons above 2.0 Mev is obtained by transforming the relation for alpha-particles. This includes the additive constant c which comes out to be 0.3 cm. By taking the probable errors in the alpha-particle curve and that of Parkinson, Herb, Bellamy and Hudson, the error in c is found to be 0.06 cm. Other errors involved in the absolute range scale for the protons are small compared to this error of 0.06 cm in c. However, for *differences* on the range energy relation for protons the accuracy is much better being about 0.02 cm.

The combination of the experimental errors and the errors in the range-energy relation gives the following errors for the ranges of the protons from the reaction $H^2(d, p)H^3$: In the forward direction, 0.10 cm and in the 90° direction, 0.09 cm. These correspond to inaccuracies in the energy of E_2^0 of 11 kev and in E_2^{90} of 10.8 kev, the slope of the range energy relation in these regions being 115 kev/cm. The difference $(E_2^0-E_2^{90})$ does not involve the absolute error in the range-energy relation, but rather a smaller error of about 0.02 cm. The error in the energy difference is then about 5 kev.

Experimentally it was not possible to determine the direction of the deuteron beam to better than 2°, and as a consequence the energy values 4.71_5 Mev and 3.22 Mev, while being accurately the energy of the protons observed, may not be E_2^0 and E_2^{90} since these two quantities are defined as the proton energies in exactly the 0° and 90° directions. The inaccuracy in θ introduces an error in Q of 72 kev and in E_1 of 52 kev. These errors are large compared to the errors arising from the range measurements, and are connected only with the determination of the beam energy and the Q value, and not with the method used in determining the energy of the emitted particle. The errors combine to give an error in Q of 74 kev and in E_1 of 54 kev.

Results

The target gases used in these experiments contained a high percentage of the heavy isotope N^{15}. Some of the earlier work was done with a sample containing 20 percent of the N^{15} and the later work with a 70-percent sample. The appreciable amount of the N^{14} in all of the samples made necessary the study of the normal nitrogen under deuteron bombardment so that the contribution of the rarer isotope could be determined. This work on normal nitrogen was essentially a repetition of the work of Cockcroft and Lewis, but since the measurements on N^{14} had to be made it was thought worth while to make them carefully.

In Fig. 7 are shown two groups of alpha-particles resulting from the bombardment of tank nitrogen which contains only about 0.4 percent of the N^{15}. The reaction involved is $N^{14}(d, \alpha)C^{12}$. In view of some work to be mentioned later the small hump occurring at about 5 cm range is probably due to the presence of the small amount of N^{15} in the tank nitrogen. The long range group at about 11.67 cm was measured in two ways.[15] The first measurement

[15] The range scale for the curves of counting rate vs. distance from the target cell is not absolute, but may differ by as much as 1 mm from the absolute value. The

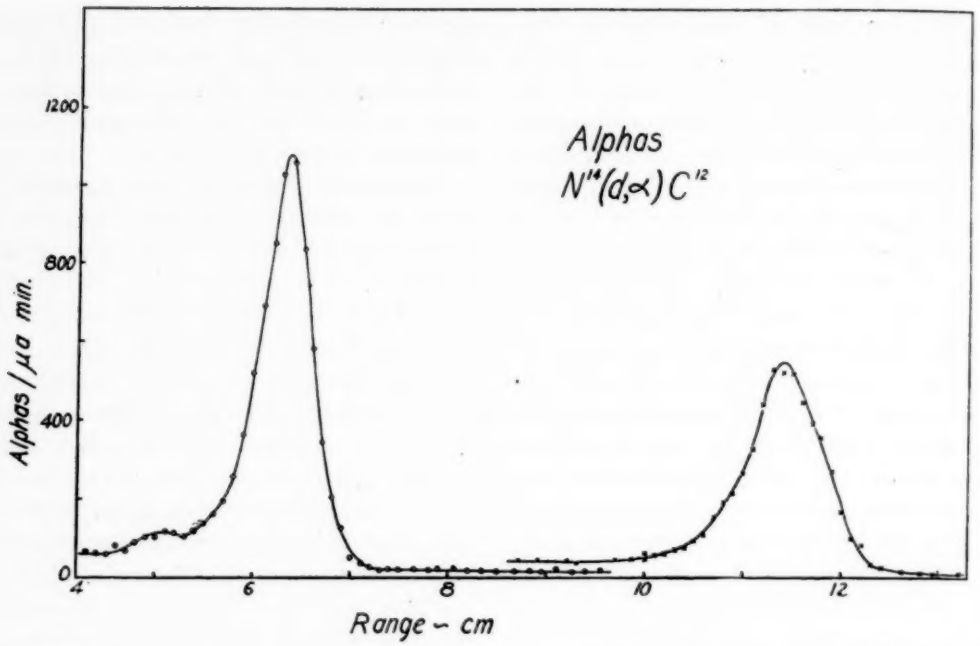

FIG. 7. Two groups of alpha-particles from the reaction $N^{14}(d, \alpha)C^{12}$. The target was tank nitrogen.

was with a foil holder between the range cell and the ionization chamber and with a copper screen as the face of the ionization chamber. The end of the range cell was covered in this case with a mica foil of about 0.88 cm air equivalent. A thick mica foil of 4.50 cm air equivalent from the calibrated set mentioned before was in the foil holder. With corrections for the stopping power of the mica and for slight obliquity the range of the group was 11.67 cm air, the bombarding energy being 1.01 Mev. The second measurement was with the 19.2-cm range cell used previously in measuring the range of the protons from the reaction $H^2(d, p)H^3$. There was no thick absorbing foil used in this measurement and the ionization chamber face was the Al foil over the collimating gridwork. The range found by this measurement was 11.97 cm at 1.02-Mev deuteron energy. The Q values for these two measurements are 13.30 Mev and 13.48 Mev, respectively; the average of these is 13.39 Mev as compared with the mass Q value of 13.36 taken from the mass tables of Barkas.[16]

The group at 6.54 cm range (deuteron energy 1.02 Mev) is also due to the reaction $N^{14}(d, \alpha)C^{12}$ in which the C^{12} is left in an excited state. The average Q value as taken from 5 separate measurements was 9.02 Mev. The two different ionization chamber heads and range cells used for 11.7-cm group were used in getting the 5 measurements of this group, although no thick mica absorber was involved.

The 6.54-cm group is shown again in Fig. 8 along with the short range group of alpha-particles at 3.47 cm, the deuteron energy being 1.02 Mev. Since these curves were taken with only tank nitrogen in the target cell it is probable that this group is from the N^{14}. Checks with the target cell evacuated and with CO_2 in the cell indicate that it is not from a casual contaminant. The fact that its intensity was not enhanced by the presence of N^{15} in large quantities makes it likely that it does not arise from N^{15}. This group at 3.47 cm appeared with the

accurate ranges are obtained from the counting rate *vs.* pressure curves. It would be much too laborious to transform each experimental point to an absolute scale, for the corrections required to get an accurate range scale are the following: (*a*) The contribution of the target cell must be corrected for pressure and temperature, (*b*) the range cell must have a similar correction, (*c*) the foils on the ends of the range cell as well as any thick absorbers must be corrected for the change in stopping power with velocity, (*d*) the chamber depth must be computed and the appropriate correction made, and (*e*) the obliquity factor computed and applied to the range. The ordinates of these curves do not represent absolute yields.

[16] W. H. Barkas, Phys. Rev. **55**, 691 (1939).

$N^{14}-N^{15}$ mixture, and with tank nitrogen in 5 distinct observations which makes it very probable that it is due to the N^{14} reaction. The average Q value from two range measurements is 5.77 Mev. Cockcroft and Lewis did not find this group of alphas, but an inspection of their published curves shows no experimental points in the region of this small peak.

In Fig. 9 are shown the alpha-particle groups obtained in the region 2- to 8-cm range when the target cell contained the gas mixture of 70 percent N^{15} and 30 percent N^{14}. In addition to the two groups at 6.54 cm and 3.47 cm there is a strong group at 5.25 cm; these ranges are for a bombarding energy of 1.02 Mev. The average of three range measurements on this group with slightly different deuteron energies gives a Q value of 7.54 Mev. This must correspond to the transition to the ground state of C^{13} in the reaction $N^{15}(d, \alpha)C^{13}$, for no alpha-groups of longer range were found which could be attributed to the presence of N^{15} in the target. The Q value as computed from Barkas' mass values is 7.51 Mev.

The very intense distribution of alphas below about 3-cm range was observed by Cockcroft and Lewis. The shortest range which could be studied by the present apparatus was about 2.1 cm, consequently any definite information concerning the short range distribution must be left for future measurements.

In the first report of this work[2] three groups of protons were attributed to the reaction $N^{14}(d, p)N^{15}$. The ranges of these groups were given as 90.8 cm, 66.1 cm and 21.0 cm. The statistics in the early work were very poor in the case of the 90.8-cm group because of its small intensity compared to the neutron recoil background. Recently it was thought advisable to repeat the measurement of the 90-cm group with an ionization chamber of 1-cm physical depth filled with krypton at two atmospheres. The ionization produced in this chamber by a neutron recoil was small compared to the ionization from a proton which went completely through the chamber. With the high thyratron bias method very few of the neutron recoils were counted. The 90-cm group is shown in Fig. 10. The small dotted curve is the one taken with the 5-mm ionization chamber filled with air. The thick mica absorbers used in this measurement amounted to 71.6 cm of air, including the correction for the change in stopping power with velocity. Rather than make corrections for the large chamber depth which would of necessity require a knowledge of the stopping power of krypton the ionization chamber was calibrated by measuring the ranges of the protons for the reactions $H^2(d, p)H^3$ and $C^{12}(d, p)C^{13}$. These two groups have a range of about 16 cm and have been carefully measured in this laboratory with the thin ionization chamber. The range of the group from the reaction $N^{14}(d, p)N^{15}$ as measured with the thick ionization chamber is 90.5 cm. The older measurements with the thin ionization

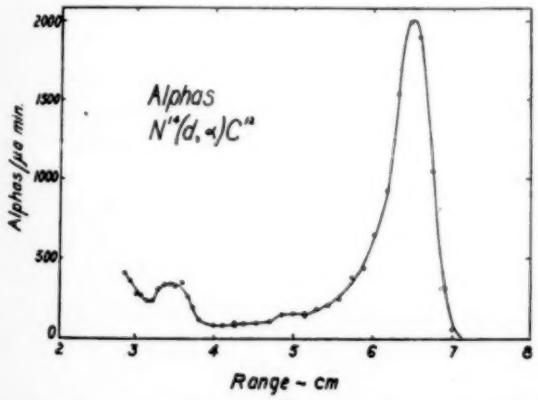

FIG. 8. Alpha-particle groups from the reaction $N^{14}(d, \alpha)C^{12}$. The group at about 6.5 cm is the same group shown in Fig. 7. The target was tank nitrogen.

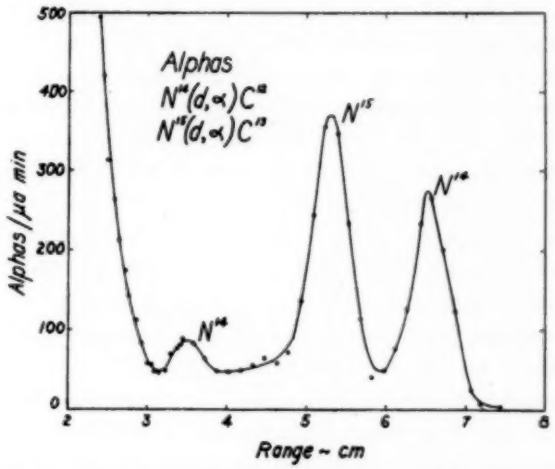

FIG. 9. Alpha-particle groups from a target of 70 percent N^{15}. The group at about 5.2-cm range is from the reaction $N^{15}(d, \alpha)C^{13}$. The other two groups were seen previously to be from the reaction $N^{14}(d, \alpha)C^{12}$.

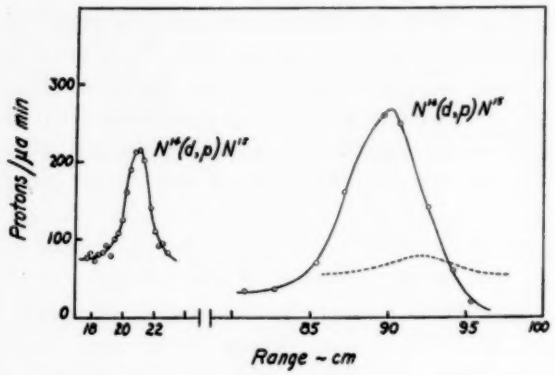

FIG. 10. The two groups of protons from the reaction $N^{14}(d, p)N^{15}$.

chamber gave 92.5 cm when corrected for change in stopping power of mica with velocity although with a different deuteron energy. Because of the much better statistics it is thought that the 90.5-cm range is the better value, and the Q value obtained with this range is 8.51 Mev as compared with the mass Q value of 8.57 Mev.

In the early work with the thin ionization chamber the proton group at 66 cm was more intense than the 90-cm group. However, with the thick krypton chamber the 66-cm group could not be found at all! Various common possible contaminants were tried but none gave the 66-cm group. Finally because the range of the group was about that to be expected from boron a target of borax was tried, and the 66-cm group appeared with a very large intensity. The problem was then to find the source of the boron in the earlier experiments and why the group did not show up when the target had been evacuated or filled with carbon dioxide but was present when tank nitrogen or the $N^{14}-N^{15}$ mixture was used. It was remembered that a Bourdon type vacuum gauge had been used on the target cell for testing the cell for leaks and that this gauge had been discarded because of a leak in its flattened tube. Further investigation revealed that this gauge had been used several years previously in the filling of boron trifluoride ionization chambers, and had been laid aside because of the leak. This explained the source of the boron in the early experiments, for presumably the cavity into which the gauge had been screwed had become saturated with the gas. The time required for taking the points for one of the long range proton groups was of the order of several hours and the $N^{14}-N^{15}$ mixture or the tank nitrogen might remain in the target cell for as much as a day. This would allow ample time for some of the boron trifluoride to seep into the bombarding cavity. However, when the tests were made with the cell evacuated or with carbon dioxide very little time was required, since the method of checking the groups was to set the ionization chamber at the position of the peak of the curve and measure the counting rate. If the counting rate was the same as the background it was assumed that the group did not come from the cell walls or the carbon dioxide. In the time required for the check it is probable that very little of the boron trifluoride got into the target cell.

The strong group of protons at 21.02 cm (deuteron energy of 1.01 Mev) is from the reaction $N^{14}(d, p)N^{15}$. The Q value is 3.15 Mev which indicates an excitation level in N^{15} of 5.42 Mev.

A group of protons might be expected to result from the reaction $N^{15}(d, p)N^{16}$. The residual nucleus N^{16} is known to be radioactive with a half-life of 8 sec. Naidu and Siday[17] measured about 240 tracks in the beta-ray spectrum of N^{16} and obtained a visually extrapolated end point at little over 6 Mev. Fowler, Delsasso and Lauritsen[18] found a visual end point of about 6 Mev and a K–U limit of 6.5 Mev. If 6.5 Mev is taken as the energy of the beta-particles given off from N^{16} in the disintegration $N^{16}\rightarrow O^{16}+\epsilon^-$ the mass of N^{16} has the lower limit of 16.007 MU and may be heavier by the energy of any gamma-rays involved in the disintegration. In the present experiment a thin-walled Geiger counter tube was set up very near to the foil window of the target cell. A chronograph was used to record every sixteenth count of the Geiger counter. With the target cell filled with the $N^{14}-N^{15}$ mixture two half-life measurements were taken of the activity produced in the gas. The first measurement showed an 8.1-sec. half-life superimposed on a 5.6-min. half-life. The second measurement gave a 10-sec. half-life on

[17] R. Naidu and R. E. Siday, Proc. Phys. Soc. London **48**, 332 (1936).

[18] W. A. Fowler, L. A. Delsasso and C. C. Lauritsen, Phys. Rev. **49**, 561 (1936).

a 7-min. half-life. It was determined that the longer periods came from the cyclotron chamber and not from the target cell and presumably this longer half-life radioactivity came from the N^{13} formed in the cyclotron chamber from carbon contamination. The somewhat small half-life value for the N^{13} is due probably to the diffusion of the radioactive nitrogen from the walls into the pumping system. With the target cell filled with tank nitrogen there was no short life component found at all, but rather one of 6.7 min. half-life, which again was found to come from the chamber. Since N^{16} has a half-life of 8 sec.[19] the short-lived activity detected as coming from the bombardment of the N^{15} with deuterons is probably from N^{16} formed in the reaction $N^{15}(d, p)N^{16}$. If this is assumed to be the case then the fact that it is possible to produce the above reaction with 1-Mev deuterons sets an upper limit of 16.0126 MU for the mass of N^{16}. This value is for zero energy of the proton which is given off in the deuteron reaction. If the value 16.007 is used for the mass of N^{16}, the Q value for the reaction $N^{15}(d, p)N^{16}$ is 4.19 Mev and with 1-Mev deuterons the energy of the emitted proton should be 4.75 Mev or a range of 31 cm of air. The entire region from 2-cm to 100-cm range was searched for protons with the $N^{14}-N^{15}$ gas mixture in the target cell, and there were found 3 groups of protons at 21 cm, 66 cm and 90 cm; these groups were also found with the tank nitrogen and their source is known. No new proton group was found. Below 12-cm range it was very difficult to detect protons because of the large numbers of alpha-particles in that region. Figure 11 shows a typical curve taken with a low bias for detecting protons. Since the weak group of alphas at 3.5 cm does not show on this curve, it is evident that a proton group would have to be rather strong to be detected over the strong background of alpha-particles. With only the results of the present experiment the matter of the protons from the reaction $N^{15}(d, p)N^{16}$ must be left in a rather inconclusive state.

In Table I the results of all these measurements are summarized. E_1 is the energy of the deuterons in the center of the gas target; E_2 is the energy of the emitted particle whose range in air (at 15°C, 760 mm Hg) is given in the third column. Q_{exp} is the Q value as computed from the present measurements and in the next two columns are given the Q values from Cockcroft and Lewis and from the mass tables of Barkas. The absolute values of the cross sections are probably accurate to a factor of 5, but the relative values are good to 50 percent.

The agreement between the Q values found in the present work and those of Cockcroft and Lewis is good except in the case of the alpha-group corresponding to the transition to the ground state of C^{12}; the difference is 0.17 Mev, which is within the experimental errors given. The agreement is excellent in every case with the corrected values deduced from Cockcroft and Lewis' experiments by Livingston and Bethe.[20] The experimental Q values reported here and the Q values obtained from mass values agree to at least 60 kev.

Consideration of the energy levels shown in the table would lead one to expect that the bombardment of nitrogen with deuterons would produce gamma-rays having energies 4.37, 7.62, 5.42 and 3.25 Mev; the last gamma would come from a transition between the 7.62- and 4.37-Mev levels in C^{12}. Gaerttner and Pardue[21] have observed five gamma-ray lines resulting from the bombardment of nitrogen with deuterons; the energies of these lines were given as 2, 4, 5.3±0.4, 7.2±0.4 and 11 Mev. The 4- and 7.2-Mev lines could correspond to the 4.37- and

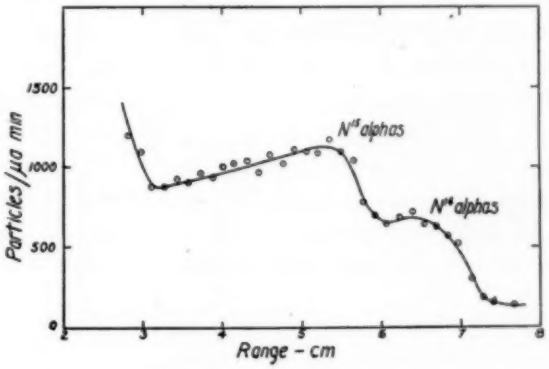

FIG. 11. Curve taken in the search for protons of range less than 8 cm.

[19] J. J. Livingood and G. T. Seaborg, Rev. Mod. Phys. 12, 30 (1940).

[20] Reference 6, pp. 279, 321 and 327.

[21] E. R. Gaerttner and Louis A. Pardue, Phys. Rev. 57, 386 (1940).

TABLE I. *Data on the bombardment of nitrogen by deuterons.*

REACTION	E_1 MEV	RANGE AIR CM	E_2 MEV	Q_{EXP} MEV	$Q_{C.\&L.}$ MEV	Q_{MASS} MEV	ENERGY LEVEL MEV	CROSS SECTION CM^2
$N^{14}(d, \alpha)C^{12}$	1.01	11.67±0.11 11.97±0.07	10.60±0.07 10.76±0.06	13.39±0.08	13.22±0.1	13.36±0.16	C^{12} g.s.	1×10^{-27}
	1.01	6.39	7.31					
	1.03	6.57	7.45					
	1.02	6.54±0.06	7.43±0.05	9.02±0.07	8.93±0.03		C^{12} 4.37	3×10^{-27}
	1.03	6.49	7.40					
	1.02	6.47	7.39					
	1.03	3.50±0.07	4.98±0.06	5.77±0.07				
	1.02	3.47±0.07	4.96±0.06				C^{12} 7.62	3×10^{-28}
$N^{15}(d, \alpha)C^{13}$	1.01	5.10±0.07	6.37±0.06					
	1.02	5.25±0.07	6.48±0.06	7.54±0.07		7.51±0.28	C^{13} g.s.	1×10^{-27}
$N^{14}(d, p)N^{15}$	0.95 (1.01)	90.5 ±1.6 (92.5)	8.75±0.1 (8.86)	8.51±0.1 (8.57)	8.53±0.1	8.57±0.23	N^{15} g.s.	4.5×10^{-28}
	1.01	21.02±0.11	3.78±0.02	3.15±0.05	3.25±0.07		N^{15} 5.42	3×10^{-27}

7.62-Mev levels in C^{12} and the 5.3-Mev line with the 5.42 level in N^{15}. The relative intensities of the particle transitions to the 4.37-Mev level in C^{12} and the 5.42-Mev level in N^{15} agree approximately with the relative intensities of the 4- and 5.3-Mev gamma-ray lines. However, it should be pointed out that the ratio of the numbers of the particle transitions to the 4.37- and 7.2-Mev levels in C^{12} is 10 whereas the ratio of the numbers of the 4- and 7.2-Mev gamma-ray quanta as given by Gaerttner and Pardue is 0.45. In order to explain this one might assume the existence of another strong group of alphas corresponding to a still higher excited state of C^{12}. Such a group would of course fall into the very short range region and could not be detected in the present measurements. The corresponding excited state of C^{12} would be unstable against alpha-emission, but it is still easily conceivable that such a state could not actually emit alpha-particles because of selection rules. If one assumes that such a state exists at about 9 Mev it is easy to account for the intensity of the 7.2-Mev line as well as the existence of the 2-Mev line which could originate in the transition from the 9 Mev to the 7.62-Mev level. This picture is given some support by the fact that the intensities of the 2-Mev and the 7.62-Mev gamma-ray lines are about the same. Crane Delsasso, Fowler and Lauritsen,[22] in addition to the first five lines reported by Gaerttner and Pardue, observed a gamma-ray line of 3.1-Mev energy. This could result from a transition between the 7.62- and the 4.37-Mev levels in C^{12}. Crane, Halpern and Oleson[23] report gamma-rays of energies 8.2, 6.6, 5.1, 4.1, and 2.5 Mev as coming from deuteron bombardment of nitrogen.

ACKNOWLEDGMENTS

The authors wish to express their appreciation of the continued encouragement and advice given them by Professors R. F. Bacher and H. A. Bethe. The N^{15} used in these experiments was kindly furnished by Professor H. C. Urey of Columbia University.

[22] H. R. Crane, L. A. Delsasso, W. A. Fowler and C. C. Lauritsen, Phys. Rev. **48**, 100 (1935).
[23] H. R. Crane, J. Halpern and N. L. Oleson, Phys. Rev. **57**, 13 (1940).

The Specific Charge of the Positron

A. H. SPEES* AND C. T. ZAHN†
Department of Physics, University of Michigan, Ann Arbor, Michigan
(Received September 20, 1940)

Previous measurements of the specific charge of beta-particles have been supplemented to include data on positrons by making a direct comparison between electrons and positrons. The positrons and electrons were obtained from artificially radioactive copper. Comparisons were made for beta-particles having approximately the velocity $\beta=0.72$. The results indicate that the ratio e/m_0 for positrons is the same as for electrons within an error of approximately two percent.

INTRODUCTION

A COMPARISON of the specific charges of negative and positive beta-rays by a deflection method was made by J. Thibaud[1] shortly after the discovery of the positron. Employing the trochoid method of collecting charged particles in a magnetic field, he observed the deflections of positrons and electrons in a combination of magnetic and electric fields and concluded that the specific charges did not differ by more than fifteen percent. Another experiment reported by E. Rupp[2] presented results indicating equality to within five percent. This work together with other articles on positrons was, however, retracted.[3] From cloud-chamber data Chadwick and his co-workers[4] obtained a comparison not of the specific charges but of the masses of positron and electron and these were found to be the same to within ten percent.

EXPERIMENTAL PROCEDURE

In view of the rather low accuracy of these previous determinations it was decided worth while to attempt measurements yielding more precise results. The method and apparatus used in the previous work on the specific charge of beta-rays[5] proved sufficient for this purpose. For convenience the method is here briefly reviewed. When the Lorentz mass formula is introduced into the formula for the curvature k of the circular orbit that a charged particle e takes in a uniform magnetic field H, one obtains:

$$e/m_0=c^2k\beta/H(1-\beta^2)^{\frac{1}{2}}.$$

Upon the determination of k and β for a fixed magnetic field H this formula yields a value of the specific charge of the particle. In the experimental arrangement employed, a diagram of which is given in Fig. 1, the curvature k is determined by geometric conditions in the magnetic field before the rays enter the velocity selector represented by the electric condenser. These geometric conditions include the relative position of the beta-ray source and the condenser, the size of the source, and the condenser spacing. Because of the latter two features the rays that are permitted to enter the condenser will have, not just a single curvature k_{00}, but curvatures in a spread dk about a curvature k_{00}. This curvature is that of a central ray which leaves the source at the center and enters the condenser in the central plane, in a direction parallel to the condenser plates.

According to the above formula for e/m_0, a definite value of $k=k_{00}$ as thus determined for a fixed field intensity H and the assumption that e/m_0 is a constant, determine a value of $\beta=\beta_{00}$. Therefore since at all times only particles having approximately $k=k_{00}$ enter the condenser space (the region of crossed electric and magnetic

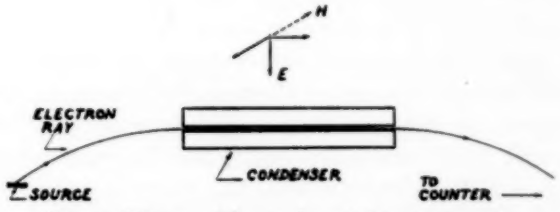

FIG. 1. Diagram of experimental arrangement.

* Now at the Detroit Institute of Technology.
† Now with the American Viscose Corporation.
[1] J. Thibaud, Phys. Rev. **45**, 781 (1934).
[2] E. Rupp, Zeits. f. Physik **92**, 485 (1934).
[3] E. Rupp, Zeits. f. Physik **95**, 801 (1935).
[4] Chadwick, Blackett and Occhialini, Proc. Roy. Soc. **144**, 235 (1934).
[5] C. T. Zahn and A. H. Spees, Phys. Rev. **53**, 357 (1938); **53**, 366 (1938). In the present article these references are referred to as papers I and II.

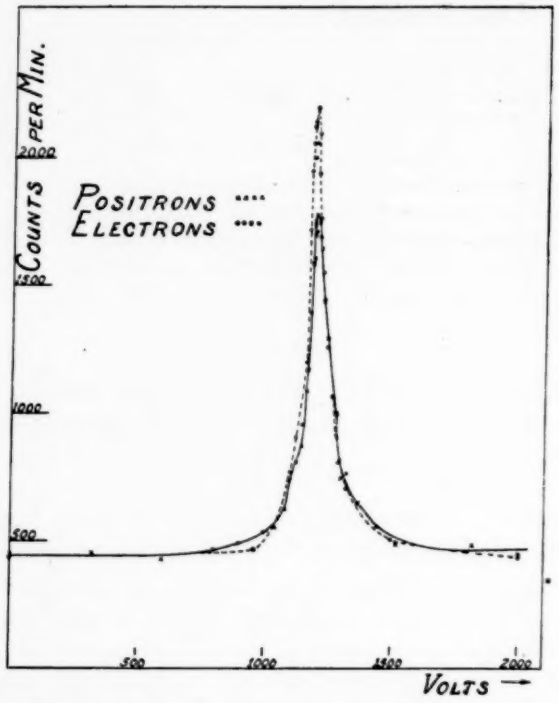

FIG. 2. Transmission peaks for positrons and electrons from a Cu source.

fields) it follows that the particles transmitted by the condenser will have approximately a velocity $\beta=\beta_{00}$. But this transmission, it is to be remembered, may occur only for a compensating setting of the electric field E, namely when $\beta_{00}=E/H$. As a consequence of such action a plot of the counts of particles emerging from the condenser space against various settings of the electric field (magnetic field constant) should show a peak indicating maximum transmission at a certain value $E=E_{00}$. An intensity peak obtained in this manner must, due to the finite resolution of an actual apparatus, have a definite spread. The quantity E determined experimentally in the fashion just outlined gives a measure of the velocity β_{00} which is to be inserted in the formula for e/m_0. Particles having different specific charges will obviously yield peaks that have different values of E_{00}.

The procedure for the problem of comparing the specific charges of electron and positron was based on the use of a beta-ray source which emits both kinds of particles. Copper when bombarded with deuterons has just this property. The unstable isotope Cu^{64} that is produced decays with the emission of both positrons and electrons, the half-life being 12.8 hours. For the present experiment this branching reaction was convenient because measurements on both kinds of particles could be made without disturbing the geometry of the apparatus. In order to change from an electron to a positron source all that was required was a reversal of the electric and magnetic fields. The procedure, therefore, was to obtain a transmission peak for the electrons and then after reversing the fields to obtain another for the positrons. The relative positions of two such peaks should give a direct comparison of the specific charges that is practically independent of any geometrical features.

The particular beta-ray sources used in the experiment were obtained from copper soldered to the end of a water-cooled probe that was placed directly between the duants of the Michigan cyclotron. With this arrangement a bombardment of 8 hours with a beam of 9-Mv deuterons gave a source of several millicuries strength. In the apparatus the source had to be shielded with lead in order to absorb some of the 0.5-Mv positron annihilation radiation that would have produced a very high background count in the particle counter.

OBSERVATIONS

The experimental peaks for two sets of measurements are given in Figs. 2 and 3. The sets differ in that the positions of the sources were slightly different and hence correspond to slightly different values of k_{00} and β_{00}. The measured points of the present peaks are slightly more scattered than those of paper II obtained from a Ra E source. This resulted from the necessity of using shorter counting periods due to the time limitation set by the shorter half-life of 12.8 hours and the additional requirement of obtaining two peaks instead of just one. As for the spreads, the present peaks are seen to have a ten percent half-width as compared with the four percent of the Ra E peaks. This change is to be expected because of an increase in source size. It was necessary to use a 1-cm square copper source because of intensity considerations; whereas the Ra E source was a 1-cm length of 0.5-mm wire. In view of this relatively large increase in source size it is indeed surprising at

first sight that the peaks turned out to be as narrow as they did. According to resolution and intensity calculations for a finite source of 1 cm the expected half-width for over-all resolution is about 6.5 percent which is to be compared with the previous result of 2 percent for a line source. As previously, the greater width of the observed peaks may be attributed to scattering. It might have been possible to increase the resolving power in the present case by using the defining slits mentioned in paper II. These, however, had to be removed to make way for the lead shielding and so were not available for the measurements with positrons.

In the transmission curves of paper II there occurred some pronounced subsidiary peaks to each side of the main peaks. An examination of the present peaks gives a slight indication of the same features. The principal reason they are not more pronounced is that the time factor did not permit drawing them out. In some preliminary work with a small condenser it was, however, definitely established that the side peaks also occur for an extended source. Thus since the side peaks arise from sources differing in size and shape, as do the Cu and Ra E sources, they can hardly be ascribed to source conditions. Furthermore an extended and more thorough resolution calculation precludes the explanation that the side peaks may arise from some second-order effect inherent in the characteristics of the instrument as a whole. Their origin, therefore, is probably the one mentioned in previous discussion, namely, scattering from the condenser plates.

Since the present investigation is concerned with relative values of the specific charge it was considered unnecessary to attempt an accurate determination of absolute values. It seems worth while, however, to discuss briefly the results in this connection. For the extended copper source used it is rather difficult to choose a proper central curvature k_{00} in that one has to allow for a non-uniform distribution of radioactivity. Hence one cannot expect the accuracy that was attained with the small Ra E source. The measured values of k_{00} for the two source positions used for Figs. 2 and 3 were corrected for stray electric field and non-uniform magnetic field, in the manner outlined in paper II. The corrected values were then used with values of the velocity as given by the graphs, namely, $\beta_{00}=0.71$ for Fig. 2 and $\beta_{00}=0.73$ for Fig. 3, to obtain values of e/m_0. In the former case the obtained value is lower than the accepted precision value by about 7 percent and in the latter case by about 10 percent. In the previous investigation with the Ra E source the observed peak position differed from the expected position by about 2.5 percent which means a discrepancy with the accepted value of e/m_0 of about five percent.

Conclusion

In conclusion, the answer to the main problem of how the specific charges of the electron and the positron compare may be read from Figs. 2 and 3. The peaks for electrons and positrons have positions on the voltage scale that correspond to voltages differing by no more than one percent. To find the corresponding difference in terms of specific charge one uses the following formula derived from the above formula for e/m_0:

$$\Delta(e/m_0)/(e/m_0)=[1/(1-\beta_{00}^2)][\Delta V/V_{00}].$$

Thus the percentage difference in e/m_0 is larger

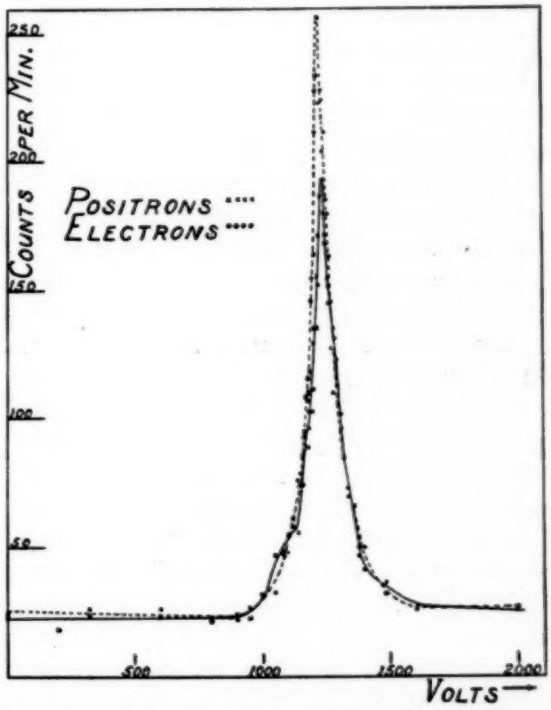

FIG. 3. Transmission peaks for positrons and electrons from a source position slightly different from that of Fig. 2.

than that in the voltages by a factor containing the compensated central velocity β_{00}. For the actual values of β_{00} used in the experiment this factor is approximately 2.0. From the percentage difference in voltage of about one percent one would therefore conclude that the specific charge of the positron is the same as that of the electron to within approximately two percent.

Acknowledgments of indebtedness are gratefully given to various members of the Michigan Physics Department who have generously contributed toward the success of this investigation: to Professor S. A. Goudsmit for helpful discussions; to Professor J. M. Cork and Dr. B. R. Curtis for aid in obtaining the necessary radioactive sources with the cyclotron; to Professor O. S. Duffendack and his co-workers for help in preparing Geiger-Müller tubes; and to Dr. J. L. Lawson for the loan of a recording circuit. Finally the authors wish to acknowledge financial support from the Horace H. Rackham Endowment Fund.

NOVEMBER 15, 1940 PHYSICAL REVIEW VOLUME 58

Successive Transformations in Nuclear Fission

N. BOHR
Institute of Theoretical Physics, University of Copenhagen, Copenhagen, Denmark
(Received August 12, 1940)

If it be assumed that fission of heavy nuclei takes place in competition with the escape of a neutron from the highly excited compound system, we should expect that, for sufficiently high excitation of the system, fission of the residual nucleus left after neutron escape may still occur. Since, in this second stage of the process, the conditions for the competition with neutron escape are in several cases more favorable than in the first stage, such effects may give rise to much increased cross sections for the fission process.

As has been shown in earlier papers,[1] it is possible to explain the principal features of the fission of heavy nuclei on the basis of the assumption that the process involves a comparatively long-lived intermediate state of the compound system in which the excitation energy is distributed over all degrees of freedom, as in temperature equilibrium. In fact, the excessive deformations of the compound nucleus leading to rupture are to be attributed to fluctuations in this energy distribution occasionally resulting in the concentration of a considerable part of the excitation energy in particular modes of oscillation of the closely coupled system of nuclear particles. The probability that a fission of the compound system takes place is therefore determined by a competition with other disintegrative or radiative processes leading to a decrease in the excitation energy of the residual system to such an extent that fission is no longer possible.

In the ordinary cases, where the compound system has an energy not greatly exceeding that required for fission, the occurrence of one or the other competing process will reduce the energy available below the critical value. If, however, the excitation of the compound system is very high, the residual system may have a sufficient excitation to permit fission. In the second stage, the probability of fission will, of course, again depend on a competition with other disintegrative or radiative processes. Such progressive transformations have already been briefly discussed (BW, p. 449) especially in connection with deuteron incited fission, but at that time no experimental evidence for their occurrence was available. Recent experiments on fission with high speed neutrons as well as with deuterons seem, however, to afford definite evidence of successive transformation and, as they at the

[1] N. Bohr, Nature **143**, 330 (1939); Phys. Rev. **55**, 418 (1939), and especially N. Bohr and J. A. Wheeler, Phys. Rev. **56**, 426, 1065 (1939), (referred to in the following as BW).

same time elucidate the competitive character of the fission process, it may be of interest here to consider them in some detail.

In the first place, it has been found by Ageno, Amaldi, Bocciarelli and Trabacchi[2] that the cross section for fission in uranium by neutron impact remains practically constant for neutron energies from about one million volts to about ten million volts, but that it increases considerably for neutrons with still higher energies, obtained by the bombardment of lithium with deuterons. This result can easily be understood by considering that, for the lower energies, we have simply to do with a competition between neutron escape from the compound nucleus $_{92}U^{239}$ and its fission, the ratio between the probability of these competing processes being nearly constant for neutron energies above 1 Mev. If, however, the neutron energy is above 10 Mev, there is a considerable probability that the residual nucleus $_{92}U^{238}$ left after neutron escape will have a sufficient excitation itself to undergo fission. Moreover, the condition for fission is, in this case, especially favorable since in $_{92}U^{238}$ we have to do with a nucleus of even charge and mass number for which, just as in the compound nucleus $_{92}U^{236}$ formed by neutron impact on the rare uranium isotope $_{92}U^{235}$, the critical energy for fission is somewhat lower than the binding energy of a neutron. Thus, for excitation energies of the nucleus $_{92}U^{238}$ just above the critical energy for fission, no neutron escape can take place; and, even at higher excitation, the probability for fission in this process is much greater than for neutron escape.

An estimate of the difference between the critical fission energy E_f and the neutron binding energy E_n can, for all the nuclei concerned, be arrived at by simple considerations (BW, pp. 430, 433), the result of which may be summarized in the following approximate formula:

$$\Delta E = E_f - E_n = 0.27(A-238) - 1.32(Z-92) + \begin{cases} -0.6 & (A-Z) \text{ even} \\ +0.4 & (A-Z) \text{ odd,} \end{cases} \quad (1)$$

giving ΔE in Mev for a compound nucleus with mass and charge number A and Z. The difference in the two constants represents just the difference of about 1 Mev between the binding energy of a neutron in a heavy nucleus for even and odd numbers $(A-Z)$ of nuclear neutrons.

For $_{92}U^{239}$ and $_{92}U^{238}$, formula (1) gives $\Delta E = +0.7$ Mev, and $\Delta E = -0.6$ Mev, from which one deduces that, for sufficiently high excitation the ratio ρ between the probabilities for neutron escape and fission, which for $_{92}U^{239}$ is about 4 : 1, will for $_{92}U^{238}$ be less than 1 : 3. For the average cross sections σ_f' and σ_f'' for uranium fission with fast neutrons in one and two stages, respectively, we get

$$\sigma_f' = \frac{1}{4+1}\sigma_0 = \frac{1}{5}\sigma_0; \quad \sigma_f'' = \frac{4}{5}\cdot\frac{3}{4}\alpha\sigma_0 = \frac{3}{5}\alpha\sigma_0,$$

where σ_0 is the cross section for formation of the compound system $_{92}U^{239}$ and the factor α roughly represents the fraction of the residual nuclei $_{92}U^{238}$ having excitation greater than the critical fission energy. Since the experiments show that the average cross section for D+Li neutrons is 40 percent higher than that for D+Be and D+B neutrons, α should in this case have an average value somewhat larger than $\frac{1}{10}$, which appears reasonable from the known spectrum of the D+Li neutrons.[3]

A comparatively larger effect from successive transformations should be expected in the case of the fission of thorium with fast neutrons. In fact, from formula (1) we get for $_{90}Th^{233}$ and $_{90}Th^{232}$ approximately $\Delta E = 1.7$ and $+0.4$, corresponding to values for ρ of about 24 : 1 and 2 : 1. In this case, we therefore get

$$\sigma_f' = \sigma_0/25, \quad \sigma_f'' = 8\alpha\cdot\sigma_0/25.$$

With the same value of α as above, we shall thus expect that the average cross section for D+Li neutrons will be almost twice that for D+Be neutrons. Still more conspicuous effects should, of course, be expected in the case of neutrons with well-defined high velocities for which α can be almost 1, giving a total fission cross section nearly 10 times greater than that obtained for neutrons with only a few million volts energy, for which α is still zero.

[2] M. Ageno, E. Amaldi, D. Bocciarelli and G. C. Trabacchi, Atti Acc. d'Italia, in press; kindly communicated to the author by Professor Amaldi.

[3] T. W. Bonner and W. Brubaker, Phys. Rev. **48**, 748 (1935).

In this connection it may be of interest to point out that similar effects can also be expected in the fission of protoactinium with fast neutrons. Here, for the compound nuclei $_{91}Pa^{232}$ and $_{91}Pa^{231}$, we get from formula (1),

$$\Delta E = +0.1 \quad \text{and} \quad \Delta E = -1.2$$

giving values for ρ of about 1 : 1 and 1 : 10, leading to

$$\sigma_f' = \tfrac{1}{2}\sigma_0, \quad \sigma_f'' = 5\alpha \cdot \sigma_0/11.$$

Thus, we shall expect an increase in fission yields of about a factor of two when comparing the effects of neutrons of a few million volts with neutrons above ten million volts.

As regards fission induced by deuterons, it follows from simple theoretical considerations (BW, p. 448) that a sufficient excitation of the compound system can only be obtained by impacts leading to a complete fusion of the deuteron and the original nucleus. The yield of the reaction will, therefore, in the first place depend on the ease with which the deuteron penetrates the electrostatic field around the nucleus, and cross sections of the order of magnitude of nuclear dimensions can only be expected for deuteron energies approaching 10 Mev. This is in agreement with the experiments of Gant[4] who reported a threshold for the process in uranium of about 8 Mev, without attempting measurements of cross sections. Such measurements for uranium as well as for thorium have recently been made at this Institute by Jacobsen and Lassen[5] who found for both elements a rapid rise in the yield of the process between 8 and 9.5 Mev, corresponding to cross sections of the order of 10^{-26} cm^2 at the latter energy.

In deuteron induced fission of uranium and thorium, we shall expect progressive transformations involving the compound nuclei $_{93}EkaRe^{240}$, $_{93}EkaRe^{239}$ and $_{91}Pa^{234}$, $_{91}Pa^{233}$, respectively. From (1), we get

$$\Delta E = -0.4 \text{ Mev} \quad \text{and} \quad \Delta E = -1.7 \text{ Mev}$$

for the successive uranium transformations, and

$$\Delta E = +0.6 \text{ Mev} \quad \text{and} \quad \Delta E = -0.7 \text{ Mev}$$

for the thorium transformations, corresponding to values of ρ of about 1 : 2 and 1 : 24 for uranium and about 3 : 1 and 1 : 4 for thorium. Thus, we shall expect for uranium

$$\sigma_f' = \tfrac{2}{3}\sigma_0; \quad \sigma_f'' = 8\alpha\sigma_0/25$$

and for thorium

$$\sigma_f' = \tfrac{1}{4}\sigma_0, \quad \sigma_f'' = 3\alpha\sigma_0/5.$$

While σ_f' for thorium is only about $\frac{1}{3}$ the value for uranium, we see that the total cross sections $\sigma_f' + \sigma_f''$ become nearly equal for the two elements if α approaches unity, as is to be expected from the high excitation (about 15 Mev) of the compound system. The experiments of Jacobsen and Lassen, showing that for 9-Mev deuterons the fission yield for thorium amounts to about 0.7 of the uranium value, seem therefore to confirm that we have here to do with successive transformations.

In the fission effects in uranium with fast neutrons and deuterons, the presence of the rare uranium isotope $_{92}U^{235}$ will, in contrast to the case with slow neutrons where it is responsible for the whole effect, be of negligible importance. In experiments with separated uranium isotopes, we shall, of course, also for $_{92}U^{235}$ expect to observe successive transformations of the same kind as those discussed here, but because of the fact that for the compound nuclei $_{92}U^{236}$ and $_{93}EkaRe^{237}$ directly formed by neutron and deuteron impacts, we have from (1) the large negative values $\Delta E = -1.2$ and $\Delta E = -2.3$, corresponding to very small values for ρ, such effects will be far less pronounced than in the cases considered above. Similar considerations apply to protoactinium fission by deuteron impact.

From this brief discussion of successive transformations in nuclear fission, it will be seen that the study of these phenomena offers a means of enlarging greatly the number of different nuclei in which the fission process may be investigated.

[4] D. H. T. Gant, Nature **144**, 707 (1939).
[5] J. C. Jacobsen and N. O. Lassen, Phys. Rev. **58**, 867 (1940), following paper.

Deuteron Induced Fission in Uranium and Thorium

I. C. JACOBSEN AND N. O. LASSEN
Institute of Theoretical Physics, University of Copenhagen, Copenhagen, Denmark
(Received August 12, 1940)

By means of deuteron beams from the cyclotron, the variation of fission yield with deuteron energy is determined for uranium and thorium. In both cases, a rapid rise is found in the region from 8 to 9.5 Mev. For an energy of 9 Mev, the cross section in uranium is estimated to be 5×10^{-27} cm², and for this energy the ratio between the cross sections for uranium and thorium is found to be 0.7, supporting the theoretical expectation that we have in these fission processes to do with successive transformations.

ACCORDING to theoretical considerations,[1] fission of heavy nuclei by deuteron impact cannot be expected to occur unless the deuteron has sufficient energy to penetrate the Coulomb field around the nucleus without breaking up. Thus, appreciable effects are not to be expected at energies much below ten million volts. This conclusion is confirmed by the experiments of Gant[2] who found a threshold for deuteron induced fission in uranium of about 8 Mev. Gant did not, however, attempt a quantitative determination of the cross section for the process. In view of the desirability of a closer study of the problem[3] and especially of a comparison between the effects induced by deuteron bombardment in thorium and uranium, experiments have recently been made in this Institute with the object of obtaining measurements of cross sections for fission at various deuteron energies in both elements.

These experiments were made by means of the cyclotron built in the Institute in the course of the last two years, the construction of which will be described in a forthcoming publication in the *Proceedings of the Copenhagen Academy*. After various recent improvements, the cyclotron is now able to give fairly steady deuteron beams of a few microamperes up to about ten million volts. The beam has an energy spread of about 0.5 Mev and has nearly constant intensity over this region.

In the measurements with uranium, four aluminum targets upon which had been evaporated thin layers of uranium (about 1.5 mg/cm²) were mounted in a rotating holder provided with absorbing foils. This holder could be inserted by means of a vacuum lock into the cyclotron chamber and each target in turn exposed to the deuteron beam, the foils serving to reduce the energy of the deuterons by a known amount for each individual target. The fission products were collected on aluminum foils fastened in the holder in such a way as not to intercept the beam. During the irradiation, the holder was rotated constantly in order to insure that all targets received the same deuteron current. After an irradiation period of ten to twenty minutes, the target holder was removed from the cyclotron chamber. Measurements of the beta-ray activity of the foils with the fission products were begun after the lapse of about ten minutes and continued for some ten hours. Separate experiments made to determine the background effect due to stray neutrons in the cyclotron showed that, for energies above 8 Mev, the number of fissions so produced was negligible compared with the deuteron effect.

The variation of fission cross section in uranium with deuteron energy is shown in Fig. 1, where the open circles indicate differences between the measured yield values for energies differing from one another by an amount which is less than the energy spread of the beam. Thus, the curve through these points is an approximation to a "differential yield" curve, corresponding to the yield to be expected from an infinitely thin target bombarded by a monochromatic beam. For a determination of the absolute value of the cross section, a single point was taken with a fixed target to which the deuteron beam current was kept as constant as possible. From the

[1] N. Bohr and J. A. Wheeler, Phys. Rev. **56**, 426 (1939).
[2] D. H. T. Gant, Nature **144**, 707 (1939).
[3] N. Bohr, Phys. Rev. **58**, 864 (1940), preceding paper.

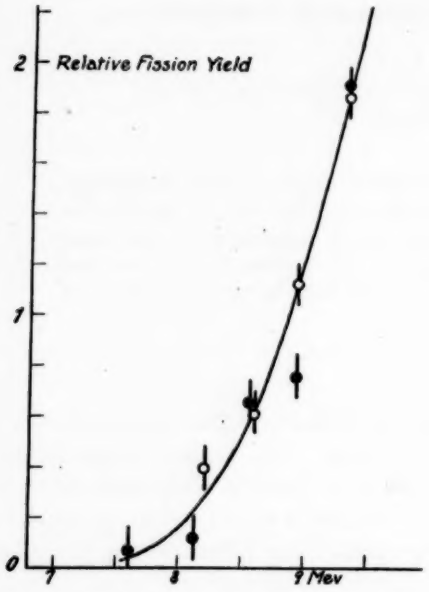

FIG. 1. Relative variation of fission yield with deuteron energy; full circles refer to uranium, open circles to thorium.

geometry of the collecting and counting arrangement, we have a means of estimating the number of fission processes occurring in the target. Assuming the average number of beta-particles given off per fission fragment during the counting period to be about three, we calculate the cross section for fission in uranium of 9-Mev deuterons to be about 5×10^{-27} cm². We observe from the curve that the rise with deuteron energy is very rapid in the interval investigated. Thus, the experiments indicate that the cross section will continue to increase for still higher energies, presumably reaching, for an energy somewhat above 10 Mev, a value comparable with nuclear dimensions, as is to be expected from the theory.

In order to make a comparison between the effects in thorium and those in uranium, two targets coated with thick layers of U_3O_8 and ThO_2 were mounted on the rotating holder in the vacuum chamber and bombarded alternately by a deuteron beam of 9- to 9.5-Mev energy. At this energy, it was found that the yield for thorium was 0.75 that of uranium. Because of the thickness of the layers of uranium and thorium oxide on the target, we should, in estimating the ratio of the cross section for fission in the two elements for a given deuteron energy, take into account that the stopping power in the uranium layer for the fission fragments escaping from it will be somewhat larger in proportion to the amount of heavy element present. In fact, because of the greater number of oxygen atoms in the U_3O_8 than in ThO_2, the relative stopping power for fission fragments can be expected to be about 10 percent greater in the uranium than in the thorium target. We may conclude, therefore, that the average fission cross section of thorium for 9- to 9.5-Mev deuterons is about 0.7 that of uranium. As explained in the paper by Bohr cited above,[3] this result confirms the view that, in the fission of uranium and thorium by deuterons, we have to do with successive transformations of the compound nucleus.

The fission yields at various energies for thorium were determined in the same way as those for uranium, using, however, in this case thick targets of ThO_2. The results are, in relative measure, represented by the full circles in Fig. 1. To facilitate comparison of the higher yields from the thick targets, the scale is chosen so that the values at a deuteron energy of 9.3 Mev for uranium and thorium are put equal. We see that the curve drawn fits equally well both sets of points, indicating that the cross section for uranium and thorium rises in very much the same way with deuteron energy in the two elements, as was to be expected from the theory on account of the small difference in charge number of the two elements.

In conclusion, the authors wish to thank the director of the Institute, Professor N. Bohr, who suggested the problem, for his continued interest in the work and for many valuable discussions of its theoretical implications. Our thanks are due also to Mr. Høffer Jensen for preparing the uranium targets.

Capture Cross Sections for Thermal Energy Neutrons. II

FRANCO RASETTI
Laval University, Quebec, Canada

(Received September 17, 1940)

Cross sections for capture of slow neutrons by a number of elements were measured by determining the intensity of the β-activity induced under standard neutron irradiation. The number of neutrons was measured by using as standard the activity induced in Mn, the cross section for capture by Mn being taken from former experiments. Data are reported for neutron capture by Na^{23}, Al^{27}, P^{31}, K^{41}, V^{51}, Cu^{63}, Cu^{65}, As^{75}, Br^{79}, Sb^{121}, I^{127}.

SINCE the early observations on the activity induced by slow neutrons, the activities have usually been reported as "strong" or "weak," but more quantitative data are very meager. Relatively accurate measurements are available only for those elements that, like Rh or Ag, possess a large cross section for activation.

It was considered worth while to perform a series of measurements on other elements, in order to determine the cross section for the neutron capture reaction. The use of a radium-beryllium source limited the investigation to the stronger activities. The work could be greatly extended if a stronger source, as afforded by a cyclotron, were available.

The source was placed inside a paraffin block, 3 cm below the surface. The detectors, 5×5 cm^2 in size, were placed above the source, on the surface of the paraffin, and covered with another paraffin block, to increase the activation by thermal neutrons.

The β-activity was measured by a small, thin-walled glass counter, the flat detectors being placed along the side of the counter, in an accurately reproducible position. The background effect was about 8 counts per minute, the measured activity seldom giving less than one hundred pulses per minute, and often a great deal more. Each activity was followed through at least one decay period in order to be certain of its identity.

It is believed that the main sources of error in the present work are due to the difficulty of securing thin uniform layers of the substances used as detectors, and to back scattering of electrons by the detector itself and by its support. Metal foils were used when possible. Compounds were generally melted on a thin Al or Ni foil, and fairly uniform thin layers were obtained by tilting the support before the substance had solidified. The activity of the Al or Ni support was negligible under the circumstances. Na and K were rolled into thin sheets between Al foils to prevent their oxidation.

No attempt was made to correct for back scattering by the support. Absorption and scattering by the detector itself and by the counter wall were accounted for by assuming an exponential "absorption," with an empirically determined coefficient. This coefficient is given, for about the same type of geometry, by Amaldi *et al.*,[1] except for a few cases where it was experimentally determined. The value used is given in Table I. No dependence of the mass "absorption" coefficient upon atomic number was considered, the experimental values generally referring to aluminum.

Since the measurements were effected inside the paraffin, it was necessary to ascertain that the presence of the detector or its support did not appreciably alter the density of the thermal neutrons. In all doubtful cases, this was checked by observing whether the activity of a rhodium detector was appreciably decreased by placing under it the substance to be investigated. No decrease of more than a few percent was recorded.

As part of the activity is generally due to resonance neutrons, a measurement was also taken with the detector covered by Cd on both sides, and the number of counts thus recorded was subtracted from the total. In some cases the activity with Cd was too weak to be measured.

To express the activity in terms of a cross section, one must know the number of thermal

[1] E. Amaldi, O. D'Agostino, B. Pontecorvo, F. Rasetti and E. Segrè, Proc. Roy. Soc. **A149**, 522 (1935).

TABLE I. *Capture cross sections for thermal neutrons.*

ELEMENT AND ISOTOPE	COMPOUND USED	G/CM² OF ISOTOPE	G/CM² OF COMPOUND	DECAY PERIOD OF ACTIVE ISOTOPE	SATUR. ACTIV. IMPULSES PER MINUTE	PERCENTAGE OF ACTIV. DUE TO RESONANCE NEUTRONS	ACTIVITY DUE TO THERMAL NEUTRONS	ASSUMED ABSORPTION COEFFICIENT OF ELECTRONS CM²/G	ACTIVITY CORRECTED FOR ABSORPTION IN DETECTOR AND COUNTER	$\sigma \times 10^{24}$ CM²	$\sigma \times 10^{24}$ CM² L.R.
Mn^{55}	Mn	0.032	0.032	2.6 hr.	3700	0.04	3500	5.0	5100	9.4	9.4
Na^{23}	Na	0.07	0.07	15 hr.	350	<0.03	350	10	980	0.35	
Al^{27}	Al	0.18	0.18	2.4 min.	750	0.02	700	4.3	1300	0.21	
P^{31}	P	0.028	0.028	14 day	~70	—	~70	7	~120	~0.2	1
K^{41}	K	0.003	0.045	15 hr.	~45	—	~45	4.0	~100	~1.4	
V^{51}	V_2O_5	0.012	0.021	3.8 min.	850	<0.02	850	4.1	1100	5.2	6.8
Cu^{63}	Cu	0.27	0.40	12.8 hr.	100	~0.03	100	27	5000	1.8	
Cu^{65}	Cu	0.13	0.40	5 min.	1000	0.03	970	5.6	3300	1.2	
As^{75}	As	0.068	0.068	27 hr.	2000	0.20	1600	4.5	2600	3.1	6.5
Br^{79}	NaBr	0.0035	0.009	18 min.	280	0.29	200	5.8	290	7	
Br^{79}	NaBr	0.0035	0.009	4.4 hr.	220	0.23	170	5.8	250	6	
Sb^{121}	Sb	0.073	0.13	2.8 day	1060	0.42	600	8	1850	3.3	
I^{127}	PbI_2	0.009	0.017	25 min.	450	0.35	300	6.3	440	6.5	6.8

neutrons traversing the detector per second. This can be determined by employing a detector whose capture cross section is already known from absorption measurements. The capture cross section of Mn^{55} ($\sigma_{Mn}=9.4\times10^{-24}$ cm²) was taken as standard since its value is one of the best known from the earlier measurements.[2] The cross section σ for any isotope is then given by

$$\sigma=\sigma_{Mn}\frac{N_{Mn}}{N}\frac{A}{A_{Mn}},$$

A being the activity (corrected for absorption), N the number of atoms of the isotope per cm², A_{Mn} and N_{Mn}, respectively, the same quantities for Mn.

Table I summarizes the results. The headings of the columns are self-explanatory. The cross section is referred to the isotope responsible for the capture process and not to the whole element. The last column gives the values found by Lapointe and Rasetti[2] in those cases where comparison is possible.

The agreement for V^{51} and I^{127} is as good as can be expected. For As^{75}, the present value is about half as large as that previously reported. A discrepancy by a factor of two cannot be altogether excluded as due to experimental errors; however, this discrepancy is more likely to be accounted for by the complex structure[3] of the β-spectrum of As^{76}. The absorption coefficient used, 4.5 cm²/g, would roughly correspond to a simple distribution with maximum energy of 2.7 Mev. In addition to this distribution, there appears to be a large number of low energy electrons, which are scarcely effective in the present experiment because of the thickness of the detector and of the counter wall. The higher value of the cross section from absorption measurements is, therefore, believed to be more accurate. For the other radioactive isotopes investigated, it is unlikely that a possible complexity of the β-spectrum will introduce a considerable error in the measurement of the activity. For the case of phosphorus, the measurement of the capture cross section from absorption was rather inaccurate, the effect being only about five times the statistical error. The present measurements indicate a considerably lower value, which is probably more accurate.

The cross sections given for Br^{79} are partial cross sections for the production of the two radioactive isomers. The difference in the fraction of the activity which is due to resonance neutrons for each of the two isomers is not significant, being within the experimental error.

[2] C. Lapointe and F. Rasetti, Phys. Rev. **58**, 554 (1940).

[3] G. L. Weil and W. H. Barkas, Phys. Rev. **56**, 485 (1939).

Elastic Scattering in Helium at 15°C

ROBERT LEE MOONEY
Georgetown University, Washington, D. C.
(Received September 24, 1940)

An angular distribution function is obtained for the scattered intensity of head-on collisions of parallel beams of helium atoms with relative velocities appropriate to a temperature of 15°C. Margenau's interaction energy is used in a form modified for small values of the separation parameter. The scattering curve does not exhibit the striking regularity obtained in calculations based on the smooth sphere model. The expected maximum at 90° is present. The total collision cross section is calculated. The "diffraction cross section" is compared with the viscosity cross section.

IT has been theoretically demonstrated that the angular distribution function, $I(\theta)$, for helium atoms scattered by helium atoms exhibits maxima and minima similar to those observed in ordinary diffraction patterns formed by plane waves passing over spherically symmetrical obstacles.[1,2] Massey and Mohr,[2] using an interaction energy given by Slater and Kirkwood,[3] have calculated an angular distribution function for elastically scattered helium atoms with relative velocities corresponding to 20°C and to −185°C. Since the publication of their results Margenau has presented a more exact expression for the van der Waals forces in helium.[4] In this paper is given an approximate distribution function obtained by numerical integration of the appropriate Schroedinger equations with Margenau's interaction energy—modified for small values of the separation parameter for the colliding atoms. The "diffraction cross section" for elastic collisions is compared with the experimentally obtained viscosity cross section. No attempt is made to take into account the Maxwellian distribution effect. The colliding atoms are moving with equal and opposite parallel relative speeds appropriate to a temperature of 15°C.

In setting up the Schroedinger equation it is convenient to consider two steady beams of infinite width moving with equal and opposite gas kinetic speeds. By considering one atom from each beam a two-particle system is obtained with the center of gravity at rest. For such a system the appropriate equation is

$$\nabla^2\psi+(2m^*/h)[\tfrac{1}{2}m^*v^2-V(r)]\psi=0, \qquad (1)$$

where $m^*=m/2$; v is the relative velocity of approach; and $V(r)$, the mutual interaction energy with r equal to the separation of the colliding particles. The solution of (1) must be of the form

$$\psi=\exp(im^*vz/h)+f(\theta)r^{-1}\exp(im^*vr/h)$$
$$+\exp(-im^*vz/h)+f(\pi-\theta)\exp(im^*vr/h)r^{-1}, \qquad (2)$$

in which the first term represents the incident wave, and the second the scattered wave as observed from the center of gravity when the colliding particles are distinguishable. However, since helium atoms are identically similar, it is necessary to add the third and fourth terms in (2) to secure a symmetrical wave function. It is then easily shown that the effective cross section for which either particle is deflected into the solid angle $d\omega$ is given by

$$|f(\theta)+f(\pi-\theta)|^2d\omega=I(\theta)d\omega. \qquad (3)$$

It has been shown[5,6] that an axially symmetric asymptotic solution of (1) for unlike particles is

$$\psi=\sum_{n=0}^{\infty}(2n+1)i^n\exp(i\eta_n)P_n(\cos\theta)L_n(r), \qquad (4)$$

where $L_n(r)$ are the solutions of the "radial part" of (1), and η_n are constants depending upon the gas kinetic and mutual interaction energies of the colliding particles. For similar particles the

[1] H. S. W. Massey and C. B. O. Mohr, Nature **130**, 276 (1932).
[2] H. S. W. Massey and C. B. O. Mohr, Proc. Roy. Soc. **141**, 434 (1933); **144**, 188 (1934).
[3] J. C. Slater and J. G. Kirkwood, Phys. Rev. **37**, 682 (1931).
[4] H. Margenau, Phys. Rev. **55**, 1137A (1939).
[5] *Vide* N. F. Mott and H. S. W. Massey, *The Theory of Atomic Collisions* (Oxford, 1933).
[6] H. Faxen and J. Holtsmark, Zeits. f. Physik **45**, 307 (1927).

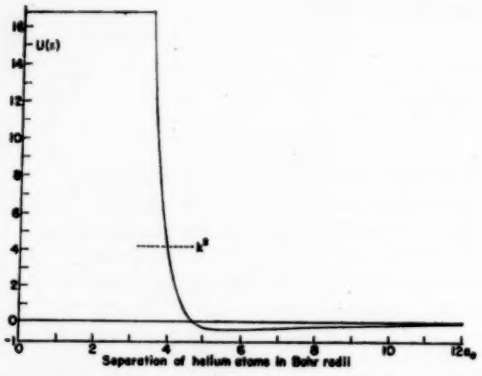

FIG. 1. Interaction potential reduced to reciprocal Bohr radii squared as a function of the separation of helium atoms.

scattered intensity is given by

$$I(\theta)=(1/4k^2)\{[\sum_{n=0}^{\infty}(4n+1)\times(\cos 2\eta_{2n}-1)P_{2n}(\cos\theta)]^2+[\sum_{n=0}^{\infty}(4n+1)\sin 2\eta_{2n}P_{2n}(\cos\theta)]^2\}. \quad (5)$$

In order to evaluate this expression, η_{2n} must be known. $L_n(r)$ must satisfy

$$\frac{1}{r^2}\frac{d}{dr}\left(r^2\frac{dL_n}{dr}\right)+\left[k^2-U(r)-\frac{n(n+1)}{r^2}\right]L_n(r)=0, \quad (6)$$

where $k=m^*v/h$ in (5) and (6). Margenau gives[4]

$$U(r)=(2m^*/h^2)[770\exp(-4.60r)-1.39r^{-6}-3.0r^{-8}]\times10^{-12}\text{ erg},$$

in which r is in angstroms. In these calculations $U(r)$ was modified as shown in Fig. 1 by making $U(r)$ constant for $r\leqslant 3.50\,a_0$ where a_0 = radius of first Bohr orbit for hydrogen. Such modification has little effect upon the asymptotic solution of (6). The asymptotic forms of $L_n(r)r^{-1}$ for r large were found for different values of n and compared with $\sin(kr-\frac{1}{2}n\pi)$. For all $n\leqslant 50$, η_n was determined for a given n from the fact that the asymptotic form of $L_n(r)r^{-1}$ is[5]

$$L_n(r)r^{-1}\sim\sin(kr-\tfrac{1}{2}n\pi+\eta_n). \quad (7)$$

For $n>50$, η_n was calculated from the expression given by Jeffreys:[7]

$$\eta_n=\pi/4+n\pi/2-kr_n+\int_{r_n}^{\infty}[(k^2-U(r)-n(n+1)/r^2)^{\frac{1}{2}}-k]dr,$$

where r_n is the first (and only) zero of

$$[k^2-U(r)-n(n+1)/r^2].$$

Figure 2 shows η_n plotted as a function of n. (It can be shown that η_n is, in general, negative for a repulsive field and positive for an attractive field.) The phase shift, η_n, becomes asymptotically less than 90° only for n greater than 78. The contribution to $I(\theta)$ by terms involving n for which $\eta_n<\pi/2$ and is approaching zero asymptotically with reasonable rapidity is relatively negligible.

The scattered intensity, $I(\theta)$ is plotted in Fig. 3. In evaluating the many terms necessary for the determination of this curve, $P_n(\cos\theta)$ for $n>6$ was computed at intervals of 2.5 degrees from the approximate formula[8]

$$P_n(\cos\theta)\backsimeq\left(\frac{2}{\pi n\sin\theta}\right)^{\frac{1}{2}}\times\left[\left(1-\frac{1}{4n}\right)\sin\varphi-\frac{1}{8n}\cot\theta\cos\varphi\right],$$

where $\varphi=(n+\frac{1}{2})\theta+\pi/4$.

The total cross section for elastic collisions was calculated from

$$Q_q=2\pi\int_0^{\pi}I(\theta)\sin\theta d\theta.$$

On account of the orthogonality of the P_n, this integral is equivalent to the sum

$$Q_q=4\pi/k^2\sum_{n=0}^{\infty}(4n+1)\sin^2\eta_{2n}.$$

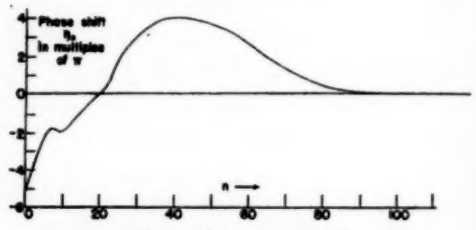

FIG. 2. Phase shift as a function of n.

[7] H. Jeffreys, Proc. Math. Soc. London [2] 23, Part 6 (1923).

[8] E. Jahnke and F. Emde, *Funktionentafeln* (Teubner, 1938), p. 117.

Planimetric integration of the integral expression for Q_v, performed as a check on the accuracy of the drawing of Fig. 3, agreed with the result of the summation expression to within 2 percent.

An inspection of Fig. 3 shows that the outer boundary of the large central maximum of the "diffraction pattern" occurs at $\theta_1 \cong 14°$. This would correspond, in the optical analogy, to the diffraction of a plane wave of wave-length λ by a sphere of diameter $\sigma_d = \lambda/\theta_1$. Here, λ is given by the de Broglie relation, $\lambda = h/mv$. Using σ_d as defined, one might introduce the "cross section for diffraction," $Q_d = \pi\sigma_d^2$.

Q_v was found to have a magnitude of 1228×10^{-16} cm². The de Broglie wave-length of one of the colliding atoms for a relative velocity of approach as given above is about 0.806A. The cross section for diffraction then would be given by $Q_d = \pi\lambda^2/\theta_1^2 = 34.21 \times 10^{-16}$ cm². Trautz and Zink[9] found for helium at 15°C a viscosity cross section $Q_v = 14.93 \times 10^{-16}$ cm². The ratio $Q_d/Q_v = 2.29$. It is of interest to note that for $\lambda = 0$, the diffraction cross section turns out to be just twice the classical value, and for $\lambda = \infty$, the ratio is 4.

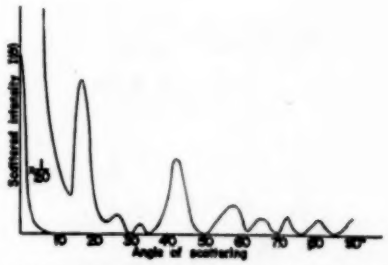

FIG. 3. Distribution in angle of scattered intensity.

The most salient feature of the scattering curve here presented is that the striking regularity exhibited by the distribution given by Massey and Mohr[1] is not duplicated. Naturally, the introduction of more complicated potential fields into the calculations leads to unanticipated results. The maximum of $I(\theta)$ at 90° found by Massey and Mohr for diffraction by smooth spheres is present here, and offers an opportunity for experimental verification, since it appears at all impact velocities. Experimental detection of this maximum would lend support to the validity of the Bose-Einstein statistics as applied to this type of collision.

[9] M. Trautz and R. Zink, Ann. d. Physik **10**, 81 (1931).

NOVEMBER 15, 1940 PHYSICAL REVIEW VOLUME 58

Comparison of X-Ray Absorption Fine Structure for Two Elements in the Same Crystal

S. T. STEPHENSON
State College of Washington, Pullman, Washington

(Received August 26, 1940)

The fine structures on the short wave-length side of the K-x-ray absorption edges of the elements Cu, Se, Br, Rb, Sr, and As in the compounds RbBr, $SrBr_2$, Cu_2Se, CuBr, ZnSe, AgBr, $CuSeO_4 \cdot 5H_2O$, $CuHAsO_3$, and $Cu(AsO_4)_2 \cdot 4H_2O$ have been investigated with a focusing transmission spectrograph. The structures of two elements in the same ionic crystal lattice are not identical, and some are different even at energy distances of 150 volts from the main edge. Some factors other than crystal structure alone are shown to influence the fine structure.

INTRODUCTION

WHEN atoms are grouped together in a crystal lattice, energy zones, characteristic of the crystal as a whole and extending sometimes several hundred volts out beyond the ordinary atomic optical levels, are formed whose existence is demonstrated by extended fine structure of the Kronig[1] type to be found on the short wave-length side of x-ray absorption edges. Secondary absorption maxima occur when electrons are ejected into outer permitted zones.

[1] R. de L. Kronig, Zeits. f. Physik **75**, 191 (1932).

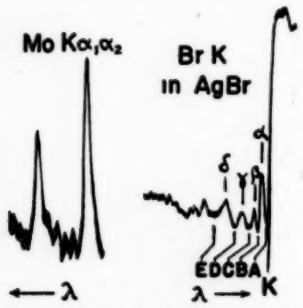

FIG. 1. Mo $K\alpha_1\alpha_2$ doublet (λ decreasing to the right) —Br K edge in the photographic emulsion (λ decreasing to the left).

Since these zones are characteristic of the crystal lattice, two different elements in the same crystal should have identical fine structures. This deduction has been verified for a few alloys (*viz.* Zn and Cu in brass[2]). However, it is not true in the case of some ionic crystal lattices. The fine structures of: Ca and S in CaS,[3] K and Cl in KCl[4] and $KClO_3$, Ca and Fe in (Ca, Mg, Fe)CO_3,[5] Ca and Ti in (Ca, Si, TiO_5) and Fe and Cr in (Fe, Cr)[(Cr, Fe)O_2]$_2$ all differ significantly and sometimes completely. In no case, however, could the structures for both edges be followed out more than 30 volts from the main edge and it has been supposed that further from the edge the structures would be similar. Kronig[6] has attempted to explain the differences observed for ionic crystals as being caused by the presence of dissimilar electric fields around anion and cation which give rise to different probabilities of transition from the K state for the two ions. This explanation is only a qualitative one and will remain so until theory is supplemented by more experimental work.

[2] D. Coster and R. Smoluchowski, Physica **2**, 1 (1935).
[3] G. P. Brewington, Phys. Rev. **46**, 861 (1934).
[4] D. Coster and G. H. Klamer, Physica **1**, 145 (1934).
[5] V. P. Barton and G. A. Lindsay, Phys. Rev. **46**, 362 (1934).
[6] R. de L. Kronig, Physik. Zeits. **36**, 729 (1935).

PURPOSE

It was thought worth while to extend the meager experimental data so far available on ionic crystals to include a comparison of the K-absorption fine structures of two elements in the same compound for those crystals containing elements of higher atomic number than the ones cited above. Available crystals containing elements from Cu to Sr were chosen for the tests. It was suggested to the author that it would be important in this connection to include some homopolar (non-ionic) crystals in this study.

EXPERIMENTAL

The curved crystal focusing spectrograph already described[7] was used. Crystals of mica 0.15–0.30 mm thick, oriented with the direction containing the two optical axes parallel to the generatrix of the focal cylinder, have given good results. More recently a quartz crystal 0.20 mm thick has proved even better. It is a laborious

[7] S. T. Stephenson, Rev. Sci. Inst. **10**, 45 (1939). The slit and ionization chamber there described are, in the present work, replaced by the conventional photographic film.

TABLE I. *Absorption fine structure. Absorption maxima A, B, etc., minima α, β, etc., distances measured in volts from the center of the K edge.*

EDGE	LATTICE	A	α	B	β	C	γ	D	δ
				Ionic Crystals					
Br in AgBr	Cubic	4	13	20	29	37	50	60	80
Rb in RbBr	Cubic	11	18	26	46	58(?)			
Br in RbBr	Cubic	9	19	32	49	62	104	137(?)	
Sr in $SrBr_2$	Cubic	17	29	49	75	101	138(?)		
Br in $SrBr_2$	Cubic	9.5	17	31	47	62			
Cu and Se in Cu_2Se	Cubic			No repeatable fine structure					
Cu in $CuSeO_4 \cdot 5H_2O$	Triclinic	13	34	68	97	128	160(?)		
Se in $CuSeO_4 \cdot 5H_2O$	Triclinic	12	50	100	150(?)				
Cu in $CuHAsO_3$	(?)	12	32	62	91				
As in $CuHAsO_3$	(?)	23	52	90	130	163			
Cu in $Cu(AsO_4)_2 \cdot 4H_2O$	(?)	14	31	60					
As in $Cu(AsO_4)_2 \cdot 4H_2O$	(?)	21	53	93	133	157			
				Homopolar Crystals					
Cu and Br in CuBr	Cubic			No repeatable fine structure					
Se in ZnSe	Cubic			No repeatable fine structure					

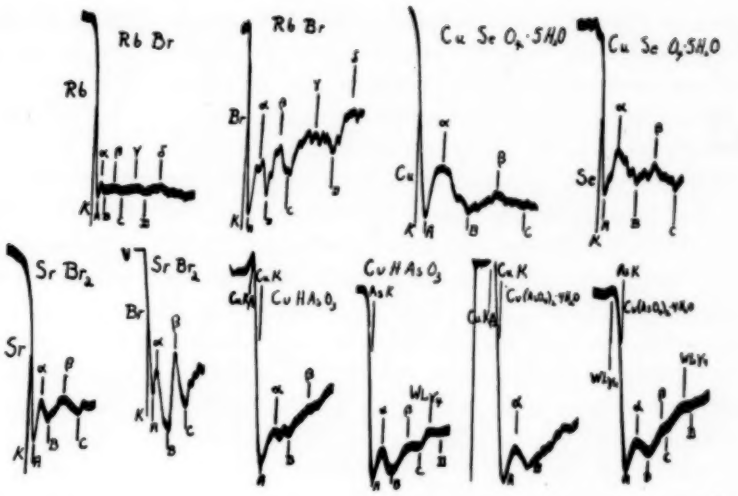

FIG. 2. K edges of Rb and Br in RbBr, Cu and Se in $CuSeO_4 \cdot 5H_2O$, Sr and Br in $SrBr_2$, and Cu and As in $CuHAsO_3$ and $Cu(AsO_4)_2 \cdot 4H_2O$ (λ decreasing to the right).

procedure to prepare a thin quartz plate of proper orientation from a large quartz crystal. A suggestion which saved the author much time and may be of general interest was that quartz crystals already cut for use in radiofrequency control might be quite suitable for this work. Accordingly, a Y cut commercial radio crystal about 0.60 mm thick was ground down to 0.20 mm thickness with FF carborundum. This crystal gave doubled lines.[8] After etching for 16 hours in dilute (about 30 percent) hydrofluoric acid nice sharp single lines were produced. The first microphotometer curve in Fig. 1 illustrates the Mo $K\alpha_1\alpha_2$ doublet obtained with this crystal. Mo $K\alpha_1$ has a half-width at half-maximum (measured at the same height as the peak of $K\alpha_2$) of 0.20 x.u. showing adequate resolution. A metal x-ray tube with either a tungsten or a molybdenum target was used at 28,000 volts peak (full wave rectification without condensers) and 10–50 milliamperes. An aluminum foil about 0.001 inch thick served as a window. Exposures were from ten to one hundred hours on regular x-ray films or plates. The absorbers were prepared by sifting the powdered compound onto cigarette papers coated with castor oil and were placed close to the curved crystal and between this crystal and the film.

RESULTS AND DISCUSSION

Representative microphotometer traces are shown in the figures. At least two different exposures were made in every case and each film or plate was microphotometered at least three times. Also blanks of the background were taken to eliminate any variations caused by the instrument. It was found in this way that the peak α in the arsenic compounds is partly affected by an unidentified weak line while all structure beyond C for these compounds is masked by $WL\gamma_4$.

Since the Br edges of the different absorbers might be affected by the AgBr of the photographic emulsion, it was necessary to examine the Br K-absorption edge recorded in the emulsion itself when no absorbers were present. A study of the structure of this edge shows that it does not affect the results for the Br edges of the other absorbers. A typical curve is shown (inverted) in Fig. 1. The resolution is sufficient to give more detailed extended structure than has been observed before.[9] The close-in structure A, α, and B agrees with that previously observed with a double crystal spectrometer.[10] The fact that the fine structure is so pronounced relative to the main edge may find its explanation in the energy zone theory of photographic action.[11] Whether or not a quantum is absorbed depends on whether an electron, after absorption of the quantum and ejection, would find itself in an allowed energy zone. If the electron can enter an allowed energy zone, it absorbs the quantum

[8] F. R. Hirsh and J. W. M. DuMond, Phys. Rev. **54**, 789 (1938).

[9] J. D. Hanawalt, Phys. Rev. **37**, 715 (1931); A. Sandstrom and E. Carlsson, Zeits. f. Physik **80**, 597 (1933).

[10] S. T. Stephenson, Phys. Rev. **50**, 790 (1936).

[11] J. H. Webb, J. Opt. Soc. Am. **26**, 367 (1936).

and is free to travel through the lattice to be trapped by an impurity and thus to contribute to the formation of a development center aiding photographic action. If the electron cannot enter a permitted zone, the quantum is not absorbed. Therefore, not only are there differences in the actual absorption of quanta by the AgBr in the emulsion for allowed and forbidden zones, giving rise to fine structure in the same fashion as for all other crystals, but those electrons going to permitted zones in the emulsion are very effective in producing development centers aiding photographic action and enhancing the absorption maxima and giving rise to more pronounced fine structure.

The results for crystals with ionic binding are illustrated in Fig. 2. It is apparent from an examination of these curves and the data in Table I that two elements in the same ionic crystal do not have identical structures in some crystals ($SrBr_2$, $CuSeO_4 \cdot 5H_2O$, $CuHAsO_3$, and $Cu(AsO_4)_2 \cdot 4H_2O$). These results differ from previous work[3-6] in two significant ways: First, the crystals have elements of higher atomic number than those heretofore examined; second, the structure differences are observable much farther from the main edge—for example, the structures of Cu and Se in $CuSeO_4 \cdot 5H_2O$ are dissimilar at least as far out as 150 volts from the main edge.

Coster and Klamer[4] emphasized that differences in structure for the two elements K and Cl in $KClO_3$ would be expected not only because of the difference in charge of anion and cation but also because of the fact that the K and Cl ions have totally different surroundings in the lattice. The same thing can be said of the two different ions in these crystals, $SrBr_2$, $CuSeO_4 \cdot 5H_2O$, $CuHAsO_3$, and $Cu(AsO_4)_2 \cdot 4H_2O$; their surroundings are different in every case and therefore differences in structure should be expected. The surprising feature about the results is that the structure differs even so far from the edge as 150 volts, for it has been supposed by most workers that the structures would be similar in position beyond about 50 volts from the edge.

The case of RbBr is interesting because it is the one ionic crystal for which significant differences in structure positions do not appear and it is the one crystal of those examined in which each ion would have similar surroundings in the lattice; also the outer electron shells for RbBr should be complete. Therefore, one would expect the least differences in structure in this crystal for its two edges, in agreement with observation.

In order to compare structures of two elements in the same compound unaffected by ionic charges, the simple homopolar[12] cubic compounds CuBr and ZnSe were studied. Unfortunately no repeatable structure could be observed although much time was spent photographing CuBr with varying absorber thicknesses under carefully controlled conditions. One can only come to the very unprofitable conclusion that Cu and Br in CuBr are similar, at least, in not showing any structure.

A comparison of the structure positions for the Cu edges in $CuSeO_4 \cdot 5H_2O$, $CuHAsO_3$, and $Cu(AsO_4)_2 \cdot 4H_2O$ shows them to be quite similar. The same result is noted if one compares the Br edges of RbBr and $SrBr_2$ or the As edges of $CuHAsO_3$ and $Cu(AsO_4)_2 \cdot 4H_2O$.

In conclusion, these results serve to emphasize the growing list of experimental data pointing to the fact that, although the crystal lattice and its energy zones are a factor affecting fine structure in ionic crystals, there are other factors of importance, for example, the ionic charge and the immediate surroundings of the ion from which the electron was ejected. These factors seem, from the present work, to be effective even further than 100 volts from the main edge.

[12] W. Hume-Rothery, *The Metallic State* (Oxford University Press, 1931), p. 334.

Note on Possible Kronig Fine Structure in X-Ray Emission Spectra*

S. T. STEPHENSON
State College of Washington, Pullman, Washington
(Received August 26, 1940)

Weak copper emission bands are observed extending 34 x.u. out on the short wave-length side of Cu $K\beta_2$. A comparison with Kronig K-absorption fine structure for copper shows that these emission bands are actually caused by absorption of the x-rays while emerging from the copper target.

INTRODUCTION

DURING the course of the experiments described in the previous paper[1] the K-absorption edge and structure of a thin copper absorbing screen was obtained as a check on the performance of the apparatus. The extended structure exhibited by copper is very pronounced and has been the subject of much study. (The excellent agreement between the results obtained here and those of Swedenborg and Claesson[2] shows how accurately this structure may now be measured. Compare columns 1 and 2 of Table I.) It occurred to the author that it might be worth while to search for emission structure from a copper target, of shorter wave-length than the absorption edge and in the same region as that in which this Kronig type absorption structure is found, because of the following considerations. In absorption an absorption maximum corresponds to a permitted energy zone for the ejected electron. In emission one could expect that electrons already in these permitted zones, normally unoccupied, might fall back to a vacant K level giving rise to an emission maximum. For this to be possible one would have to have: first, vacant K levels caused by electron bombardment of the copper target; second, electrons in the higher permitted energy zones of the copper crystal lattice caused again by the continual electron bombardment of the copper target; and third, transition probabilities which allow this type of transition. Cauchois[3] and Hayasi[4] have reported emission bands for Cu and Ni which might be explained by these considerations.

PROCEDURE AND RESULTS

The apparatus has been described in the preceding paper. For the copper absorption experiments a tungsten target was used with a copper foil absorber 12μ thick.** For the copper emission experiments a copper target was used with the x-rays coming off at an angle of about 20° with the plane of the target face. The results obtained are illustrated by the microphotometer traces of Fig. 1 (curve 1 is absorption and curve 2 is emission) and the data in columns 2 and 3 of

TABLE I. *Copper absorption and emission fine structure. Distances listed in x.u. from* Cu $K\beta_2$.

PEAKS OR VALLEYS	ABSORPTION		EMISSION
	OTHER AUTHORS[3]	PRESENT	PRESENT
α	7	5.5	6
β	9	10.5	11
γ	19	18.5	18
δ	28	28	29(?)
ϵ	40	41	
ζ	54	55	
A	5	3.5	4.5
B	8	7.5	8
C	14	14	14
D	23	23	22
E	35	34	34(?)
F	48	47	
G	62	62	

** Some of the plates showed more marked absorption structure than that illustrated in Fig. 1, curve 1. Curve 1 was chosen for illustration, however, because it was taken with the same positioning and dispersion as curve 2, thus facilitating comparison between the two. (The tungsten target consisted of a tungsten button sunk in the end of a hollow copper rod to facilitate cooling. Some electrons strike the sides of the rod and give rise to weak copper emission which is not strong enough to affect results in the region on the short wave-length side of the copper absorption edge. Curve 1 is a trace of a twenty-five-hour exposure and this copper emission was sufficient, in this time, to give the Cu $K\beta_1$ line whose base is observed.)

* S. T. Stephenson, Phys. Rev. **57**, 353A (1940).
[1] S. T. Stephenson, Phys. Rev. **57**, 873 (1940).
[2] H. Swedenborg and M. Claesson, Ann. d. Physik **28**, 159 (1937).
[3] Y. Cauchois, Comptes rendus **201**, 1359 (1935).
[4] T. Hayasi, Sci. Rep. Tohoku **25**, 785 (1936–37).

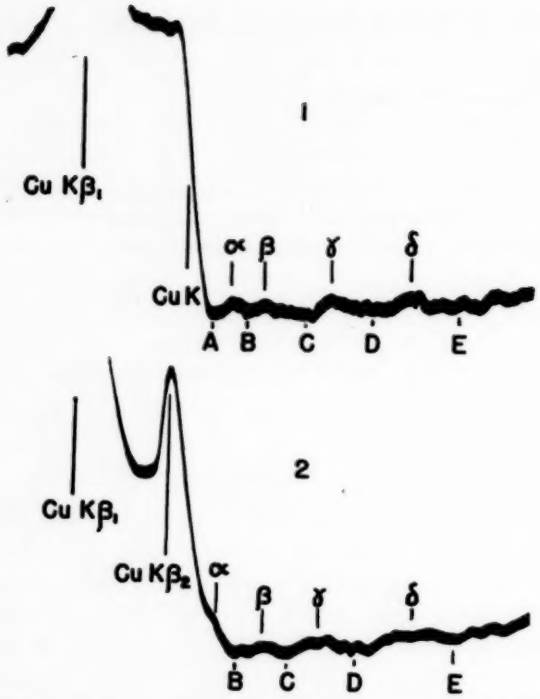

FIG. 1. Curve 1, copper K absorption with 12μ Cu foil and W target (25-hr. exposure). Curve 2, copper K emission with Cu target and no absorber (70-hr. exposure).

Table I. The emission structure on several of the films was quite visible to the unaided eye. This structure did not appear when other targets were substituted in the tube and therefore must have its origin in the copper target.

DISCUSSION

If the structure from the copper target is caused by excited lattice electrons falling into a vacant K level as postulated in the Introduction above, then the emission maxima (peaks) of curve 2 should have the same wave-length as the absorption maxima (valleys) of curve 1 and similarly the valleys of curve 2 should correspond to the peaks of curve 1. A comparison of the curves and of the data (columns 2 and 3 of Table I) indicates that this is not true. Rather the peaks and valleys for the absorption curve and for the emission curve come at the same places within experimental error (except perhaps for A and α, the closest structure[8]). This may be taken as evidence that the structure observed from the copper target is self-absorption of the Kronig type in the target itself, brought about as the x-rays produced beneath the surface of the target pass through a thin layer of copper before emerging.

It must be concluded that the observed structure is caused by an absorption process and not an emission process and that the considerations discussed in the Introduction do not lead to emission bands strong enough to be observed in this experiment. Probably the difficulty is that there are too few electrons in the upper lattice levels caused by the target bombardment. This result is considered important because others have observed some fine structure bands in the emission spectra of Cu and Ni and have speculated as to their origin. Cauchois[3] mentions a series of soft bands extending to the short wave-length side of Cu $K\beta_2$ and a possible conduction electron origin of these bands. She gives no curves or data to indicate the exact position or extent of this structure. Hayasi[3] gives curves and data for emission structure for copper extending out 12 x.u. to the short wave-length side of Cu $K\beta_2$. He ascribes this structure to double electron jumps: one electron jumping from an optical level to a K level and another between two allowed lattice levels in the crystal. From the present work it seems probable, however, that self-absorption accounts for the structure (except perhaps that within about 6 x.u. of Cu $K\beta_2$) observed by both of these authors.

[8] The region within 4 x.u. of Cu $K\beta_2$ has been examined at high resolution with a double crystal spectrometer (Beeman and Friedman, Phys. Rev. **56**, 392 (1939)) and showed emission structure caused by electrons in the lower permitted zones in the Cu lattice which are normally filled.

Isotope Shift in Boron

JOHN P. VINTI
Worcester Polytechnic Institute, Worcester, Massachusetts
(Received September 7, 1940)

Mrozowski's microphotometer curves for the lines λ2497, 2498 of B I due to $2^2P_{\frac{1}{2},1\frac{1}{2}}-3^2S_{\frac{1}{2}}$ and λ3451 of B II due to $(2s)(2p)\,{}^1P_1-(2p)^2\,{}^1D_2$ showed asymmetries which he resolved into isotope shifts arising from the isotopes 10 and 11. Subtraction of the corresponding normal shift from each of his observed values leads to observed specific shifts of -0.373 cm^{-1} for λ2497, -0.366 cm^{-1} for λ2498, and $+0.734$ cm^{-1} for λ3451. The present note gives a calculation of these specific shifts with the aid of Morse, Young, Haurwitz wave functions. The results are -0.3665 cm^{-1} for either member of λ2497, 2498 of B I and $+0.566$ cm^{-1} for λ3451 of B II. Reasons are suggested why the agreement with experiment is better in the case of the B I lines than in the case of the B II line, and also why the present calculation for the B I lines agrees better than that due to Opechowski and DeVries, who calculated -0.33 cm^{-1} for λ2497, 2498. The possible spread due to nuclear spin is estimated with the use of triplet separations and Morse, Young, Haurwitz functions and found to be of the order 0.03 cm^{-1} in each case, thus explaining on the basis of smallness the absence of nuclear spin h.f.s. in Mrozowski's plates.

MROZOWSKI[1] has recently investigated with high resolving power apparatus the boron spectrum excited in a hollow cathode discharge. Photometric investigation of the doublet lines λ2497 and λ2498 of B I, due to $2^2P_{\frac{1}{2}}-3^2S_{\frac{1}{2}}$ and $2^2P_{1\frac{1}{2}}-3^2S_{\frac{1}{2}}$, respectively, and of the line λ3451 of B II due to $(2s)(2p)^1P_1-(2p)^2\,{}^1D_2$ showed in each case an asymmetry. This asymmetry Mrozowski interpreted as indication of an isotope shift. Resolution of the photometric curve of each line into two symmetrical components, each of the typical shape due to Doppler effect, led to values for the abundance ratio B^{11}/B^{10} in good agreement with mass-spectrograph values. Letting $\Delta\nu\equiv\nu_{11}-\nu_{10}$, we may summarize his results as follows:

B I, λ2497: $\Delta\nu=-0.175\pm0.012$ cm^{-1},
B I, λ2498: $\Delta\nu=-0.168\pm0.010$ cm^{-1},
B II, λ3451: $\Delta\nu=\ 0.877\pm0.004$ cm^{-1}.

There was no indication of h.f.s. splitting due to nuclear spin.

It is the purpose of this note to give a theoretical calculation of the expected isotope shifts due to nuclear motion and an estimate of the possible spreads due to nuclear spin. The notation of the author's paper on isotope shift in Mg I[2] will be followed. Thus for the line $A\rightarrow B$, $\Delta\nu=(\Delta\nu)_N+(\Delta\nu)_\sigma$, where the normal shift $(\Delta\nu)_N=(1/11-1/10)1838^{-1}(\tau_A-\tau_B)$, where, e.g., τ_A is the term value in cm^{-1} of level A, and the specific shift $(\Delta\nu)_\sigma=-(1/11-1/10)1838^{-1}\,2\ \mathrm{Ry}(k_A-k_B)=1.0855(k_A-k_B)$ cm^{-1}. From the observed term values we have, to sufficient accuracy, $(\Delta\nu)_N=0.198$ cm^{-1} for either λ2497 or λ2498 of B I, and $(\Delta\nu)_N=0.143$ cm^{-1} for λ3451 of B II. These values lead to specific shifts of -0.373 cm^{-1} for λ2497, -0.366 cm^{-1} for λ2498, and 0.734 cm^{-1} for λ3451.

For the doublet λ2497, 2498 of B I, the level A is $(1s)^2(2s)^23s\,{}^2S_{\frac{1}{2}}$ and B is $(1s)^2(2s)^22p\,{}^2P_{\frac{1}{2},1\frac{1}{2}}$. From reference 2, Eqs. (1), (4), (5), and the relation $\bar\sigma\equiv-2(m/M)$ Ry k, we obtain:

$$k_A=0$$
$$k_B=\tfrac{1}{3}[J^2(2p,\,1s)+J^2(2p,\,2s)]. \qquad (1)$$

In deducing (1) the fact has been used that it is valid to calculate $\bar\sigma$ in the SLM_LM_S representation, in which the wave functions in the above simple cases are single determinants corresponding, respectively, to the configurations $1s^+1s^-2s^+2s^-3s^\pm$ and $1s^+1s^-2s^+2s^-2p^\pm_m$. In evaluating the J's the variational radial functions of Morse, Young, and Haurwitz[3] will be used. Use of the parameters for $(1s)^2(2s)^22p\,{}^2P$ as given by them leads, after some simple integrations, to $J^2(2p,\,1s)=0.7590$ and $J^2(2p,\,2s)=0.2539$,

[1] S. Mrozowski, Zeits. f. Physik **112**, 223 (1939).
[2] J. P. Vinti, Phys. Rev. **56**, 1120 (1939).
[3] P. M. Morse, L. A. Young, and E. S. Haurwitz, Phys. Rev. **48**, 948 (1935). This paper is subsequently referred to as MYH; the radial factors of the MYH functions are written explicitly in reference 2.

with the result that $k_B=0.3376$, so that $k_A-k_B=-0.3376$ and $(\Delta\nu)_s=-0.3665$ cm^{-1}. Thus for each member of the doublet line $(1s)^2(2s)^2 3s\ ^2S \rightarrow (1s)^2(2s)^2 2p\ ^2P$ there results the calculated specific shift -0.3665 cm^{-1}, as against Mrozowski's observed values of -0.373 cm^{-1} for λ2497 and -0.366 cm^{-1} for λ2498. At this point it should be mentioned that a calculation by Opechowski and DeVries[4] of this shift gave a value -0.33 cm^{-1}. Their calculation was carried out with the aid of Hartree radial functions obtained by Brown, Bartlett, and Dunn.[5] Thus their radial functions correspond to the solution of a variational problem in which the trial function has as much flexibility as is consistent with the requirement that it be a product of single-electron wave functions. The MYH functions, on the other hand, although not so flexible as the Hartree functions, take proper symmetry into account at the very start. This fact may account for the better agreement with observation obtained with the use of the MYH functions.

For λ3451 of B II the transition is $(1s)^2(2p)^2\ ^1D_2 \rightarrow (2s)(2p)^1P_1$. For $(1s)^2(2p)^2\ ^1D_2$ we use the fact that $\bar{\sigma}$ is the same in the SLM_LM_S representation as in the $SLJM_J$ representation, and that its value in the SLM_LM_S representation is independent of M_S or M_L. We may then compute its value for $M_S=0$, $M_L=2$, for which the wave function is the single determinant corresponding to the configuration $1s^+1s^-2p^+_1 2p^-_1$. Then from Eqs. (1), (4), and (5) of reference 2 and the relation connecting $\bar{\sigma}$ and k, we have:

$$k_A=\tfrac{2}{3}J^2(2p,\ 1s), \tag{2}$$

where the subscript A refers to the initial level $(2p)^2\ ^1D_2$. For the final level $B\equiv(1s)^2(2s)(2p)^1P_1$ we make use of the diagonal sum rule, in the manner of reference 2. In the use of this method we have to assume that a given single orbit function, e.g. $2p$, is the same for $(2s)(2p)^1P$ and $(2s)(2p)^3P$; in the final formulas for the singlet and triplet, however, we may use the proper (different) values of the parameters as found by MYH. This procedure is justified by the fact that if we actually wrote the wave function in each case as the proper linear combination of determinants and then calculated $\bar{\sigma}$, we should obtain essentially the same formulas as would be given by the method of sums, the only difference being that the correct (different) parameters would appear in the final formulas. The method of sums here goes very much as it does for $(3s)(3p)$ of Mg I, for which the process was given in reference 2, p. 1124; thus for the triplet:

$$\bar{\sigma}_t=-\tfrac{2}{3}(m/M)\ \text{Ry}\ [J^2(2p,\ 1s)+J^2(2p,\ 2s)] \tag{3}$$

and for the sum for singlet and triplet:

$$\bar{\sigma}_t+\bar{\sigma}_s=-(4/3)(m/M)\ \text{Ry}\ J^2(2p,\ 1s). \tag{4}$$

By difference, we obtain:

$$\bar{\sigma}_s=-\tfrac{2}{3}(m/M)\ \text{Ry}\ [J^2(2p,\ 1s)-J^2(2p,\ 2s)], \tag{5}$$

so that

$$k_B=\tfrac{1}{3}[J^2(2p,\ 1s)-J^2(2p,\ 2s)]. \tag{6}$$

Using in Eq. (2) the MYH parameters for $(2p)^2\ ^1D$ and in Eq. (6) the MYH parameters for $(2s)(2p)^1P$, we find after some simple integrations that $k_A=0.8019$ and $k_B=0.2804$. These values give $(\Delta\nu)_s=+0.566$ cm^{-1}, as compared with Mrozowski's observed value of $+0.734$ cm^{-1}, a discrepancy of 23 percent. The fact that the agreement is less satisfactory for the B II line than for the B I lines may possibly be due to the MYH functions. Examination of the term values given by the B I and B II functions of MYH shows that the wave functions for B I are probably much better than those for B II, MYH finding indeed that their term value discrepancies are always much less when there is only one electron in the outermost shell than when there are two or more.

It still remains to be explained why no h.f.s. due to nuclear spin is observed in either case, since B^{10} and B^{11} both have nuclear magnetic moments. The obvious answer would be that the spread due to nuclear spin is too small to be resolved; this indeed turns out to be the case. The spread due to nuclear spin can be estimated for the line $3s\ ^2S_{\frac{1}{2}} \rightarrow 2p\ ^2P_j$ of B I; for B^{11} it is of the order 0.034 cm^{-1} for $j=\frac{1}{2}$, 0.022 cm^{-1} for $j=\frac{3}{2}$; for B^{10} it would be still smaller. For $(2p)^2\ ^1D_2 \rightarrow (2s)(2p)^1P_1$ of B II it comes out 0.031 cm^{-1} for B^{11} and smaller for B^{10}. Since shifts

[4] W. Opechowski and D. A. DeVries, Physica [6] 9, 913 (1939).
[5] F. W. Brown, J. H. Bartlett, Jr., and C. G. Dunn, Phys. Rev. 44, 296 (1933).

even of 0.7 cm^{-1} were not actually resolved by Mrozowski, but gave rise only to asymmetries in the microphotometer curves, it is clear that the splitting due to nuclear spin would be entirely unobservable in Mrozowski's plates.

Since Opechowski and DeVries[4] have indicated the method of estimating the nuclear spin spread for the doublet line of B I, we shall outline only the somewhat less obvious estimate for the B II line. We use the notation and methods of a paper by Goudsmit,[6] in which a or b denotes, respectively, the interaction parameter in the sense of Goudsmit's Eq. (3) for a single p electron or a single s electron with the nuclear magnetic moment, and $A(J)$ is the coupling coefficient occurring in the expression $A\,\mathbf{I}\cdot\mathbf{J}$ for the interaction energy of the electrons with the nucleus, where $\mathbf{I}$ is the nuclear spin and $\mathbf{J}$ the total electronic angular momentum. The single electron parameters a or b are given by the expression

$$\mathrm{Ry}\,\alpha^2 g(I)1838^{-1}\langle 1/r^3\rangle_{Av}=(5.82)1838^{-1}g(I)\langle 1/r^3\rangle_{Av}\ \mathrm{cm}^{-1}, \quad (7)$$

where Ry is the Rydberg energy, α the fine structure constant, $g(I)$ the nuclear gyromagnetic ratio, and r is expressed in units of the Bohr radius. For a hydrogenic nonpenetrating orbit $\langle 1/r^3\rangle_{Av}$ has the value $Z^{*3}/n^3l(l+\frac{1}{2})(l+1)$, Z^* being the effective nuclear charge.

For $(2s)(2p)$ we denote the singlet A by $A'(1)$ and the triplet A's for $J=1$ and 2 by $A(1)$ and $A(2)$. Then the method of sums gives:

$$\begin{aligned} A(2)&=\tfrac{3}{4}a+\tfrac{1}{4}b,\\ A(1)+A'(1)&=2a+\tfrac{1}{4}b. \end{aligned} \quad (8)$$

Applying now the method of sums to the interaction energy of the orbital magnetic moments only with the nucleus and then to the interaction energy of the spin magnetic moments only with the nucleus, we find:

$$\begin{aligned} A_{\mathrm{orb}}(2)&=\tfrac{1}{2}a,\\ A_{\mathrm{orb}}(1)+A'_{\mathrm{orb}}(1)&=1\tfrac{1}{2}a, \end{aligned} \quad (9)$$

$$\begin{aligned} A_{\mathrm{sp}}(2)&=-(1/10)a+\tfrac{1}{4}b,\\ A_{\mathrm{sp}}(1)+A'_{\mathrm{sp}}(1)&=\tfrac{1}{2}a+\tfrac{1}{4}b, \end{aligned} \quad (10)$$

where the meaning of the symbols is evident, so $A(2)=A_{\mathrm{orb}}(2)+A_{\mathrm{sp}}(2)$, etc. If we now apply Goudsmit's Eq. (33) for the $A(J)$ of a multiplet, we find:

$$\begin{aligned} A(2)&=\tfrac{1}{2}\lambda-\tfrac{1}{2}\sigma+\tfrac{1}{2}\beta,\\ A(1)&=\tfrac{1}{2}\lambda+\sigma+\tfrac{1}{2}\beta,\\ A'(1)&=\lambda. \end{aligned} \quad (11)$$

Here λ, σ, and β denote, respectively, parameters for interaction with the nucleus of the total orbital angular momentum $\mathbf{L}$, of the total spin $\mathbf{S}$, and of the spin of an "unbalanced" s electron such as occurs in sp. It is worth mention that Goudsmit's Eq. (33) can be derived very easily for all the special cases that are here considered. Equations (11) can now be decomposed as follows:

$$\begin{aligned} A_{\mathrm{orb}}(2)&=\tfrac{1}{2}\lambda, & A_{\mathrm{sp}}(2)&=-\tfrac{1}{2}\sigma+\tfrac{1}{2}\beta,\\ A_{\mathrm{orb}}(1)&=\tfrac{1}{2}\lambda, & A_{\mathrm{sp}}(1)&=\sigma+\tfrac{1}{2}\beta,\\ A'_{\mathrm{orb}}(1)&=\lambda, & A'_{\mathrm{sp}}(1)&=0. \end{aligned} \quad (12)$$

Comparison of Eqs. (9), (10), and (12) leads to the relations $\lambda=a$, $\sigma=\frac{1}{2}a$, $\beta=\frac{1}{2}b$; thus the desired $A'(1)=a$. For $(2s)(2p)\,{}^1P_1$, therefore, we need only the p parameter a.

For $(2p)^2$ we denote the A of the ${}^1D_2$ by $A'(2)$ and the A's of the ${}^3P$ by $A(1)$ and $A(2)$. Then, from the method of sums:

$$\begin{aligned} A(2)+A'(2)&=(8/5)a,\\ A(1)&=0, \end{aligned} \quad (13)$$

and from the general multiplet formula:

$$\begin{aligned} A'(2)&=\lambda,\\ A(1)&=\tfrac{1}{2}\lambda+\sigma,\\ A(2)&=\tfrac{1}{2}\lambda-\tfrac{1}{2}\sigma. \end{aligned} \quad (14)$$

Comparison of Eqs. (13) and (14) gives $\lambda=a$ and $\sigma=-a/2$, so that the desired $A'(2)=a$.

For $(2p)^2\,{}^1D_2$ the hydrogenic expression for $\langle 1/r^3\rangle_{Av}$ gives $a=5.82(Z^{*3}/24)g(I)/1838\ \mathrm{cm}^{-1}$. From the work of Millman, Kusch, and Rabi,[7] $g(I)$ is known to have the value 1.788 for B^{11}; also Z^* may be estimated from the triplet separations for $(2p)^2\,{}^3P$ to be 2.80.[8] These values lead to $a=0.0052\ \mathrm{cm}^{-1}$ for $(2p)^2\,{}^1D_2$. For $(2s)(2p)\ {}^1P_1$ we take Z^* from the triplet separation for $(2s)(2p)\ {}^3P$, *viz.* 2.82,[8] and obtain $a=0.0053\ \mathrm{cm}^{-1}$. The $\langle 1/r^3\rangle_{Av}$ values may also be estimated from the MYH functions: for $(2p)^2\,{}^1D_2$ one finds $(\langle 1/r^3\rangle_{Av})_{2p}=\frac{1}{3}(1.385)^3=0.883$, leading to $a=0.0050$; for $(2s)(2p)\ {}^1P$ one finds $(\langle 1/r^3\rangle_{Av})_{2p}=\frac{1}{3}(1.335)^3=0.793$, leading to $a=0.0045$. The two methods check about as well as could be expected;[9] to obtain an upper limit for the spread in each case we take the slightly larger values of a obtained from the Z^*. Then since $A=a$ in each case, we have $A=0.0052\ \mathrm{cm}^{-1}$ for $(2p)^2\,{}^1D_2$ and $A=0.0053\ \mathrm{cm}^{-1}$ for $(2s)(2p)\ {}^1P_1$. Each hyperfine level is then given by

$$\delta\nu=A/2[F(F+1)-J(J+1)-I(I+1)]; \quad (15)$$

where F is the hyperfine quantum number and I is the nuclear spin, for which the value $1\frac{1}{2}$ has been suggested[7] as the most reasonable value for B^{11}. Use of Eq. (15) for each level plus the selection rule leads to the hyperfine components; the spread is then given by the sum of the absolute values of the largest positive and largest negative $\delta\nu$'s. The result is $(0.0078+0.0232)\ \mathrm{cm}^{-1}=0.031\ \mathrm{cm}^{-1}$.

[6] S. Goudsmit, Phys. Rev. **37**, 663 (1931).

[7] S. Millman, P. Kusch, and I. I. Rabi, Phys. Rev. **56**, 165 (1939).

[8] L. Pauling and S. Goudsmit *The Structure of Line Spectra* (McGraw-Hill, 1930), p. 101.

[9] For the level $2p\ {}^3P$ of B I an estimate of $(\langle 1/r^3\rangle_{Av})_{2p}$ from MYH functions leads to a value of A which is 10 percent larger than that estimated from doublet separations (the method of Opechowski and DeVries).

A Theorem on Nuclear Motion in Atomic Spectra

JOHN P. VINTI
Worcester Polytechnic Institute, Worcester, Massachusetts
(Received September 7, 1940)

A theorem is derived concerning the energy shift of an atomic level due to nuclear motion. Since the expression obtained (Eq. (12) below) does not involve derivatives, it may be useful for calculations of isotope shifts due to nuclear motion in those cases where the radial wave functions are known not as analytical expressions but only as tables of numerical values.

SUPPOSE we consider an atom of atomic number Z with n electrons, the energy operator for a fixed nucleus being H_0. Then, as shown by Hughes and Eckart,[1] the effect of nuclear motion can be expressed exactly by the addition to H_0 of a term

$$G=(2M)^{-1}(\sum_{i=1}^{n}\mathbf{p}_i)^2, \tag{1}$$

where M is the nuclear mass and $\mathbf{p}_i$ the momentum of the ith electron relative to the nucleus. The calculation of isotope shifts due to nuclear motion involves the evaluation of the quantum-mechanical average of G for each level considered. It is customary to split G into two parts N and σ,[2] where the average $\bar{N}$ of the "normal" term N can be obtained by use of the virial theorem and the energy of the given level, but where the average $\bar{\sigma}$ of the "specific" term σ must be specifically evaluated for each level of each atom by the use of wave functions. The present note is the result of an attempt to find some general method which would put the calculation of the specific effect on a par with that of the normal effect. This attempt, although not successful, led to a simple expression for G which does not involve derivatives. It may, therefore, prove useful in calculations of isotope shifts due to nuclear motion in cases where the radial wave functions are known not as analytical expressions but simply as tables of numerical values. The derivation is very much like one which can be given for the general virial theorem.

With the omission of G and spin orbit terms, the Schrödinger equation for a stationary state of an atom can be written:

$$-(h^2/8\pi^2m)\sum_{1}^{n}\nabla_k^2\psi+V\psi=E_0\psi, \tag{2}$$

where

$$V=-Ze^2\sum_{1}^{n}1/r_j+e^2/2\sum\sum_{j\neq l}1/r_{jl}. \tag{3}$$

We first derive a preliminary theorem, Eq. (7) below; m denotes the electronic mass, $\mathbf{r}_\mu$ the radius vector of the μth electron, and the subscript $_N$ quantum-mechanical averages over stationary states. To do so, we first apply the operator ∇_r to Eq. (2), form the scalar product with $\psi^*\mathbf{r}_\mu$ (where the asterisk denotes the complex conjugate), and then integrate over configuration space. We obtain:

$$-(h^2/8\pi^2m)\sum_{k=1}^{n}\int\psi^*\mathbf{r}_\mu\cdot\nabla_k^2(\nabla_r\psi)d\tau+\int\psi^*(\mathbf{r}_\mu\cdot\nabla_r V)\psi d\tau=\int\psi^*(E_0-V)\mathbf{r}_\mu\cdot\nabla_r\psi d\tau. \tag{4}$$

Some simple transformations now give:

$$\int\psi^*\mathbf{r}_\mu\cdot\nabla_k^2(\nabla_r\psi)d\tau=\int\nabla_r\psi\cdot\mathbf{r}_\mu\nabla_k^2\psi^*d\tau+2\delta_{\mu k}\int\nabla_r\psi\cdot\nabla_k\psi^*d\tau. \tag{5}$$

[1] D. S. Hughes and C. Eckart, Phys. Rev. **36**, 694 (1930).
[2] J. P. Vinti, Phys. Rev. **56**, 1120 (1939).

We now sum Eq. (5) on k from 1 to n, transform the resulting first term on the right side by Eq. (2), and integrate by parts the resulting second term on the right side. (The last step here, as in the derivation of Eq. (5), involves the rejection of a surface integral at infinity and thus restricts our proof to discrete states.) We obtain

$$\sum_{k=1}^{n}\int\psi^*\mathbf{r}_\mu\cdot\nabla_k^2(\nabla_\nu\psi)d\tau=-(8\pi^2m/h^2)\int(\mathbf{r}_\mu\cdot\nabla_\nu\psi)(E_0-V)\psi^*d\tau-2\int\psi^*\nabla_\mu\cdot\nabla_\nu\psi d\tau. \tag{6}$$

We now insert Eq. (6) into Eq. (4), cancel a term common to both sides of the resulting equation, and use $(h/2\pi i)\nabla_\mu=\mathbf{p}_\mu$. There results:

$$\langle\mathbf{p}_\mu\cdot\mathbf{p}_\nu\rangle_{Av}=m\langle\mathbf{r}_\mu\cdot\nabla_\nu V\rangle_{Av}. \tag{7}$$

From Eqs. (1) and (7) we find:

$$\bar{G}=(m/2M)\langle\sum_\mu\sum_\nu\mathbf{r}_\mu\cdot\nabla_\nu V\rangle_{Av}=(m/2M)\langle\sum_\mu\mathbf{r}_\mu\rangle\cdot\langle\sum_\nu\nabla_\nu V\rangle_{Av}. \tag{8}$$

Equation (3) gives:

$$\nabla_\nu V=Ze^2\mathbf{r}_\nu/r_\nu^3-e^2\sum_{j(\neq\nu)}\mathbf{r}_{j\nu}/r_{j\nu}^3, \tag{9}$$

so that

$$\sum_\nu\nabla_\nu V=Ze^2\sum_\nu\mathbf{r}_\nu/r_\nu^3-e^2\sum_{j\neq\nu}\sum_\nu\mathbf{r}_{j\nu}/r_{j\nu}^3. \tag{10}$$

The second term on the right side of Eq. (10) vanishes because of cancellation in pairs; physically this cancellation arises from the fact that this term is simply the sum of the interaction forces of the electrons. We now readily obtain from Eqs. (8) and (10):

$$\bar{G}=Z(e^2m/2M)\langle\sum_\mu\sum_\nu\mathbf{r}_\mu\cdot\mathbf{r}_\nu/r_\nu^3\rangle_{Av}. \tag{11}$$

With the Bohr radius a_0 and the Rydberg energy $e^2/2a_0$ as units of length and energy, respectively, we may write:

$$\bar{G}=Z(m/M)Q,\quad\text{where}\quad Q\equiv\langle\sum_\mu\sum_\nu\mathbf{r}_\mu\cdot\mathbf{r}_\nu/r_\nu^3\rangle_{Av}. \tag{12}$$

By use of the virial theorem an expression can now be written down for $\bar{N}$ as an average of a function of the coordinates, which together with Eq. (12) will lead to an expression for $\bar{\sigma}$ as a similar average. Since, however, the resulting expression for $\bar{\sigma}$ is somewhat more complicated than Eq. (12) for $\bar{G}$, the usual procedure of finding $\bar{N}$ by the virial theorem and $\bar{\sigma}$ by calculation with wave functions would not be so simple as direct evaluation of the total energy shift $\bar{G}$ from Eq. (12). Then for a line $A\rightarrow B$ the shift $\Delta\nu\equiv\nu(\mu_1)-\nu(\mu_2)$, where μ_1 and μ_2 are mass numbers of isotopes, is given by:

$$\Delta\nu=Z1838^{-1}(1/\mu_1-1/\mu_2)109740(Q_A-Q_B)\ \text{cm}^{-1}.$$

The above derivation shows that Eq. (12) will give the same value for $\bar{G}$ as will Eq. (1), provided that exact wave functions are used. In any actual calculation there may of course be a discrepancy between the values obtained by the two methods, due to inaccuracy in the wave function. One cannot say on general grounds which value will be the better when such an approximate wave function is used; agreement between the values obtained by the two methods might well serve as an additional criterion for the accuracy of a wave function.

Finally it may be remarked that in a paper published some years ago by the writer,[3] there is contained implicitly an entirely different proof of the present theorem. A comparison of Eq. (5) of that paper with the equation about one-fourth of the way down the page on p. 436 leads directly to Eq. (8) of the present paper.

[3] J. P. Vinti, Phys. Rev. **41**, 432 (1932).

Pressure Effects of Homogeneous Rubidium Vapor on Its Resonance Lines

CH'EN SHANG-YI*
Norman Bridge Laboratory of Physics, California Institute of Technology, Pasadena, California
(Received September 23, 1940)

The broadening of the resonance lines of rubidium in absorption under pressures up to 150 mm of its own homogeneous vapor was studied by means of a 21-foot grating. Under pressures below 1 mm the broadening of the lines was very symmetrical and the line contours could be described by the dispersion formula, but when the pressure was high the lines exhibited asymmetrical broadening of van der Waals type. The $^2P_{1/2}$ component showed red, while the $^2P_{3/2}$ component showed violet asymmetry. Both lines showed the proportionality of the width with N, the concentration of Rb atoms. The experimental width at half-maximum is greater than that predicted by Houston's theory by a factor of 1.5 and the width of the transition from $^2P_{3/2}$ is greater than that from $^2P_{1/2}$ by a factor of 1.6. A narrow diffuse band was observed near the shorter wave-length side of the $^2P_{1/2}$ component and a similar one near the longer wave-length side of the $^2P_{3/2}$ component.

THE development of the new corrosion resistant MgO windows[1] has made feasible many experimental researches. Using the new windows Hughes and Lloyd[2] first made an experimental study of the resonance broadening of potassium resonance lines under pressures up to 20 mm. In the present research the corresponding problem for rubidium was studied and observations were made for Rb pressures up to 150 mm under which the two broadened component lines (with a separation of 147A) began to overlap.

EXPERIMENTAL

Absorption tubes of 1.5 cm inside diameter with MgO windows on both ends were used. Three tube lengths were employed, *viz.* 15, 7.5 and 0.2 cm. The construction of the 2-mm tube is shown in Fig. 1. The tube was made of steel. A small capsule containing rubidium was placed inside the hole A, and the end of the hole was closed by a copper tap screw whose coefficient of thermal expansion was higher than that of steel. Thus the hole was always tightly closed throughout the experiment. B was an annealed copper ring which served as a gasket when the tube C was compressed onto the tube D at high temperatures. The copper ring was too hard, but had the advantage over aluminum of not alloying with rubidium.[3] The length of the absorption tube could be easily determined from the thickness of the section S.

The absorption tubes were mounted in a vacuum furnace. By means of a sylphon it was possible to move the tube C and thereby seal off the absorption tube while a vacuum was maintained in the furnace. The entire tube was heated uniformly and its temperature was kept constant within 1°C as indicated by a Chromel-Alumel thermocouple in contact with the absorption tube.

Light from a tungsten filament lamp passed through the absorption tube and was photographed in the first order of a 21-foot grating in a Rowland mounting. Eastman type 1 R plates hypersensitized with ammonia were used, the second-order violet being eliminated with a Wratten F filter. The plates were calibrated by means of two step-weakeners mounted just in front of the plate on both sides of the absorption lines.

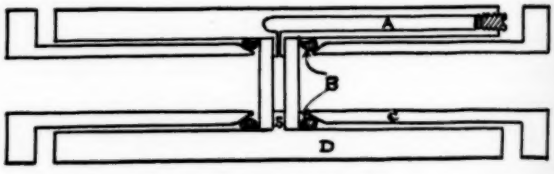

FIG. 1. The 2-mm tube.

* Research Fellow of the China Foundation for the Promotion of Education and Culture. Now at Yenching University, Peiping, China.

[1] J. Strong and R. T. Brice, J. Opt. Soc. Am. **25**, 207 (1935).

[2] D. S. Hughes and P. E. Lloyd, Phys. Rev. **52**, 1215 (1937).

[3] An aluminum ring was tried. When the tube was heated to 300°C or higher a large amount of silvery liquid alloy of rubidium and aluminum appeared and the tube gave no more absorption lines.

TABLE I. *The width at half-maximum of the two doublet components.*

Tube Length in cm x	Temperature Kelvin T	Vapor Pressure in mm P	Number of Atoms per cc N	Width at Half-Maximum ($\Delta\nu_{1/2}$) $\times 10^7$ Divided by N $(^2P_{3/2})$	$(^2P_{1/2})$	$\frac{(\Delta\nu_{1/2})(^2P_{3/2})}{(\Delta\nu_{1/2})(^2P_{1/2})}$
15.06	409	1.87×10^{-3}	4.42×10^{13}	1.84	1.41	1.3
15.06	445	1.14×10^{-2}	2.44×10^{14}	1.06	0.62	1.7
7.50	454	1.35×10^{-2}	2.88×10^{14}	1.04	0.63	1.7
7.50	491	9.80×10^{-2}	1.94×10^{15}	1.43	0.77	1.9
0.20	563	9.83×10^{-1}	1.69×10^{16}	0.72	0.42	1.7
7.50	575	1.183	1.99×10^{16}	1.51	0.84	1.8
7.50	601	2.361	3.89×10^{16}	1.09	0.60	1.8
0.20	600	2.32	3.75×10^{16}	1.06	0.61	1.7
0.20	621	3.84	5.67×10^{16}	1.19	0.79	1.5
0.20	651	7.57	1.14×10^{17}	0.76	0.54	1.4
0.20	660	9.18	1.34×10^{17}	1.80	0.63	1.7
0.20	664	9.98	1.45×10^{17}	0.52	0.36	1.4
0.20	699	19.9	2.75×10^{17}	0.29	0.19	1.5
0.20	721	29.6	3.97×10^{17}	0.16	0.12	1.3
0.20	766	62.2	7.87×10^{17}	0.11	0.09	1.2
0.20	797	98 ?	1.2×10^{18}	0.09 ?	0.07 ?	1.3
0.20	829	152 ?	1.8×10^{18}	0.07 ?	0.06 ?	1.2

The line contours were traced by a Kruss microphotometer and were compared with those given by the dispersion formula:

$$\alpha x=\frac{\rho\gamma}{2\pi\{(\delta\lambda)^2+(\gamma/2)^2\}} \tag{1}$$

in which ρ is the area under the absorption curve, γ is the width, in wave-length units, of the absorption line measured between points of half-maximum absorption coefficient, α is the absorption coefficient at wave-length $\delta\lambda$ from the central maximum, and x is the length of the absorption tube. If I/I_0 is the fraction of the light of wave-length $\lambda\pm\delta\lambda$ transmitted by the absorption tube, this yields

$$(\delta\lambda)^2=\frac{\rho\gamma\log_{10}e}{2\pi\log(I_0/I)}-\left(\frac{\gamma}{2}\right)^2. \tag{2}$$

Therefore a plot with $(\delta\lambda)^2$ as ordinate against $(\log_{10}I_0/I)^{-1}$ as abscissa is a straight line with slope $(\rho\gamma\log_{10}e)/2\pi$ and intercept $(\gamma/2)^2$. The intercept $(\gamma/2)^2$ was practically nil. However, since

$$\rho=\int_{-\infty}^{+\infty}\alpha x d(\delta\lambda)=\pi e^2\lambda_0^2Nf_{21}x/mc^2, \tag{3}$$

the width at half-maximum, γ, could be calculated from the experimentally determined slope, the number of Rb atoms per cc, N, the tube length, x and the oscillator strength f_{21} of the line components. N was found from the vapor pressure data

$$\log_{10}p=-52.23(76/T)+6.976, \tag{4}$$

where T is the temperature and p is the vapor pressure in mm. The width at half-maximum was then expressed in wave number units ($\Delta\nu_{1/2}$) by means of the relationship $\Delta\nu_{1/2}=c\gamma/\lambda^2$.

Results and Discussion

The lines were very symmetrically broadened when the vapor pressure was below about 1 mm Hg. But for plates taken when the temperature of the tube was raised to about 290°C or more, the lines exhibited more and more asymmetrical broadening of the van der Waals type, and a shadow of absorption was observed near the broadened line components.

A. Observations of the line broadening under low pressures

(*a*) *Theoretical formulas for resonance broadening.*—It is possible to compare the symmetric broadening at the lower pressures with that predicted by the theory. The Lorentz collision theory has been quantum theoretically modified by various persons, including Weisskopf[4] and Margenau and Watson.[5] The result given by Margenau and Watson is

$$\Delta\nu_l=e^2\lambda Nf_{12}/2\pi mc, \tag{5}$$

[4] V. Weisskopf, Zeits. f. Physik **75**, 287 (1932).
[5] H. Margenau and W. W. Watson, Rev. Mod. Phys. **8**, 22 (1936).

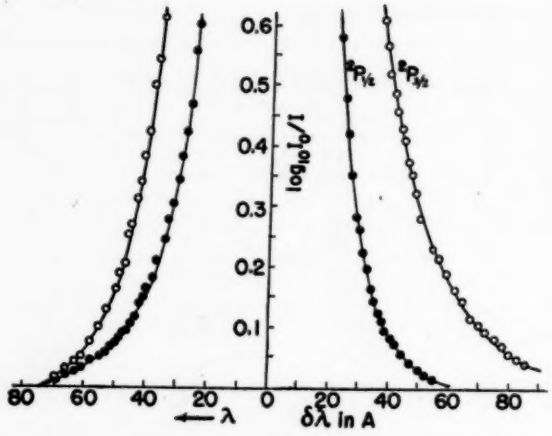

FIG. 2. The asymmetrically broadened lines. $T=766°K$; $p=62.2$ mm Hg; $x=0.196$ cm.

where f_{12} is the oscillator strength of the line in question. The numerical factor 2π is the result of a crude approximation and might be in error by as much as a factor 2.

The features of this expression that are subject to test are the dependence on N, the approximate correctness of the numerical factor, and the dependence on f_{12}. In Weisskopf's work no distinction is made between f_{12}, which is the same for both members of the doublet, and f_{21} which is twice as great for one member as for the other. The oscillator strength f_{12} is approximately $\frac{1}{3}$ in this case, and Margenau and Watson indicate clearly that f_{12} is to be used.

Another treatment of the problem, with special attention to the relative broadening of the members of a multiplet, has been given by Houston.[6] His result is

$$\Delta\nu_{\frac{1}{2}}=\frac{6^{\frac{1}{2}}S(1,2)N}{\hbar(2J_1+1)(2J_2+1)}=\frac{3\times 6^{\frac{1}{2}}}{2(2J_1+1)}\frac{e^2\lambda}{2\pi mc}Nf_{12}. \quad (6)$$

The quantity $S(1, 2)$ is the line strength as defined by Condon and Shortley,[7] while J_1 and J_2 are the inner quantum numbers of the ground and the excited states, respectively. This expression has the same dependence on N as has Eq. (5), it has a somewhat different numerical factor, and it definitely predicts that all members of a Russell-Saunders multiplet should have the same width, except for a factor equal to the ratio of the wave-lengths.

[6] W. V. Houston, Phys. Rev. **54**, 884 (1938).
[7] E. U. Condon and G. Shortley, *The Theory of Atomic Spectra* (Cambridge, 1935), p. 98.

(*b*) *Comparison of theory with experiment.*— In Table I are listed the experimental values of the width at half-maximum divided by N the number of absorbing atoms per cc. The ratios are listed separately for the two components of the resonance doublet corresponding to transitions from the $^2P_{3/2}$ and the $^2P_{1/2}$ states. In the range below 1 mm of vapor pressure, in which the lines are observed to be symmetrical and in which one may expect the theory to apply, the width at half maximum is found to be proportional to N as predicted by theory. In this range the average values of the ratio are

$$(\Delta\nu_{1/2})(^2P_{3/2})/N=1.22\times 10^{-7},$$
$$(\Delta\nu_{1/2})(^2P_{1/2})/N=0.77\times 10^{-7}.$$

In comparison Houston's formula (6) predicts the ratio

$$(\Delta\nu_{1/2})(^2P_{3/2})/N=0.65\times 10^{-7},$$
$$(\Delta\nu_{1/2})(^2P_{1/2})/N=0.66\times 10^{-7}.$$

The differences in the absolute values of the experimental and theoretical ratios are probably not greater than can be explained by the approximations used in the theoretical derivation. On the other hand, the great difference between the observed line widths of the two components at every pressure is definitely not predicted by the present theories.

B. Observational line broadening under higher pressures

When the temperature of the tube was raised to 290°C, corresponding to a Rb vapor pressure of 1 mm, the absorption lines began to show traces of asymmetry which became more pronounced as still higher pressures were reached. The $^2P_{1/2}$ component was asymmetrical towards the red and the $^2P_{3/2}$ component towards the violet. Figure 2 gives sample curves showing this asymmetry. Obviously the whole of these asymmetrical lines cannot be represented by the dispersion formula (1). If $(\delta\lambda)^2$ is plotted against $(\log I_0/I)^{-1}$ for each side of these lines separately it is found that a fairly straight line is obtained for the shorter wave-length wing of the $^2P_{3/2}$ component and the longer wave-length wing of the $^2P_{1/2}$ component while the opposite wings of these components yield strongly curved lines. The values of the width at half-maximum divided

by N listed in Table I for the pressures above 1 mm were calculated from the slopes of these straight lines. The values for these higher pressures do not therefore represent true widths at half-maximum. They are merely convenient parameters for indicating the form of one wing of each component in terms of formula (1).

The fact that the shorter wave-length wing of the $^2P_{1/2}$ component and the longer wave-length wing of the $^2P_{3/2}$ component deviate strongly from the dispersion formula (1) is not only due to the asymmetry but is also due to the appearance at these higher pressures of a faint structureless band near each of the component lines. Because the bands are diffuse and faint and are located near to the doublet lines the position of the bands could not be determined with great accuracy. The first of these bands extends for approximately 6A to the red of a fairly sharp edge at 7964.5A while the second extends about 10A to the violet of an edge at 7817.6A. While these bands have apparently not been observed before, similar bands have appeared in the absorption spectra of other alkalis.

In conclusion the author wishes to express his gratitude to Professors I. S. Bowen and W. V. Houston for their supervision and encouragement. He is also indebted to Dr. P. E. Lloyd for his generosity in discussing his experiences during research on K resonance lines.

NOVEMBER 15, 1940 PHYSICAL REVIEW VOLUME 58

The Energy Losses Attending Field Current and Thermionic Emission of Electrons from Metals*

G. M. Fleming† and Joseph E. Henderson
University of Washington, Seattle, Washington

(Received September 10, 1940)

The energy losses accompanying field emission and thermionic emission have been measured in the same experimental tube. This was accomplished by observing the thermal electromotive force in a junction from which the emission currents were drawn. No measurable temperature change was observed for field emission up to thermionic temperatures. For thermionic emission, temperature changes were observed which, when correlated with the power losses from the filament as a function of temperature, yield a calorimetric value for the work function of tungsten of 4.46±0.09 volts. A theoretical expression is given for the average net energy loss per electron emitted in thermionic and field current emission. The experiment gives strong additional evidence that in field emission the electrons escape by penetrating rather by surmounting the surface potential barrier as in thermionic emission.

Introduction

It has frequently been observed that during the emission of large thermionic currents of electrons there is a very noticeable decrease in the temperature of the emitting body. This phenomenon provides direct evidence that the electrons furnishing the emission current partake of the thermal energy of the solid. Evidently the electrons leaving a metal at the high temperatures occurring in thermionic emission have more temperature energy than those which are supplied to replace them. The difference in the average energy of the electrons emitted by the cathode and of those supplied to the cathode results in a loss of power and in a corresponding decrease of temperature. The power loss producing the temperature change, when translated in terms of the average net energy loss per electron emitted, yields a value of the work function of the emitting metal in very satisfactory agreement with that obtained by independent methods.[1]

* Abstracts: J. E. Henderson and G. M. Fleming, Phys. Rev. **48**, 486 (1935); **54**, 241 (1938); **56**, 853 (1939).
† Now at Russell Sage College.

[1] Saul Dushman, Rev. Mod. Phys. **2**, 394 (1930).

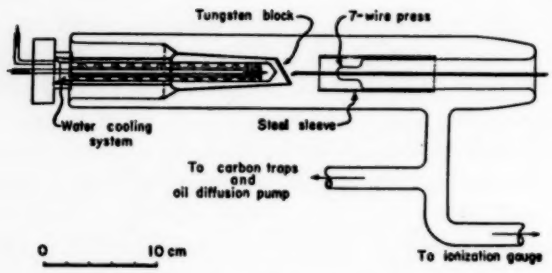

FIG. 1. Section through the experimental tube.

Since the knowledge of the energy losses by a metal emitting electrons provides information concerning the mechanism of emission it is important to make measurements in the case of field current emission where electrons are supposed to escape from the metal by penetrating rather than by surmounting the barrier as in thermionic emission. The only at all satisfactory theoretical explanations[2] of the current-voltage relationships for field emission, as well as the form of the energy distribution curves[3] for field emission support this mechanism. The almost complete independence of these energy distributions as a function of temperature[4] as well as the remarkably small temperature dependence of field emission characteristics as obtained by Ahearn[5] and others[6] makes the region extending to thermionic emission of particular interest. The present experiment deals with the problem by measuring the cooling of a field current emitter in this region. The amount of cooling depends, as in thermionic emission, on the amount of temperature energy possessed by the emitted electrons.

METHOD

The essential feature of the method is to incorporate a thermocouple junction in the emitting cathode and to use the changes in the electromotive force of this junction to measure changes in temperature of the cathode during emission. This information coupled with a knowledge of the physical properties of the cathode is sufficient to determine the rate at which energy is carried away by the emission current. The cathode can be designed to permit measurements at temperatures extending from room temperature into the thermionic range.

APPARATUS

Since large power losses must be dissipated at the target in this experiment, it was necessary to provide a water-cooled anode. Consequently, the thermocouple cathode assembly was installed in place of the regular cathode of a General Electric XP–DF x-ray tube the anode of which is water cooled. Figure 1 shows a section through the experimental tube. A seven-wire press was installed to permit the testing of various cathode-thermocouple arrangements. Of the four different arrangements that were tried, only the one which yielded the best experimental results will be described here. Since very good vacuum conditions are necessary for stable field current emission, the tube was evacuated with a two-stage oil diffusion pump used with charcoal.[7] Consistent space vacuums of the order of 10^{-8} mm of Hg were maintained throughout the experiments.

The potentials necessary for field emission were provided by a filtered, valve rectified x-ray supply, of approximately 30 kv. To insure steady currents, a radiator type x-ray tube was used in series with the experimental tube. In the portion of the experiment dealing with thermionic emission the potential was provided by batteries.

Of the various cathode-thermocouple combinations tried, the one illustrated in Fig. 2 proved most satisfactory. The thermocouple was formed by wires of 0.004-inch tungsten and 0.005-inch

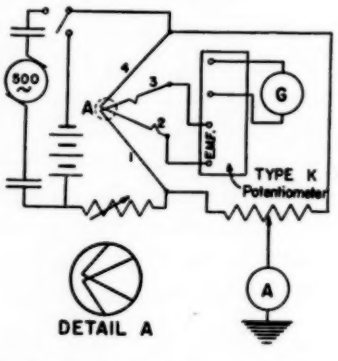

FIG. 2. Schematic diagram of the point assembly and measuring circuit.

[2] R. H. Fowler and L. Nordheim, Proc. Roy. Soc. **A119**, 173 (1928).
[3] J. E. Henderson and R. K. Dahlstrom, Phys. Rev. **55**, 473 (1939).
[4] J. E. Henderson and R. K. Dahlstrom, Phys. Rev. **45**, 764 (1934).
[5] A. J. Ahearn, Phys. Rev. **44**, 277 (1933); **50**, 238 (1936).
[6] R. A. Millikan and C. F. Eyring, Phys. Rev. **27**, 51 (1926).
[7] J. E. Henderson, Rev. Sci. Inst. **6**, 66 (1935).

tantalum spot-welded together near A. These were bent and shaped to the form of points close to the weld and placed opposite the anode to serve as the field emitter. Legs 1 and 3 are one continuous wire of tungsten and legs 2 and 4 are continuous tantalum. The thermal electromotive force of the junction formed by legs 2 and 3 was measured by a type K potentiometer capable of reading to 10^{-6} volt. Either leg, 1 or 4, furnished the path from ground for the emitted electrons.

For temperatures above room temperature, the cathode was heated either by a current from a battery or from a 500-cycle generator. The 500-cycle current was found convenient, since it permitted isolation of the measuring circuits across various portions of the cathode by means of a choke. Temperatures were determined by resistance measurements up to where a Leeds and Northrup optical pyrometer could be used. Since the temperatures of the various parts of the cathode were not the same, the reference temperature is taken as that of the region of maximum temperature, t_m, along the heated legs. The temperature of the junction may be as much as 200°C from this for the highest temperatures quoted. Corrections were made for absorption of light by the glass walls by measurements upon the temperature of a similar filament observed through both walls of the tube. The experimental plots in Figs. 3 and 4 show, respectively, the values

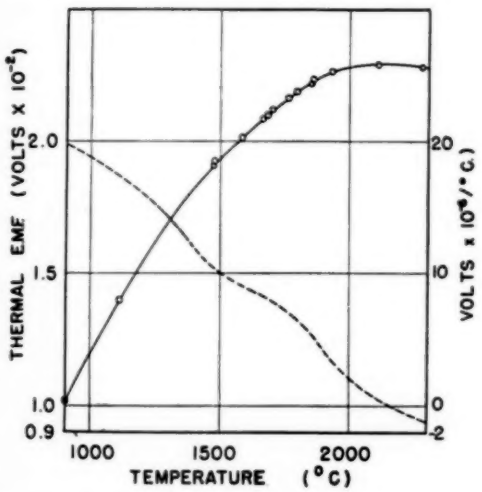

FIG. 3. The thermal electromotive force, K, of the tungsten-tantalum junction of the cathode shown in Fig. 2 as a function of the maximum temperature, t_m, along the heated wires. The dotted curve shows dK/dt_m or the thermal electromotive power as a function of t_m.

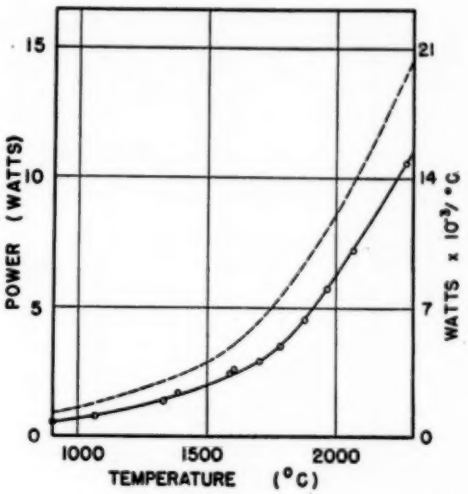

FIG. 4. The power, P, supplied by the heating current to the point assembly as a function of the maximum temperature, t_m. The dotted curve shows dP/dt_m as a function of t_m.

of the thermal electromotive force, K, as a function of t_m, and the power, P, supplied by the heating current as a function of t_m. In the same figures are shown the derivative curves giving the rate at which the thermal electromotive force and power supplied by the heating current change with the maximum temperature t_m. These data were taken when the heating was produced by the current supply. In the experiment itself the changes in power corresponding to changes in t_m as well as to changes in the e.m.f. of the junction will depend upon the distribution of this supply to the cathode. For example, during emission of electrons the power associated with this current is drained from the region of the cathode from which emission occurs, thus changing the distribution of the net power supplied to the cathode, and the temperature, t_m, may not be that corresponding to the same total power supplied solely by the heating current. That is, $(dP/dt_m)(W)$, where the power change is produced through the heating current, is in general different from $(dP/dt_m)(i)$, where the change in power occurs with the change of emission current. The relation between these two quantities depends upon the region from which emission current is drawn.

Use was made of the values of the ir drops in the cathode in estimating the distribution of the areas active in field current emission. It was

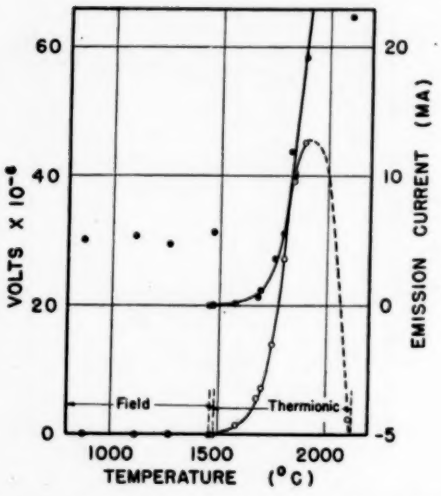

FIG. 5. The change in electromotive force produced by emission. The full circles represent the emission current and the open circles the corresponding changes in electromotive force.

found that at room temperatures emission occurred from the tips of the cathode, very close to the junction and nearest the anode; thus, in this case, the effectiveness of power changes due to emission to produce a change in temperature of the junction was twice that of power changes due to the heating current. The effect of higher temperatures of the cathode was, in general, the redistribution of the emission, frequently to regions of the surface at which the field strength was less than the maximum, and the predominant emission was not correlated with the position of highest temperature. This shifting with temperature was perhaps due to the migration of an impurity patch of lower work function or to a change of the crystal structure along the surface. The estimation of the actual distribution of current could be roughly made, but the effectiveness of power losses in producing a change in temperature of the junction was uncertain because of the ambiguity of the position along the cathode at which the emission occurred. Correspondingly the temperature of the portion of the metal from which the emission took place was uncertain within limits. At the highest temperatures for which measurements were made with field currents the effect of power losses was uncertain by a factor of about two, and the temperature of the emitting region by about 200°C. Because of the nature of the results obtained, this uncertainty is unimportant except for the highest value of the temperature given for field emission.

In the case of thermionic emission both the position of emission and the temperature can be specified because the emission current occurs predominantly at the region of highest temperature, thus allowing a calculation of the effect of the power losses due to emission. Approximate expressions for $(dP/dt_m)(W)$ and $(dP/dt_m)(i)$ can be calculated from an equation obtained giving the temperature variations along the wire. The relation between them is:

$$\left(\frac{dP}{dt_m}\right)(i)=\frac{1}{1.16}\left(\frac{dP}{dt_m}\right)(W).$$

The highest temperatures along legs 1 and 4 occurred at positions about one-third of the length of the leg away from the junction, and for thermionic emission the maximum along leg 1, of tungsten, was higher than that along the tantalum leg by a small amount varying from 30° to 50°C. The value of the ir drops in the cathode during emission showed that only a small part of the total emission current was furnished by the tantalum leg, this fraction varying from practically zero at lower temperatures to one-fifth at the highest temperature used. The way in which the temperature of the junction, or the equivalent electromotive force, K, varies with t_m for the two types of power changes likewise must be known. With sufficient accuracy, calculations showed that

$$(dK/dt_m)(i)=(dK/dt_m)(W).$$

RESULTS

Data were taken by measuring the difference in thermal e.m.f. of the junction with the emission current alternately on and off. Figure 5 shows the results for both field current and thermionic emission. The remainder of the curve for field currents, omitted in the figure, extends for the range from 800°C down to room temperature along the axis. The temperatures used in plotting are again those of the position of maximum temperature along the cathode. The emission currents are represented by full circles and the corresponding changes in e.m.f. by open circles. The field currents were produced by the

high voltage supply and were usually adjusted to be about 5 milliamperes. The thermionic currents, except for the one at the highest temperature, were produced with 140 volts accelerating potential. The last value, for which about 90 volts was used, shows lack of saturation by departure from the curve rising exponentially at lower temperatures. The changes in electromotive force, K, for emission due to the high electric fields were less than the experimental error at all temperatures used. In the thermionic range the effects were easily measurable. Figure 6 shows the trend of the points, giving the values of ΔK per unit emission current in microvolts per milliampere. The decrease in the ordinate for the thermionic range with increasing temperature is associated with two characteristics of the cathode. First, as the temperature of the cathode increases, the amount of power change necessary to produce a given temperature change increases (see Fig. 4), and, second, the thermoelectric power of the junction decreases in this range (see Fig. 3).

The power loss per unit current for field current emission is less than that measurable by the apparatus. Therefore, only an upper limit can be given for the average net energy loss per electron emitted. At room temperature the sensitivity of the apparatus sets this limit at 0.002 ev/electron. At higher temperatures the sensitivity of the apparatus is less, and for the highest temperature at which field emission can be said to have been produced in this case, 1250°C, the energy loss per electron emitted was not greater than 0.08 ev/electron.

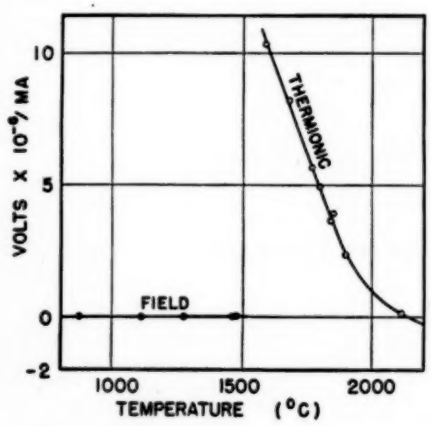

FIG. 6. The change in electromotive force per unit emission current as a function of temperature for field current and thermionic emission.

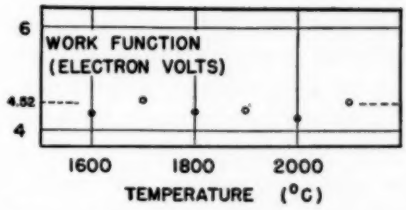

FIG. 7. Values of the work function of tungsten calculated from the experimentally measured energy losses found at different temperatures.

The values of $\Delta K/i$ found for thermionic emission are used to calculate the associated power loss per unit emission current or the equivalent energy loss per electron emitted. The power change per unit current, $\Delta P/i$, corresponding to $\Delta K/i$ is

$$\frac{\Delta P}{i}=\left(\frac{dP}{dt_m}\right)(i)\frac{\Delta K/i}{(dK/dt_m)(i)}$$

$$=\frac{1}{1.16}\left(\frac{dP}{dt_m}\right)(W)\frac{\Delta K/i}{(dK/dt_m)(W)},$$

where the quantities on the right can be obtained at each temperature from the curves in Figs. 3, 4, and 6. The result, expressed in watts per milliampere, can be alternatively given in terms of electron volts per electron by the relation:

$$w=10^3\cdot\Delta P/i,$$

where w is the loss of energy per electron.

The values of w as a function of temperature can be compared with those given by theory in the relation:

$$w=\phi+3.2kT,$$

ϕ being the work function of the emitting metal, and T, the absolute temperature. Conversely, by use of this relation a value of ϕ may be obtained which can be compared with the known value for the emitting metal. The values for ϕ obtained in this way are shown in Fig. 7. The accepted value for the work function of tungsten, 4.52 ev,[8] is indicated. The average of the experimental results displayed is 4.46 ± 0.09 ev.

THEORETICAL DISCUSSION

It is interesting to compare the values obtained by theory with the experimental values of the net

[8] See A. L. Hughes and L. A. DuBridge, *Photoelectric Phenomena* (McGraw-Hill, 1932), p. 76.

energy loss per electron emitted. The energy losses occurring during electron emission from metals can be computed for a simple triangular type of potential barrier such as assumed by Fowler and Nordheim.[2] The calculations are made for electrons within the metal having Fermi-Dirac statistics.

The number of electrons per unit volume having velocity v in the range dv is

$$f(v)dv=\frac{2m^3}{h^3}\frac{dv_x dv_y dv_z}{e^{-(\mu-E)/kT}+1}=\frac{8\pi m^3}{h^3}\frac{v^2 dv}{e^{-(\mu-E)/kT}+1}$$

given by the Fermi-Dirac distribution function. The electron parameter μ is determinable from the number of electrons per unit volume. Assume that the emitting metal has a temperature T and is connected to a metal at 0°K from which the supply of electrons to the cathode is taken. Electrons passing between the regions of different temperature undergo a redistribution in energy to correspond to the temperature of the region occupied. The group of electrons passing from a region of lower to one of higher temperature gains heat energy from the metal, while the group passing in the opposite direction gives up energy to the cooler metal. When no emission occurs the net current within the metal is zero and the energy lost by the hot portion is gained by the cool portion of the metal. During emission the net current in the metal is not zero but is equal to the emission current. Those of the emitted electrons which possess temperature energy, that is, for which $E>\mu$, are replaced by electrons originally from the cool supply which have acquired heat energy on arriving at the emitting region at temperature T. A net loss of energy occurs as a result of this replacement equal to the difference between the energy of the emitted and the added electrons.

In order to calculate the heat energy which must be supplied to the electrons emitted it is necessary to find the average energy of the levels in the current supply out of which these electrons are raised. The number of electrons per unit time of each energy which gains temperature energy is proportional to the rate at which electrons of this energy enter the warmer metal and to the fraction of the number of levels of this energy which are vacant at temperature T.

The current of electrons of energy E coming from the 0°K supply is computed as follows. The number of electrons per unit volume having velocity v in dv which also have velocity v_x (in the direction of increasing temperature) in dv_x is

$$f(v)dv\cdot dv_x/2v=(4\pi m^3/h^3)vdvdv_x$$

and the current per unit area in this direction is

$$(4\pi m^3/h^3)vdvdv_x\cdot v_x=(4\pi m/h^3)dEdW$$

with $W=\frac{1}{2}mv_x^2$. The total current density of electrons of energy $E=\frac{1}{2}mv^2$ in dE is

$$\int_{W=0}^{W=E}\frac{4\pi m}{h^3}dEdW=\frac{4\pi m}{h^3}EdE.$$

The fraction of the total number of levels which should be vacant at T is

$$e^{-(\mu-E)/kT}/(e^{-(\mu-E)/kT}+1)$$

and, therefore, the rate at which electrons of energy E increase their energy on entering the region of temperature T is

$$\frac{4\pi m}{h^3}E\frac{e^{-(\mu-E)/kT}}{e^{-(\mu-E)/kT}+1}dE.$$

The average energy of the levels from which the electrons in the current are removed is

$$\int_0^\mu\frac{Ee^{-(\mu-E)/kT}}{e^{-(\mu-E)/kT}+1}dE\cdot E\Big/\int_0^\mu\frac{Ee^{-(\mu-E)/kT}}{e^{-(\mu-E)/kT}+1}dE=\mu-\frac{0.81}{\ln 2}kT=\mu-1.2kT.$$

In the emitted current the energy distribution is modified by the transmission coefficient of the barrier. The current density of emitted electrons at E is given by

$$\frac{4\pi m}{h^3}\frac{dE}{e^{-(\mu-E)/kT}+1}\int_0^E D(W)dW,$$

where $D(W)$ is the transmission coefficient of the barrier for electrons of normal energy W. The net loss of energy associated with this current is, then,

$$\frac{4\pi m}{h^3}\int_\mu^\infty \frac{(E-\mu+1.2kT)dE}{e^{-(\mu-E)/kT}+1}\int_0^E D(W)dW$$

and the average energy loss per electron emitted in the total current is

$$w=\int_\mu^\infty \frac{(E-\mu+1.2kT)}{(e^{-(\mu-E)/kT}+1)}dE\int_0^E D(W)dW \Big/ \int_0^\infty \frac{dE}{e^{-(\mu-E)/kT}+1}\int_0^E D(W)dW.$$

The above expression is to be evaluated for two cases: for field current emission at temperatures up to the thermionic range, and for thermionic emission. For field emission Fowler and Nordheim[2] give the transmission coefficient as

$$D(W)=(4/C)W^{\frac{1}{2}}(C-W)^{\frac{1}{2}}\exp\left[-4\kappa(C-W)^{\frac{1}{2}}/3F\right],$$

where

$$\kappa=2\pi(2m)^{\frac{1}{2}}/h.$$

The temperature of the metal from which field currents were produced was always below the range for which appreciable thermionic emission occurred, and therefore the upper limit of the integral on E can be put at C, the height of the barrier. Substituting for $D(W)$, setting $\mu-W=x$ and dropping terms of higher power than the first in x in the expansion about $x=0$, we find

$$w=\frac{\displaystyle\int_\mu^C \frac{(E-\mu+1.2kT)}{e^{-(\mu-E)/kT}+1}dE\int_{\mu-E}^\mu\left[1+x\left(\frac{1}{2\phi}-\frac{1}{2\mu}\right)\right]e^{-2\kappa\phi^{\frac{1}{2}}x/F}dx}{\displaystyle\int_0^C \frac{dE}{e^{-(\mu-E)/kT}+1}\int_{\mu-E}^\mu\left[1+x\left(\frac{1}{2\phi}-\frac{1}{2\mu}\right)\right]e^{-2\kappa\phi^{\frac{1}{2}}x/F}dx}.$$

These approximations are valid for the values of the field used[9] where the greatest contribution to the emission current comes from the range around $W=\mu$. The net energy loss per electron emitted is upon integration:

$$w=\frac{kT\left[1.2\left(\dfrac{1}{1-\alpha kT}-\dfrac{1}{2-\alpha kT}+\cdots\right)+\left(\dfrac{1}{(1-\alpha kT)^2}-\dfrac{1}{(2-\alpha kT)^2}+\cdots\right)\right]}{\left(\dfrac{1}{\alpha kT}-\dfrac{1}{1+\alpha kT}+\cdots\right)+\left(\dfrac{1}{1-\alpha kT}-\dfrac{1}{2-\alpha kT}+\cdots\right)}$$

with

$$\alpha=2\kappa\phi^{\frac{1}{2}}/F=1.03\times10^8\phi^{\frac{1}{2}}/F.$$

For $T=300°\mathrm{K}$ and $F=10^8$ volts/cm, $\alpha kT\ll1$, and

$$w=1.6\alpha(kT)^2=0.0025 \text{ ev/electron}.$$

[9] J. E. Henderson and R. K. Dahlstrom quote values of the field as high as 10^8 volts/cm; other estimates range from this value down to 10^7 volts/cm.

At 1550°K with $F=10^8$ v/cm, $\alpha kT=0.29$, and

$$w=0.07 \text{ ev/electron.}$$

The magnitude of the computed energy loss per electron at 300°K is much too small to be detected by this experiment, but that calculated for 1550°K is very close to the limit detectable.

In the thermionic range the accelerating potentials used were relatively small, and the transmission coefficient is chosen as:

$$D(W)=0, \qquad W<C,$$
$$D(W)=\bar{D}, \text{ a constant}, \quad W\geqslant C.$$

The energy loss per electron is then readily seen to be

$$w=\phi-3.2kT; \quad \phi=C-\mu.$$

The use of this relation between w and ϕ in obtaining a satisfactory value of the thermionic work function of tungsten from the experimental data establishes that the agreement between theory and experiment is good.

Discussion of Results

This experiment demonstrates clearly that there is no net measurable loss in energy from the emitter in field emission over the temperature range from room temperature to that temperature at which thermionic emission begins to furnish more than a negligible fraction of the total emission. Corresponding to this temperature and above there is a definite measurable energy loss. These conclusions show that there is a fundamental difference involved in the mechanism responsible for the two types of emission.

The calculations show that the Fowler-Nordheim theory of metals provides a picture essentially in agreement with these results. The theory describes field current emission as taking place by penetration of the surface barrier and, consistent with experiment, predicts a cooling effect at room temperatures much smaller than that measurable and only slightly within the limits of error of the method at 1250°C. In the thermionic range, where emission occurs without the application of high electric fields, only the electrons of normal energy greater than that corresponding to the top of the barrier are emitted and thus carry away heat energy. On this basis from the net energy loss per electron emitted, the thermionic work function of the emitting metal has been computed, agreeing well with the accepted value.

The relation between the temperature of the emitter and field emission has been attacked by two other types of experiments. In the first of these the striking independence of temperature of the total current in field emission was established first by Millikan and Eyring[6] and later for pure metals by Ahearn.[5] The other type of experiment deals with the energy distribution of the emitted electrons. Henderson and Dahlstrom[4] show that the energy distribution for the electrons emitted under the action of intense electrical fields changes only slightly with temperature. Their work shows a small but detectable increase in the high energy groups with temperature. These changes in the high energy groups doubtless represent temperature energy carried away from the metal but the small number of electrons involved make the total energy they represent undetectable in this experiment.

Both of these experiments differ from this investigation in their fundamental approach in that they deal with the properties of the emitted electrons whereas this experiment deals with the effect of the emission upon the metal itself. Evidently the majority of the electrons involved in field emission are practically independent of the temperature of the emitter, at least up to that temperature at which thermionic emission becomes the predominant form of emission, and carry away an inappreciable amount of temperature energy above that possessed by the electrons that replace them.

The authors are much indebted to the General Electric X-Ray Corporation for the gift of the water-cooled x-ray anode which formed the basis of the experimental tube used in this research.

Interactions in the Tungsten Atom, W I, in a Magnetic Field

J. H. ROBERSON AND J. E. MACK
University of Wisconsin, Madison, Wisconsin

AND

G. R. HARRISON
Massachusetts Institute of Technology, Cambridge, Massachusetts

(Received September 5, 1940)

General theoretical expressions are given for the magnetic field dependence of the energies and intensities belonging to neighboring levels (regardless of coupling) of an atom. The energy dependence is tested experimentally for the levels $21{,}448_2$ and $21{,}453_1$ of W I in fields up to 4.5 cm^{-1} ($=9.7\times10^4$ c.g.s.), where the pattern of levels extends more than 30 cm^{-1}. The values found for the constants are $\Delta\nu_0=5.154$ cm^{-1}, $g(214_2)=1.4787$, $g(214_1)=2.5113$, $k^2(214_1, 214_2)=0.0447$. The deviations $\nu_{obs}-\nu_{calc}$, obtained from individual determinations at different field strengths, are in some instances as great as 0.05 cm^{-1}, which is somewhat greater than the estimated error in the observations; they may be attributed in part to slight repulsive effects from other levels and similar disturbances of the reference lines, which have not yet been calculated in detail.

INTRODUCTION

IN a magnetic field, each level of an atom splits into $2J+1$ nondegenerate sublevels with magnetic quantum numbers ranging from $+J$ to $-J$. When the Larmor precession frequency $c\eta(=eH/4\pi mc)$ is small compared with the no-field frequency separations $c\Delta\nu_0$ between the level under consideration and neighboring levels with the same parity that differ by not more than 1 in J value, the sublevels are equally spaced, symmetric about the field-free level, and linear in the field (linear or ordinary "anomalous" Zeeman effect), if we neglect a certain small effect[1] (diamagnetic quadratic Zeeman effect). When η is not small compared with the $\Delta\nu_0$'s, the dependence upon the field is more complicated: the approximate equidistance, symmetry, and linearity are lost through an interaction that may be described as a mutual repulsion of sublevels with the same M. Thorough studies have been made of the interactions among the levels of an LS-coupling multiplet (Paschen-Back effect, called "incipient" when the asymmetries are slight), but hardly any attention has been paid to the more general case, presumably because levels other than members of the same "good" multiplet rarely lie close enough together to give rise to noticeable interactions in the fields commonly used.[2-8]

The work reported here is a detailed study of the mutual influence of any two levels of an atom in a magnetic field, with the experimental behavior of the levels 214_1 and 214_2 of W I as an

[1] Shown in references 12 and 23 to be negligible in the cases considered here.

[2] For the interesting case of Hg I $6s6d\ ^3D_1$, "1" $^3D_2$, which lie only 3.2 cm^{-1} apart, see P. Zeeman, Proc. Amst. Acad. Sci. **10**, 351 (1907); Physik. Zeits. **10**, 217 (1909); P. Gmelin, Physik. Zeits. **9**, 212 (1908); Ann. d. Physik **28**, 1079 (1909); Physik. Zeits. **11**, 1193 (1910); M. M. Risco, Physik. Zeits. **13**, 137 (1912); J. B. Green and R. A. Loring, Phys. Rev. **46**, 888 (1934); E. U. Condon and G. H. Shortley, *Theory of Atomic Spectra* (Cambridge University Press, 1935), p. 294. The interaction of these levels is complicated by their relatively great hyperfine structure; cf. S. Goudsmit and R. F. Bacher, Phys. Rev. **43**, 894 (1933).

[3] Asymmetric Zeeman effect patterns were reported for several Mo I and W I lines by R. Jack, diss. Göttingen (1908); Ann. d. Physik **28**, 1032 (1909); Proc. Roy. Soc. Edinburgh **29**, 75 (1908).

[4] Incipient Paschen-Back effect in certain configurations $2p^5nl$ of Ne I, where the coupling is intermediate, has been studied by K. Murakawa and T. Iwama, Tokyo Inst. Phys. Chem. Research **13**, 283 (1930); J. B. Green and J. A. Peoples, Phys. Rev. **56**, 54 (1939).

[5] The qualitative explanation of certain of the asymmetries[3] in W I, and preliminary reports on the present quantitative study, were given by J. E. Mack and O. Laporte, Phys. Rev. **51**, 291 (1937); J. H. Roberson and J. E. Mack, Phys. Rev. **55**, 1126 (1939); **57**, 1074 (1940).

[6] A surprising intensity anomaly in the Zeeman effect of Ni I is attributed to interaction between levels 28 cm^{-1} apart labeled $3d^84s5s\ ^5F_1$ and $3d^94d\ ^3D_1$, but unfortunately without data on the positions of the sublevels, by H. Dijkstra, Physica **4**, 81 (1937).

[7] J. B. Green and J. F. Eichelberger, Phys. Rev. **56**, 51 (1939) discuss the theory of the Paschen-Back effect for intermediate coupling.

[8] The general considerations in this paper apply to hyperfine structure levels if J is replaced by F throughout.

example. These levels are particularly suitable because, while their nearest neighbor with the same parity is almost 1400 cm^{-1} away, they are only 5 cm^{-1} apart, and, moreover, one of them has an exceptionally large g value. All the levels specifically referred to in this paper are listed in Table I;[9] of course, it is understood that except for parity and J, the designations of quantum numbers in this complex spectrum are only crude approximations. In a prospective paper[10] a study will be made of several smaller interactions in W I and the dependence of the interaction constants k upon the structure of the atom.

TABLE I. *Levels of* W I *referred to in this paper. The designation "PF" for* 13_2 *indicates an approximately equal mixture of two L values.*

NAME	DESIGNATION	ENERGY	g*
D_0	$5d^46s^2\ {}^5D_0$	0.00	0/0
S_3	$5d^56s\ {}^7S_3$	2951.27	1.9751
13_2	$5d^46s^2\ {}^3PF_2$	13777.71	—
18_1	$5d^46s^2\ {}^3D_1$	18082.84	—
$214_2°$	$5d^46s6p\ {}^7F_2$	21448.65	1.4787
$214_1°$	$5d^46s6p\ {}^7D_1$	21453.80	2.5113
$261_3°$	$5d^46s6p\ {}^7D_3$	26189.11	1.7408
$353_2°$	—	35311.46	—
$415_2°$	—	41583.16	—
44_2	$5d^46s7s\ {}^7D_2$	44919.74	1.9470

* The g's given here were determined in this study. In the cases indicated by dashes, it was unnecessary to know the g's.

THEORY[11]

In considering the interaction of levels in a magnetic field, we shall assume that it is sufficient to take into account the mutual influence of only two levels at a time; and[12] that

$$\eta \ll h/\pi mc\Sigma[x^2+y^2]_{Av}.$$

The energy of an atom in a magnetic field differs from the no-field energy by an amount proportional to $\Sigma j_z+\Sigma s_z$, where j_z and s_z are the projections, respectively, of the total angular momentum and the spin angular momentum in the direction of the field, and the summation takes place over all electrons. In consequence of a general theorem regarding the matrix elements of a component of a vector,[13] the matrix elements of the contribution of the magnetic field to the Hamiltonian of the atom can be written:

$$(aJ_aM_a|H_{mag}|bJ_bM_b)=hck_{ab}f\eta\cdot\delta(M_a,M_b), \quad (1)$$

$$\text{where } f=\begin{cases} M, & \text{if} \quad J_a=J_b. \\ (J^2-M^2)^{\frac{1}{2}}, & \text{if} \quad |J_a-J_b|=1. \\ 0, & \text{if} \quad |J_a-J_b|>1. \end{cases}$$

Here J stands for the greater of the two values J_a, J_b; and M, for the common value $M_a=M_b$ where M is used. The coefficient k_{ab} is the same for all the sublevels, characterized by different M values, of the two levels. The indices a and b, which are used simply to distinguish different states with the same parity, may be interchanged throughout any expression, here and in the discussion below. It will be observed that for a diagonal element the coefficient k_{aa} is the ordinary weak-field g factor of the Zeeman effect.

The simplicity of the general discussion in the previous paragraph arises from the fact that one may start with exact wave functions in no field; even though these functions are not explicitly known, they are known to have the above-mentioned properties.

For the special case of LS coupling, all the k's are zero[14] except in the case of two states within the same multiplet, and in that case[15]

[9] O. Laporte and J. E. Mack, J. Research Nat. Bur. Stand., in preparation.

[10] J. H. Roberson, in preparation.

[11] We are indebted to Professor Breit for essential help in the preparation of this section.

[12] The term on the right is the value of η at which the diamagnetic quadratic effect would equal the normal effect ($\doteq 5\times10^3$ cm^{-1} for the lowest, and 5×10^2 cm^{-1} for the highest level listed in Table I; cf. reference 23).

[13] Cf. M. Born and P. Jordan, *Elementare Quantenmechanik* (Julius Springer, Berlin, 1930), Section 29.

[14] Here we assume n to be a good quantum number. In a better approximation there is an interaction closely related to the famous sharing of intensity among members of a series; E. Fermi, Zeits. f. Physik **59**, 680 (1929). For a heavy atom like W the radial functions are not strictly the same for the orbits $nl_{l+\frac{1}{2}}$ and $nl_{l-\frac{1}{2}}$, and not strictly orthogonal for nl_j and $n'l_j(n'\neq n)$ to such a good approximation as in the lightest elements. For this reason, on the one hand there may be incipient "Paschen-Back" interactions between different series members (although a rough calculation shows that these effects are negligible in practical cases), and on the other hand the exact validity of Eq. (2) is subject to doubt because the calculation of this formula presupposes that the radial functions are strictly the same for $nl_{l+\frac{1}{2}}$ and $nl_{l-\frac{1}{2}}$. While this departure from simplicity, associated with large ls interaction energy, may be properly described as a breakdown of LS coupling, it is not always recognized as such because it cannot be read directly from the elementary vector model; for instance, it occurs even in one-electron spectra.

[15] P. Güttinger and W. Pauli, Zeits. f. Physik **67**, 743 (1931); cf. E. U. Condon and G. H. Shortley, *Theory of Atomic Spectra*, Eqs. 10^32a, 10^32b. Güttinger and Pauli's derivation does not cover the case of more than one multiplet with the same L and the same S in a configuration, but Professor Breit informs us that $k=0$ between different multiplets even in this case as a consequence of

$$k(J, J)=1+[J(J+1)+S(S+1)-L(L+1)]/2J(J+1), \quad (2a)$$

$$k(J, J-1)=k(J-1, J)=[(J+L-S)(J-L+S)(L+S+1+J)\times(L+S+1-J)/4J^2(4J^2-1)]^{\frac{1}{2}}, \quad (2b)$$

where it will be noticed that $k(J, J)$ is the well-known LS coupling weak-field g value and $k(J, J-1)$ is the coefficient leading to the well-known expression for the Paschen-Back effect. The sign of k depends, in general, upon a convention in the choice of phases for the wave functions, but we may, without loss of generality, use the positive sign throughout this paper.

In any case where the values of the coefficients for the transformation between the actual case and the ideal LS coupling case are known, k_{ab} may be determined. The interpretation of k_{ab} for particular cases, and the discussion of the inverse problem of interpreting actual levels from experimental values of k_{ab} is postponed.[10]

This paper is concerned especially with the nondiagonal coefficients k_{ab}, $a \neq b$. Reference hereafter to k_{ab} (or for brevity, k) implies a nondiagonal coefficient unless the contrary is specified.

The secular equation from Eq. (1) for the two sublevels with the same M, of the interacting levels a and b, has the solutions

$$\nu=\nu_0'+Mg'\eta\pm[(\nu_0''+Mg''\eta)^2+k^2f^2\eta^2]^{\frac{1}{2}}, \quad (3)$$

where ν_0' and ν_0'' are half the sum and half the difference, respectively, of the no-field wave numbers ν_{0a} and ν_{0b}, and g' and g'' are half the sum and half the difference, respectively, of the weak-field g factors, g_a and g_b.

Equation (3) is the equation of a hyperbola with its center at

$$\eta_{\text{cent}}=-\nu_0''Mg''/(M^2g''^2+k^2f^2), \quad (4a)$$

$$\nu_{\text{cent}}=\nu_0'-\nu_0''M^2g'g''/(M^2g''^2+k^2f^2) \quad (4b)$$

and asymptotic slopes

$$(d\nu/d\eta)_\infty=Mg'\pm(M^2g''^2+k^2f^2)^{\frac{1}{2}}. \quad (4c)$$

The wave numbers at η_{cent}, which is the point of minimum energy separation of the branches, are

$$\nu_{\text{min sep}}=\nu_{\text{cent}}\pm\nu_0''kf(M^2g''^2+k^2f^2)^{-\frac{1}{2}}. \quad (4d)$$

The intensity of a line component is

$$I_a=(I_{0a}^{\frac{1}{2}}x\pm I_{0b}^{\frac{1}{2}})^2/(1+x^2), \quad (5)$$

where I_{0a}, I_{0b} are the intensity contributions of the two sublevels with the same M to the no-field lines, and

$$x\equiv kf\eta/(\nu-\nu_{0a}-Mg_a\eta).$$

It will be noticed that $x=1$ when η has the value $-\nu_0''/Mg''$ at which the linear approximation would predict the crossing of the sublevels. At this field the intensities of two Zeeman effect sublines are equal in the important case where I_{0a} or I_{0b} is zero, for instance on account of a selection rule. When I_{0a} and I_{0b} are both different from zero, the general expression for the intensity, Eq. (5), contains an ambiguity in sign that can be removed in any special case.

Figure 1*A* shows the results of the calculations for a representative case. The values used for the seven constants J_a, J_b, g_a, g_b, ν_{0a}, ν_{0b}, and k are those found experimentally for the levels 214_1 and 214_2 of W I. Although negative values of η have no physical meaning, it is convenient to draw the curves for the two values of M that differ only in sign, on opposite sides of the $\eta=0$ axis, for then they form a single complete hyperbola. This simple property arises from the fact that all the results depend, not upon the signs of M and η separately, but only upon the sign of the product $M\eta$. Thus Fig. 1*A* shows the complete hyperbola representing the $M=\pm1$ sublevels, and in addition the reflection in the $\eta=0$ axis of the (dotted) portion representing $M=+1$.

An approximate solution, valid for incipient asymmetry, $\eta \ll |\Delta\nu_0|$, in agreement with second-order perturbation theory, is

$$\nu_a \doteq \nu_{0a}+Mg_a\eta\pm k^2f^2\eta^2/(\Delta\nu_0+M\eta\Delta g), \quad (7)$$

where in any particular case only the "repulsive" sign is to be chosen in front of the last term. Neglecting this $k^2f^2\eta^2$ term leads, of course, to the linear Zeeman effect.

Apparatus and Exposures

The study in fields $\eta<2$ cm^{-1} was made at Wisconsin. The magnet, containing $\frac{3}{4}$ ton of iron,

the orthogonality of the space components of the wave functions, following the general treatment of spectroscopic terms given in E. Wigner, *Gruppentheorie* (F. Vieweg, Braunschweig, 1931).

was built in the shape of a Θ. The current was supplied by means of 48 pancake coils of copper tubing in parallel. The tubes were cooled by distilled water, pumped through a closed circulating system and cooled by city water at an interchanger. The resistance of the coils was about 1 ohm. The field became sufficiently steady for Zeeman effect work after about 30 minutes of running. The current, which was about 10 amperes for $\eta=1$ cm^{-1} and 160 amperes for $\eta=1.9$ cm^{-1}, was supplied by a 200-volt, 200-ampere motor generator. The pole pieces consisted mainly of Armco iron rods 12 cm in diameter; but each was furnished with a tip of Permendur[16] carefully threaded into the pole piece with a minimum of clearance, and ending in a cone with a half-angle of 56°, truncated at a diameter of 6 mm. During the exposures the tips were from 3.0 to 4.5 mm apart.

The source was an arc, enclosed in a Back chamber that has already been described[17] and was made over for this use. The pole tips were protected by quartz plates about 0.5 mm thick, each mounted upon a brass ring machined to fit the conical tip and to allow the quartz to rest almost in contact with the Permendur face; but for the strongest fields, requiring the greatest crowding, the quartz was omitted from the tip next to the grounded electrode. The arc was produced across a gap, longitudinal to the field, between electrodes made of pure tungsten rods[18] or 50-mil tungsten wires placed in pairs, filed to form plates about 1 mm thick. One electrode was placed on a pivoted rod and agitated by a motor-driven eccentric shaft to make about 5 contacts per second, and an inductance was introduced into the arc circuit to help maintain a fairly steady current.

The exposures at Wisconsin were made with the Physics Department's 21-foot Rowland mounting and 5.6-inch, 15,000 lines/inch Rowland grating. The exposures were made in the second order, with a dispersion of about 1.33A/mm. Eastman 33 and 40 plates were used; the greatest exposure time required, with the strongest fields, was about 2 hours.

The study in fields $\eta>2$ cm^{-1} was made at Massachusetts Institute of Technology. The apparatus and the technique of exposure have been described.[19] Gratings *F* and *G* were used in the first order. In exposures[20] 2.4, 3.5, and 4.2, and in no others, the π and σ components were separated with the aid of a Rochon prism.

Measurements and Reduction of Data

The lines studied were ν21,453 $(=D_0-214_1)$, and $\nu\nu$23,465, 23,471 $(=214_{1,2}-44_2)$. The former was studied principally for $\eta<2$ cm^{-1} and the latter, only for $\eta>2$ cm^{-1}. The former was carefully examined for self-reversal, with negative results.

Each of the readings recorded on our data sheets, of the position of a spectrum line on a plate, is the result of several settings to 1 micron (0.004 to 0.006 cm^{-1}) made on the large Société Génevoise comparator at Wisconsin. After each group of settings the plate was moved, so that the next group would be shifted to a different point along the length of the line, i.e., to different grains of the emulsion.

A serious difficulty arose in our attempt to provide reference lines. If we had attempted to use field-free lines of any element as standards, it would have been necessary to try to avoid the possibilities of error inherent in any attempt to superimpose the radiation diffracted by the grating from two sources separated in time or in space. Instead, we used as actual reference points for each line the centers of the patterns of two neighboring lines (or only one, as discussed in the next paragraph). For D_0-214_1 the reference lines were ν21,533 $(=13_2-353_2)$ and ν21,359 $(=D_3-261_3)$, and for $214_{1,2}-44_2$, ν23,500 (18_1-415_2) and ν23,237 $(=S_3-261_3)$. Our method has the serious defect that any departure of the center of the pattern of any reference line from the no-field wave number introduces an error into the result. For that reason, these pairs of reference line patterns were selected in each case only after a careful study had shown both patterns to be symmetric and their centers to have the same separation as the no-field lines, within 0.02 cm^{-1}. Yet, even for lines thus chosen, we have been forced to tolerate the undesirable

[16] Kindly furnished by the Bell Telephone Laboratories.
[17] A. E. Whitford, Phys. Rev. **39**, 898 (1932).
[18] Kindly furnished by the General Electric Company.
[19] F. C. Bitter and G. R. Harrison, Phys. Rev. **56**, 15 (1940).
[20] Each exposure is designated by the first two digits in η.

possibility of bodily shifts away from their no-field positions as a possible source of error in our final result.

Since every sufficiently intense and well-resolved line between ν23,471 and ν23,237 was found to wander with respect to ν23,500 and ν23,237, and experience showed that $\nu\nu$23,471, 23,465 could be measured as accurately with reference to ν23,500 alone as by interpolation between ν23,500 and ν23,237, some of the measurements upon $\nu\nu$23,471, 23,465 were made with reference to ν23,500 alone. These measurements required the independent determination of the dispersion curve of each plate involved, for different plates from the same grating were found to differ as much as 0.1 percent in dispersion.

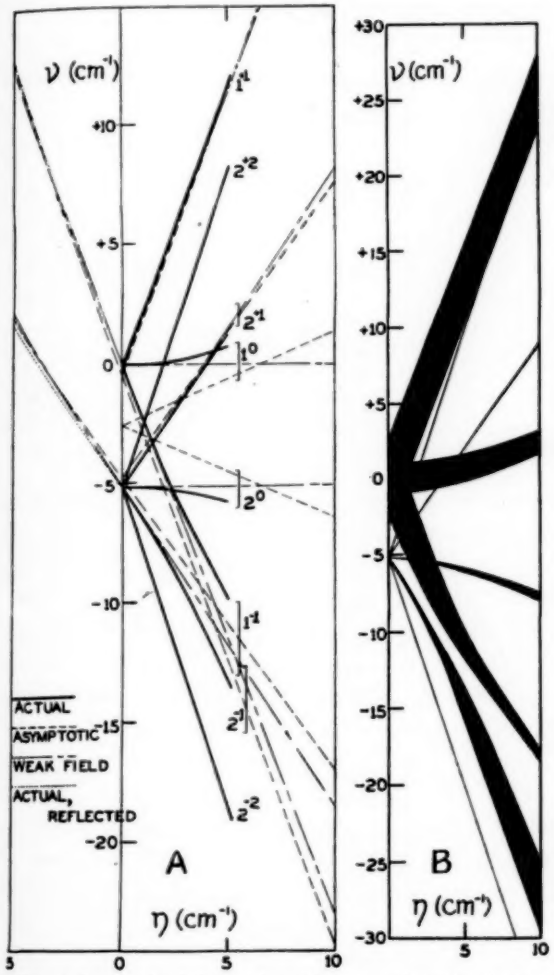

FIG. 1A. Typical behavior of two otherwise isolated atomic energy levels in a magnetic field, predicted by Eq. (3) and found for the W I levels $21{,}453.80_1$, $g=2.511$, and $21{,}448.65_2$, $g=1.479$. *B*, Sharing of properties between the levels shown in Fig. 1*A*, as predicted by Eq. (5) and qualitatively found. The thickness of each line (above that of the thinnest) is proportional to the intensity of a transition to a $J=0$ level, permitted for $J=1$ but forbidden for $J=2$.

In order to eliminate false relative shifts of the differently polarized components arising from possible imperfections of adjustment in the cases of the exposures taken with the Rochon prism, all measurements of any line component in these exposures were made with respect to reference line components similarly polarized.

Although the wave-length dispersion $d\lambda/dx$ is sensibly constant over any one line pattern, the approximation involved in considering the wave number dispersion $d\nu/dx$ to be constant over a pattern would have introduced errors (almost 0.002 cm^{-1} for our widest patterns, 17 cm^{-1} wide) in our calculations. Of course the words "symmetry," "center," etc., in our discussion of the patterns, refer to the patterns reduced to a wave number scale, rather than to the photographic plates themselves. The equations used in our routine reductions were as follows, where λ_0 refers to the wave-length in air of the no-field line (or of the no-field line involving the level 214_1 in the case of patterns arising from 214_1 and 214_2, which were always considered as single patterns); $\delta\lambda$, $\delta\nu$, and δx to deviations from the no-field line; and $\delta\nu'$ to an approximation to the vacuum wave number deviation, $\delta\nu$, obtained in an intermediate step:

$$\left.\begin{aligned} \delta\lambda &= \delta x\, d\lambda/dx \\ \delta\nu' &= -\delta\lambda/\lambda_0{}^2 \\ \delta\nu &= \delta\nu'/n_{\text{air}} + \lambda_0(\delta\nu')^2. \end{aligned}\right\} \quad (8)$$

FIELD DETERMINATIONS

Because no quantitative determinations have been made heretofore of magnetic fields as great as those used in this work, it was necessary to give careful consideration to the question of field determination. The procedure finally selected was: first, to determine as our principal field standard[21] the field $\eta=(4.093\pm0.006)$ cm^{-1} found for an auxiliary exposure, calculated as discussed below from certain patterns chosen for theoretical reasons from among the lines of several

[21] $\pm$ here refers to probable error.

TABLE II. *Individual determinations of sublevels of $214_{1,2}$ from exposure 3.5($\eta=3.552$ cm^{-1}). Superscripts in the body of the table give M for the even sublevel of the transition. A = shift of D_0^0 with respect to the center of (supposedly symmetric) 44_2, determined to be -0.036 cm^{-1} by adjustment to best agreement with the other line ($214_{1,2}-44_2$). Dashes indicate lines too faint to measure, or missing.*

LINE	GRATING	ν_1^{+1}	ν_1^0	ν_1^{-1}	ν_2^{+2}	ν_2^{+1}	ν_2^0	ν_2^{-1}	ν_2^{-2}
$214_{1,2}-44_2$	G	$+9.089^{+2}$	$+0.400^{+1}$	-8.158^0		—	-5.572^{+1}	-11.186^0	-15.662^{-1}
		$.092^{+1}$	$.408^0$	$.171^{-1}$	$+5.351^{+2}$	-0.082^{+1}	—	—	$.673^{-2}$
		—	—	—	$.371^{+1}$	$.072^0$	$.545^{-1}$	$.173^{-2}$	
$214_{1,2}-44_2$	F	$.124^{+2}$	$.428^{+1}$	$.107^0$		—	—	$.149^0$	$.634^{-1}$
		$.115^{+1}$	$.407^0$	$.155^{-1}$	$.351^{+2}$	$.081^{+1}$	—	—	$.654^{-2}$
		—	—	$.139^{-2}$	$.368^{+1}$	$.077^0$	$.550^{-1}$	$.166^{-2}$	
D_0-214_1	F	$.139^0+A$	$.456^0+A$	$.079^0+A$		$.046^0+A$	$.526^0+A$	$.119^0+A$	
mean		+9.105	+0.413	−8.141	+5.360	−0.079	−5.557	−11.165	−15.656

TABLE III. *Observed sublevels of 214_1 and 214_2 referred to $\nu_0(214_1)$. All quantities are expressed in cm^{-1}; uncertainty $\sim\pm0.010$ cm^{-1}. B—Impossible to determine value on account of line blends. b—Value with unusually large uncertainty on account of partly resolved blends. Exposures listed in brackets are plotted together in Fig. 2.*

η	ν_1^{+1}	ν_1^0	ν_1^{-1}	ν_2^{+2}	ν_2^{+1}	ν_2^0	ν_2^{-1}	ν_2^{-2}
1.586	+4.068	+0.117	−3.835					
1.586	+4.080	+0.098	−3.835					
1.588	+4.093	+0.098	−3.878					
1.646	+4.222	+0.123	−4.013					
1.664	+4.258	+0.123	−4.062					
1.666	+4.277	+0.117	−4.050					
1.667	+4.277	+0.129	−4.050					
1.679	+4.295	+0.123	−4.074					
1.693	+4.338	+0.110	−4.099					
1.698	+4.350	+0.110	−4.154					
1.915	+4.897	+0.153	−4.627					
2.252	+5.727	+0.179	−5.420	*B*	−1.885	−5.330	−8.696	*B*
2.426	+6.208	+0.234	−5.821	+2.035	−1.649	−5.326	−9.015	−12.276
3.552	+9.105	+0.413	−8.141	+5.360	−0.079	−5.557	−11.165	−15.656
4.285	+11.016	+0.602	*B*	+7.540	+0.966	−5.688	−12.721	−17.802
4.533	+11.677	+0.674	−9.947*b*	+8.272	+1.320	−5.795	−13.307	−18.584*b*

elements introduced as impurities; and second, to determine the field for each exposure from the separations, assumed to be linear in the field, within the W I line $\nu 23{,}237$ ($=S_3-261_3$), which was especially selected as the reference line from theoretical and experimental considerations discussed below. The necessity of considering the value of a transformation factor between field and energy separation is automatically eliminated by the use of the Lorentz unit ($\eta=1$ cm^{-1}, or about 2.142×10^4 c.g.s.) instead of the c.g.s. unit of magnetic field, because the unit is dimensionally the same as that in which we measure the separation of the levels.

The impurity lines used to determine our principal standard of field were the resonance doublets of Ca II, Sr II, and Ba II. The concentration of each impurity was sufficiently low to produce sharp lines without self-reversal. The exposure was gauged to bring out the impurity lines and the W I reference lines with optimum blackening for measurement. The two directions of polarization were not separated. The field was calculated by making use only of the five intervals in each doublet that would have been, for weak fields, symmetric about no-field lines. This method compensates for all nonlinear effects that do not influence the interval within any pair of sublevels of a level that differ only in the sign of M, i.e., to a good approximation, for the diamagnetic quadratic Zeeman effect and for incipient mutual repulsion effects such as the Paschen-Back effect (cf. the last subsection of this paper). The error introduced in the calculations by the approximate treatment of the Paschen-Back effect can be seen from Eq. (7) to be, to the next approximation,

$$2M\Delta g\cdot k^2f^2\eta^3/(\Delta\nu_0)^2.$$

This error, which we have neglected, amounts to no more than 1.3×10^{-3} cm^{-1} in line separation, or 2.0×10^{-3} cm^{-1} in η, in any case. Earlier tenta-

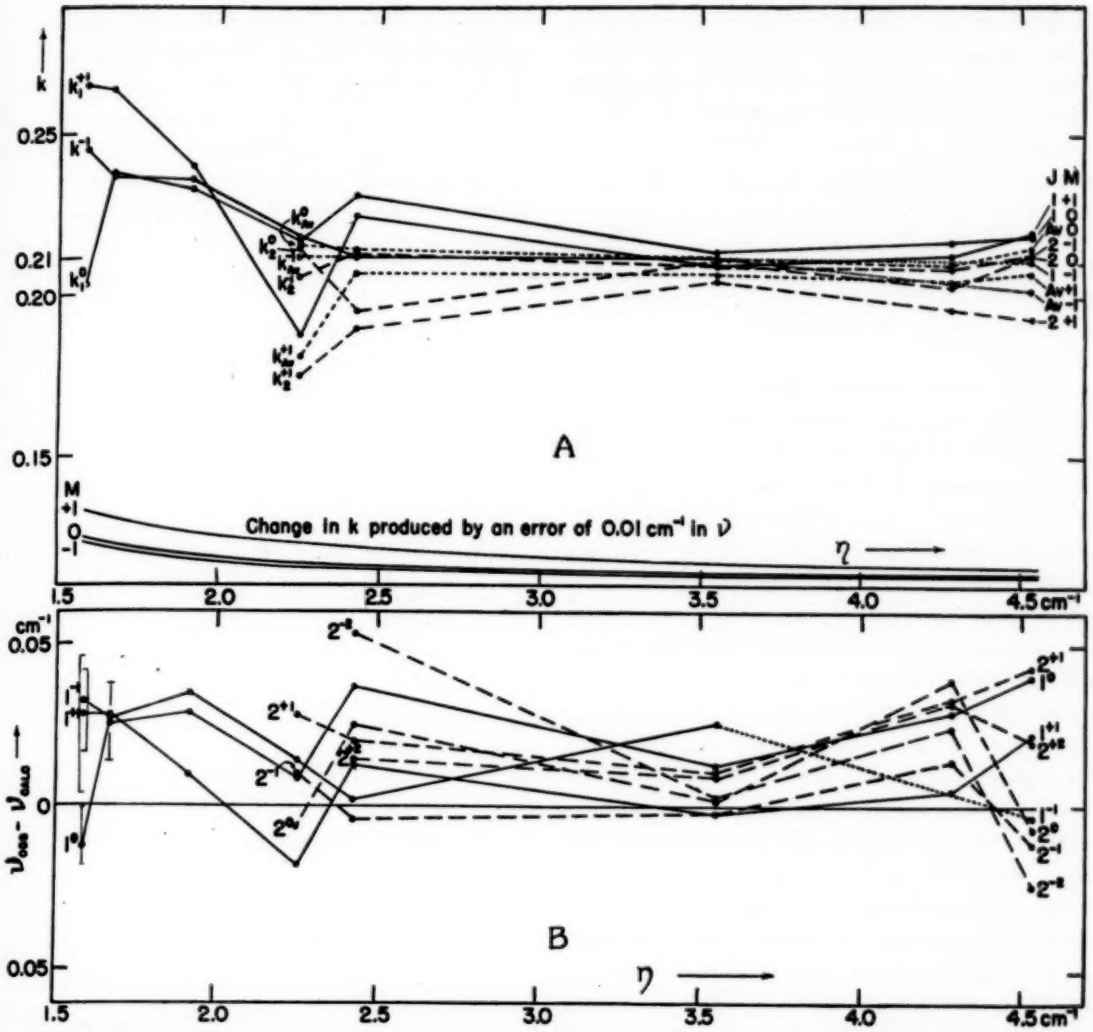

FIG. 2*A*, Values of $k(214_1, 214_2)$ observed for each sublevel in each of a number of fields. Full lines, $J=1$; dashes, $J=2$; filled circles, relatively unreliable values obtained from line blends. The ordinate labeled "0.21" should be labeled "0.211." *B*, Discrepancies, $\nu_{obs}-\nu_{calc}$, between the energy levels observed and those calculated from Eq. (1) with the best values of the constants. The scale of ordinates (discrepancy) is spread out tenfold compared with that of abscissas (field).

tive field values calculated from Al, Ca, and Sr impurities in two of the exposures listed in Table III, were $\eta=3.543$ and 4.267 cm^{-1}, lower by 0.3 and 0.5 percent, respectively, than the accepted values; but these values were abandoned on account of the relatively poor observational quality of the impurity lines, some of which were self-reversed.

The W I reference line ν23,237 was chosen primarily for experimental reasons: its great width ($\doteq 5\eta$), the relative slightness of its observed asymmetry, its stable distance from certain other relatively symmetric patterns, and its general favorable appearance on the plates. A secondary reason for the choice was the fact that the theoretically estimated[10] nonlinearities for both levels are small (although, as in all other levels in the spectrum, there are enough levels near to each level to make one expect some asymmetry). The observed pattern in the largest field (expressed as $\Delta\nu/\eta$, where $\eta=4.533$ cm^{-1}) was

2.445 2.209 *1.976* *1.741* 1.502 1.272 (*0.710* 0.466 0.237 $\bar{0}$ $\dot{0}$.236 0.466 *0.710*) 1.272 1.505 *1.743* *1.975* 2.212 2.447
236 233 235 239 230 244 229 473 230 244 233 238 232 237 235

The greatest discrepancy between this pattern and the weak-field one calculated from the accepted g values, $g(S_3)=1.9751$ and $g(26l_3)=1.7408$, is 0.022 cm^{-1} ($\sim$5 microns).

Results and Comparison with Theory

Although only the energies and not the intensities were measured, it may be remarked that the intensities were found, by visual estimation, to be qualitatively in agreement with Eq. (5) and Fig. 1*B*.

By means of an auxiliary study, the level 44_2 was found to be very nearly symmetric, with $g(44_2)=1.9470$. In the calculation, levels D_0 and 44_2 were assumed to follow the weak-field formula.

Table II shows the results of all the readings recorded for levels $214_{1,2}$ from exposure 3.5. It is typical except that the discrepancies (average deviation from accepted means, 0.011 cm^{-1}) are rather larger than in most exposures and that it is derived from both the line pair $\nu\nu$23,471, 23,465 and the line ν21,453, the former having been photographed simultaneously with two gratings, while usually the data for one field were determined from one line or pair photographed on one plate. In Table II and throughout the paper, a subscript (except 0, *a*, *b*) stands for J and a superscript stands for M. Table III is a summary, showing the final values of the sublevels observed in each field. The no-field interval between the levels was found to be

$$2\nu_0''\equiv\Delta\nu_0=(5.154\pm0.002)\ cm^{-1}.$$

In the calculations discussed below, all line components were given equal weight, except for partly resolved blends (marked *b*), which were recorded but given no weight when other readings were available for the same quantity, and unresolved blends (marked *B*), which were not recorded. Each interval was weighted by a factor proportional to its magnitude. In averaging the k's, each value was weighted by a factor inversely proportional to the change that would result in k from an arbitrary small alteration of a single reading (Fig. 2*A*, bottom).

The calculations and the comparison of the observed with the calculated sublevels proceeded as follows: g_2 and g_1 were determined in that order, and then k (called $k_J{}^M$), independently for each sublevel, for all the exposures with $\eta>2$ cm^{-1}; and finally the wave number difference $\nu_{obs}-\nu_{calc}$ between the observed and the calculated value was determined for each sublevel in each field. Each calculation for one constant used the best (the weighted mean) value for each one previously listed; e.g., all the calculations for g_1 used $g_2=1.4787$. From the linear theory

$$g_2=(\nu_2{}^{+2}-\nu_2{}^{-2})/4\eta. \tag{9}$$

From the linear theory, modified by an interaction with spur invariance:

$$g_1=(\nu_1{}^{+1}+\nu_2{}^{+1}-\nu_1{}^{-1}-\nu_2{}^{-1})/2\eta-g_2. \tag{10}$$

The results for the g's are as follows:

$\eta(cm^{-1})$	g_2	g'
2.252	*B*	1.9936
2.426	1.4754	1.9986
3.552	1.4792	1.9940
4.285	1.4785	*B*
4.533	1.4811*b*	1.9993*b*
weighted mean	1.4787	1.9950

An independent determination of $k_J{}^M$ was made for each sublevel in each field, where $k_J{}^M$ was available, by solving Eq. (3) for k:

$$k_J{}^M=[(\nu_J{}^M-\nu_0'-Mg'\eta)^2-(\nu_0''+Mg''\eta)^2]^{\frac{1}{2}}/f\eta \quad \begin{cases} M=+1,\ 0,\ -1 \\ J=1,\ 2. \end{cases} \tag{11}$$

In addition to these six $k_J{}^M$ there were calculated for each field the following weighted means: three k^M from $k_1{}^M$ and $k_2{}^M$; two k_J, from $k_J{}^{+1}$, $k_J{}^0$, and $k_J{}^{-1}$; and one k from all six $k_J{}^M$. Finally the grand average k was computed from all the fields with complete (six) $k_J{}^M$ data, i.e., from fields 2.2, 2.4, 3.5, and 4.5. The values are shown in Fig. 2*A*. The grand average k is

$$k(214_1,\ 214_2)=0.211.$$

The best value of k squared (formerly[5] called K and given a tentative value of 0.06) is 0.0447.

The $k_J{}^M$ show small systematic trends, and it should be noted that the values of $k_1{}^M$ are consistently larger than those of $k_2{}^M$.

The values of ν_{calc} were obtained from Eq. (3) with the best values of the constants. The resulting curves are shown in Fig. 1*A*. The constants of the hyperbolas, calculated from Eq. (4),

are:

M	η(center)	ν(center)	$(d\nu/d\eta)_\infty$
±1	$-3.312M$ cm^{-1}	-9.195 cm^{-1}	$\begin{cases}2.632M\\1.364M\end{cases}$
0	0.000	-2.577 cm^{-1}	±0.424

The values of $\nu_{\text{obs}}-\nu_{\text{calc}}$ are shown in Fig. 2*B*. The discrepancies are somewhat greater than our estimated experimental uncertainty, and are almost all positive.

In interpreting Fig. 2*B*, two distinct types of discrepancy ought to be considered: (1) *Experimental error.* Of all the factors possibly contributing to the accumulated experimental errors in our results, two deserve special mention here: First, the wandering of the reference levels. Each energy determination for $214_{1,2}$ depends upon the assumption that each of five reference levels exhibits in certain respects the weak-field behavior described in the second sentence of this paper.[22] The fact is that most of the discussion in the next paragraph is applicable to the reference levels as well as to levels $214_{1,2}$. Second, the repeated application of the same measurements in the determination of several constants: For instance, the same readings upon $\nu_1{}^{+1}$ and $\nu_1{}^{-1}$ were used successively in determining $g(44_2)$, g_1 and k, each of which depends upon its predecessors, as shown above. Thus, although we estimate our probable error in setting upon the line components to be not more than 0.010 cm^{-1} ($\sim$2.5 microns), the total error in $\nu_{\text{obs}}-\nu_{\text{calc}}$ may be considerably larger than if independent data had been used for each constant with a consequent statistical canceling of errors.

(2) *Inadequacy of the calculation.* The calculation took explicitly into account only the interaction between the two levels under special consideration. Each sublevel is subject to other disturbances that we have not tried to evaluate, such as the diamagnetic quadratic Zeeman effect and incipient interactions with many other levels in the neighborhood. The disturbances specified can be expressed as a series in ascending powers of η. The first and most important member of the series is the η^2 one, which includes the incipient interactions with more distant levels, insofar as they can be described by Eq. (7), as well as the diamagnetic quadratic Zeeman effect[23] term:

$$\Delta\nu_{\text{diamagnetic quadratic}}\doteq\tfrac{1}{4}\pi mch^{-1}\eta^2 \times\sum[(r^2)_{kl}\cdot 2(l^2+l-1+m_l{}^2)/(2l-1)(2l+3)]. \tag{12}$$

Thus the η^2 member is, to a close approximation, an even function of M. Advantage was taken of this property in the determination of the constants, as follows: Eqs. (9) and (10) depend not upon individual ν's, but only upon differences $\nu_J{}^{+M}-\nu_J{}^{-M}$; and in the determination of the grand average k, Eq. (11) was used in effect only to determine the values of k_J, from pairs $\nu_J{}^{+M}$ and $\nu_J{}^{-M}$. Consequently the constants g_1, g_2, and k used in the calculations are independent of all disturbances that are even functions of M and η.

No such immunity can be claimed, however, for the individual determinations shown in Fig. 2. Parabolic terms are not evidently predominant in the discrepancies shown in Fig. 2*B*. Nevertheless, it is hoped that the outstanding discrepancies between the observations and the calculations can be improved, especially with respect to the general upward trend in Fig. 2*B* and the associated fact that the values of $k_1{}^M$ are on the whole higher than those of $k_2{}^M$, after a more detailed study[10] of the influence of more distant levels.

[22] Since the energies were measured with respect to 44_2 (assuming the field-independence of the zero point interpolated from 18_1-415_2 and S_3-261_3) in fields $\eta>2$ cm^{-1}, and with respect to $^5D_0$ (assuming the field-independence of the zero point interpolated from 13_2-353_2 and D_3-261_3) in fields $\eta<2$ cm^{-1}, a false discontinuity might be expected to appear at the junction of the two regions in Fig. 2*B* (as well as in Table III). On the assumption that the effect is proportional to η^2, the value found for the quantity A (Table II, caption) at $\eta=3.5$ cm^{-1} leads one to expect the magnitude of the discontinuity to be about 0.01 cm^{-1}, the ordinate for strong fields being less than that for weak fields. Indeed such a discontinuity, probably from this cause, may be recognized in Fig. 2*B*.

[23] J. H. Van Vleck, *The Theory of Electric and Magnetic Susceptibilities* (Oxford, Clarendon Press, 1932), Chapter 6, Eqs. 105, 106. The summation, which is to be carried out over all electrons, is simplified by the fact that the contribution of any closed subshell is just $\Sigma 2(r^2)_{kl}/3$. From certain equations and susceptibility data (especially for Au^+) in Chapter 8 the value of $\Delta\nu$ (diamagnetic quadratic) for W I may be roughly estimated to range from about $+0.003$ cm^{-1} to about $+0.005$ cm^{-1} for the levels listed in our Table I, leading to absolute changes not greater than about 0.002 cm^{-1} for any line with which we are concerned. Thus the shifts of the lines under study relative to the reference lines are too small to detect.

Ionic Mobilities in Insulating Liquids

ANDREW GEMANT
The Detroit Edison Company, Detroit, Michigan
(Received July 15, 1940)

A simple method is suggested which allows ionic mobilities in insulating liquids to be computed from conductivity-time curves obtained after application of a d.c. potential. The ionic radii and the concentration of the corresponding particles can be computed from the mobilities obtained. The method is applied to some data of J. B. Whitehead, and ionic mobilities of the order 10^{-7} cm/sec. per volt/cm are obtained.

1. INTRODUCTION

THIS paper is concerned with the possibility of determining the mobility of ions present in insulating oils. This is one of the fundamental problems regarding insulating materials in general. Measurements of the conductivity supply only the product of mobility and ionic concentration, and a separation of the two factors is not possible without some additional information. In aqueous or alcoholic solutions such additional information is obtained from osmotic data or electrode potential measurements, methods which, with very few exceptions,[1] have not up to now been extended to insulating liquids.

It has long been recognized that the decay of the current passing through an insulating liquid after the application of a d.c. potential is, partly at least, caused by the removal or accumulation near the electrodes of the ions present. If this assumption holds, it should be possible, by an analysis of the current-time curve, to draw certain conclusons with regard to the ionic mobilities, and from them to the size and concentration of the free ions.

K. F. Herzfeld[2] has applied the theory of ionic distribution to a potential distribution curve obtained by J. B. Whitehead,[3] and computed values for the ionic mobilities on the basis of rather involved equations. Continued interest in this matter is shown also by some recent publications of a more mathematical nature by B. Gross.[4]

A simple theory allowing ionic mobilities to be computed from the initial current-time curves will be presented. The greatest difficulty in interpreting such curves is the fact that several mechanisms are overlapping. Because of the widely differing time constants of these single processes it is possible, however, approximately at least, to separate several regions of the current-time curves, corresponding to different mechanisms.

Orientation of dipoles usually has a very small time constant, and the separation of this process is generally easy. An identification of charging currents, corresponding to internal surfaces is, on the other hand, a hard task, and a definite solution of this problem does not yet exist.

Electrolytes dissolved in homogeneous media, with which this paper is concerned, can be of two kinds. First there are ions which can be considered as pertaining to an electrolyte in a state of "total dissociation." These are generally large ions of a more or less colloidal nature. In restricting our consideration to liquids having a total charge of zero, these large ions must have their oppositely charged equivalent counterpart either in equally large, or smaller ions. Second, there are electrolytes in a state of partial dissociation of a type investigated by Kraus[5] and co-workers. Ions of this type are of a molecular size. The first type is relatively quickly removed from the liquid and is expected to cause a sharp drop in the conductivity after application of a d.c. potential in a comparatively short time. The second type, however, is continuously regenerated, and its effect upon the conductivity is, therefore,

[1] Andrew Gemant, "Electrochemical potentials at the boundary copper-insulating oil," presented at the National Research Council meeting, Cambridge, Massachusetts, November, 1939.
[2] K. F. Herzfeld, Phys. Rev. **37**, 287 (1931).
[3] See J. B. Whitehead, *Impregnated Paper Insulation* (Wiley, New York, 1935).
[4] B. Gross, Phys. Rev. **57**, 57 (1940). Compare also a recent paper by J. L. Oncley and W. C. Hollibaugh, presented at the Summer Convention AIEE, 1940. They mention that ionic mobilities can be computed from current-time curves, but do not give any equations.
[5] C. A. Kraus, Science **90**, 281 (1939).

either negligibly small, or just a very slow decrease. A separation of the two types appears possible on this basis.

The dissociation process will not be discussed here. It is the fast drop in conductivity with which this paper is concerned, and it should be shown how the mobilities of the respective charge carriers can be computed from that part of the current-time curve.

The ions accumulating near the electrodes might either be discharged or persist as charged particles. Which of the two cases actually prevails will essentially depend on the chemical nature of the ions. In case they persist, it is to be expected that a space charge develops, and, after removing the voltage, a discharge current flows. Whereas the space charge was detected by J. B. Whitehead, as also by others, the discharge current appears to be more elusive. The fact that the original value of the conductivity is sometimes restored after removal of the d.c. potential[6] clearly indicates that the ions are not discharged, but persist, at least to a certain extent, in a number of cases.

In deducing the equations controlling the current-time curve, this accumulation of ions near the electrodes has to be taken into account. One can see that there will be two reasons for the decrease of the conductivity. One is the decrease of the number of carriers in the liquid phase; the other is a decrease of the voltage drop across the liquid, since part of the voltage is used up in the polarization voltage at the electrodes. This latter effect is analogous to that encountered in the electrolysis of aqueous solutions.

2. General Equations of Current Flow

Let us consider a condenser of 1 cm² cross section and separation a. The total initial conductance A_t of the cell is the sum of A_0, the totally dissociated part referred to above, and A_f, the final conductance, the change of which should be negligible. Thus

$$A_t = A_0 + A_f$$

and, similarly, the conductance at any time t after application of a d.c. voltage E_0 is given by a sum:

$$A' + A_f.$$

Considering the term A', let us take the general case that the ions removed accumulate near the electrodes forming a double layer of capacitance C and voltage drop E_c. The total charge removed is then CE_c, corresponding to a loss of CE_c/a in charge concentration. This again corresponds to a loss of mCE_c/a in specific conductivity, if m = mobility of ions. The loss in conductance is then mCE_c/a^2. We have then the relation

$$A' = A_0 - bCE_c$$

with

$$b = m/a^2.$$

It is assumed here that the remainder of the ions is always redistributed uniformly by means of diffusion, an assumption which holds only approximately. The charging of the capacitance C will then be controlled by the differential equation

$$CdE_c/dt = (A_0 - bCE_c)(E_0 - E_c).$$

In replacing E_c by E according to

$$E = E_0 - E_c,$$

where E is the voltage drop across the liquid, the differential equation can be solved. With the boundary condition $E = E_0$ for $t = 0$, the equation gives:

$$E = \frac{(A_0 - bCE_0)E_0 e^{-\beta t}}{A_0 - bCE_0 e^{-\beta t}},$$

where

$$\beta = A_0/C - bE_0. \tag{1}$$

The total current is now given by

$$E(A' + A_f)$$

and the apparent conductance A by:

$$A = E(A' + A_f)/E_0.$$

Putting the above value of E into the equation for A, we obtain

$$A = \frac{A_0(A_0 - bCE_0)(A_t - bCE_0)e^{-\beta t} - A_f(A_0 - bCE_0)bCE_0 e^{-2\beta t}}{(A_0 - bCE_0 e^{-\beta t})^2}. \tag{2}$$

[6] J. Sticher and D. E. F. Thomas, Elect. Eng. 58, 709 (1939).

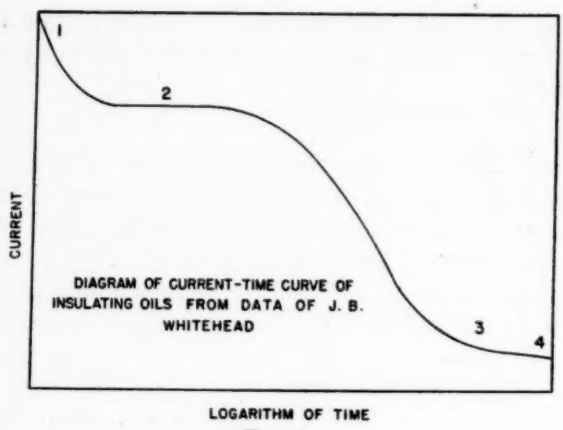

FIG. 1.

Equation (2) shows the following peculiarities: For $t=0$

$$A=A_i$$

as required.

For $t=\infty$, two cases must be considered, according as β is larger or smaller than zero. If β is positive,

$$A_0/bC>E_0.$$

The expression A_0/bC is the maximum possible polarization voltage corresponding to the case that all ions contributing to A_0 had left the liquid. A positive β then means that the liquid will finally be deprived of any finite electric field. Equation (2) for $t=\infty$ gives in this case, $A=0$, as expected.

On the other hand, for a negative β, Eq. (2) gives, for $t=\infty$,

$$A=(E_0-A_0/bC)A_f/E_0.$$

This again is according to expectations, since the bracket contains the final voltage drop across the liquid.

Another useful equation to be derived from Eq. (2) is the following:

$$(dA/dt)_{t=0}=-A_0(bE_0+A_i/C),$$

which is the slope of the $A(t)$ curve at the origin.

3. SPECIAL EQUATIONS

Equation (2) shows that it has to be used in its complete form only if the term A_0/bC is of the order of E_0. If the former is, at least, say, ten times larger than E_0, then the change of the voltage drop is the dominating factor, the process then amounts to charging a condenser across the liquid as resistance.[7] This special case will not be considered here any further.

If, on the other hand, E_0 is, at least, say, ten times larger than A_0/bC, or in other words, if

$$bCE_0/A_0\gg 1, \tag{3}$$

then the decrease of the ionic concentration is the chief factor. Equation (2) then becomes considerably simplified. In order to show that Eq. (3) usually holds, it shall first be given the form:

$$m\epsilon F/4\pi\lambda\sigma_0\gg 1, \tag{3a}$$

where ϵ = dielectric constant of liquid, F = applied field, λ = thickness of double layer accumulating at the electrodes, σ_0 = specific conductivity, corresponding to the large ions, being equal to A_0a. Taking likely orders of magnitude, we now have $m\sim 10^{-7}$ cm/sec. per volt/cm, $\epsilon\sim 3$, $F\sim 10^4$ volts/cm, $\lambda\sim 10^{-3}$ cm, $\sigma_0\sim 10^{-2}$ abs. e.s.u., and the left-hand side of Eq. (3a) becomes 25. This means that the second approximation will generally hold, and we shall now consider the simplified equation referring to this case.

Equation (2), with Eq. (3) valid, takes the form

$$A=A_0e^{-bE_0t}+A_f \tag{4}$$

or, writing Eq. (4) in terms of specific conductivities σ, and replacing b by m/a^2:

$$\sigma=\sigma_0e^{-mE_0t/a^2}+\sigma_f. \tag{4a}$$

Equation (4), as does Eq. (2), operates with one mobility m, which seems to be an unlikely specialization. The equation can be generalized easily by taking account of several ions with different mobilities. On the other hand, it is always desirable to operate with equations with a minimum of constants. Thus Eq. (4) should be extended only to two different mobilities, those of the positive and negative ions. In this case the relative factors of the two terms, generally unknown, also can be computed. If m and m' are the mobilities, the respective transference numbers are $m/(m+m')$ and $m'/(m+m')$. Consequently we have, instead of Eq. (4a):

$$\frac{\sigma-\sigma_f}{\sigma_0}=\frac{m}{m+m'}e^{-mE_0t/a^2}+\frac{m'}{m+m'}e^{-m'E_0t/a^2}. \tag{5}$$

[7] Compare S. F. Acree, E. Bennett, G. H. Gray and H. Goldberg, J. Phys. Chem. **42**, 871 (1938).

Equation (5) is the final answer to our question, for with it ionic mobilities may be computed from $\sigma(t)$ curves.

It should be pointed out here that according to Eq. (5) the $\sigma(t)$ curve depends upon the voltage. If conditions were such as to make the expression bCE_0/A_0 smaller than unity (say for small field intensities or large initial conductivities), then the $\sigma(t)$ curve should become independent of the potential applied. This circumstance supplies an experimental method to differentiate between the two cases.

In order to estimate the size of the ions, it first has to be decided whether the Stokes equation or the Helmholtz cataphoresis equation holds. This depends upon whether the thickness of the double layer around the ions is larger or smaller than the particle radius. The thickness of the double layer (ionic cloud) around the particles is given by the expression:[8]

$$.(\epsilon RT/8\pi F^2c)^{\frac{1}{2}},$$

where R=gas constant, T=absolute temperature, F=Faraday constant, c=molar ionic concentration per cc, and if c is estimated from the residual conductivity to about 10^{-14}, then the thickness becomes of the order 10^{-3} cm. Since the particle size is much smaller than that, it follows that Stokes equation will control the motion.

Applying this equation, we have for the ionic radii:

$$r=en/6\pi\eta m, \tag{6}$$

where e=electronic charge, n=valency of ion, η=viscosity of liquid.

Finally the number of particles can be computed from σ_0 and the mobilities obtained, as outlined in the introduction. Evidently this number is given by:

$$\sigma_0/en(m+m'). \tag{7}$$

4. Numerical Application of the Theory

The last equations now shall be applied to experimental data on mineral oils obtained by J. B. Whitehead[3] and co-workers. Figure 1 shows diagrammatically a typical current-time curve.

The part 1–2 is a decay of very short duration (around 10^{-3} sec.) which is possibly due to the orientation of dipolar constituents. At 2 the current becomes constant until about 1 sec. and then starts to drop again fairly rapidly until the region indicated by 3 (around 10^3 sec.) is reached. The region 3–4 is one of a very slow continuous decrease where the curve frequently runs nearly horizontally with a scarcely perceptible slope. Thus we might assume that the portion 2–3 has a mechanism of its own, and corresponds to the above discussed removal of large ions. If 3–4 has a slope different from zero, then this decrease is due to a mechanism different from that between 2 and 3, and very likely corresponds to electrolytes in a state of partial dissociation.

Figure 2 shows a plot, carried out on Whitehead's data, referring to his oil B-4 at 60°C. The abscissae are seconds, the ordinates are $\log_{10}\sigma_0/(\sigma-\sigma_f)$, σ_0, and σ_f being taken from the experimental data. It can be seen that the curve gives the impression of being the superposition of two different slopes, one effective between 0 and 0.6 of the ordinate scale, the other beyond about 1.2, the intermediate region showing a smooth transition. It should be mentioned that other curves of Whitehead show a similar behavior. This is in agreement with Eq. (5).

Applying Eq. (5) to Fig. 2, in which case E_0 was 1500 volts, a=0.1 cm, $\sigma_0=114\times10^{-15}$ mho/cm, and $\sigma_f=36\times10^{-15}$ mho/cm, the following values were obtained: $m=3.1\times10^{-7}$ and $m'=0.37\times10^{-7}$ cm/sec. per volt/cm. Table I shows the degree of agreement between experimental and calculated σ values.

Table II shows the results referring to another oil, B-6, the figures being somewhat less certain in that σ_f had to be estimated (Point 3 in Fig.

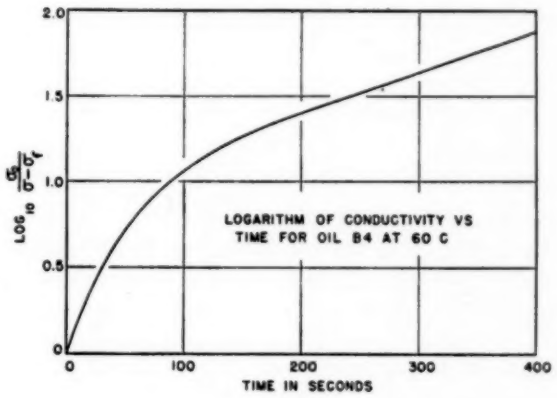

FIG. 2.

[8] A. Gemant, J. Phys. Chem. **43**, 743 (1939).

1) in contradistinction to the previous case for which the branch 3–4 was horizontal. Here a and E_0 have the same values as before, $\sigma_0 = 3.24 \times 10^{-15}$, and $\sigma_f = 0.81 \times 10^{-15}$. The values 1.0×10^{-7} and 0.31×10^{-7} were obtained for m and m', respectively. The agreement is somewhat less satisfactory than in the previous case. Figure 3 shows the theoretical curves and experimental points for both oils considered. The larger mobilities, m, probably correspond to the positive ion (solvated H-ion?), the smaller ones, m', to the negative ion.

In computing ionic radii according to Eq. (6), n for the cation will be taken as one. The viscosities are 1.1 poise for the *B*-4 oil at 60°C, and 9.0 poise for *B*-6 oil at 30°C. The corresponding cation radius for the first oil is 2.5×10^{-7} cm, and 9.4×10^{-8} cm for the second.

TABLE I. *J. B. Whitehead's B-4 Oil at 60°C.*

TIME IN SEC.	σ(MHO/CM) EXPERIMENTAL	CALC. WITH EQ. (5)
10	108 $\times 10^{-15}$	112 $\times 10^{-15}$
40	64	61.5
100	46	44
200	40.5	40.0
400	37.5	37.3
1000	36.0	36.0

TABLE II. *J. B. Whitehead's B-6 Oil at 30°C.*

TIME IN SEC.	σ(MHO/CM) EXPERIMENTAL	CALC. WITH EQ. (5)
10	3.67×10^{-15}	3.62×10^{-15}
20	3.19	3.24
40	2.32	2.68
100	1.45	1.73
200	1.25	1.19
400	0.96	0.93

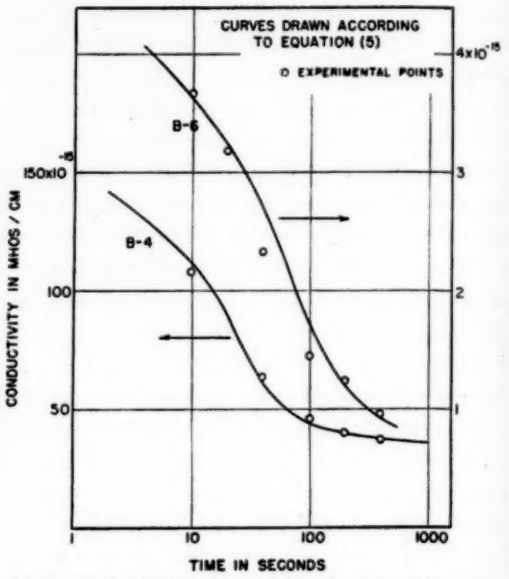

FIG. 3. Comparison of conductivities computed from Eq. (5) with experimental values.

The number of charges carried by the anion is unknown; because of association it probably increases with decreasing temperature, while at higher temperatures it approaches unity. Thus for the first oil at 60°C, and with $n = 1$, the value is 2.1×10^{-6} cm, whereas for the second oil at 30°C we can only write $0.3 \times 10^{-6}\ n$ cm.

In computing the concentration of ions from Eq. (7) that for the cations ($n = 1$) is 2×10^{12} per cc for oil *B*-4 and 1.5×10^{11} per cc for oil *B*-6. The number of anions is the same with the restriction that it contains $1/n$ as a factor.

In spite of these uncertainties it is felt that some useful information is obtained by the method suggested, and that it should be worth extending Whitehead's method to insulating liquids of known chemical constitution.

Ferromagnetic Anisotropy and the Itinerant Electron Model

HARVEY BROOKS
Harvard University, Cambridge, Massachusetts
(Received October 3, 1940)

The purpose of the present investigation is to explore the possibilities of the "itinerant" or "collective" electron picture in the theory of metals to explain the quenching of orbital angular momentum in solids and, through the introduction of l,s coupling, the phenomenon of ferromagnetic anisotropy in cubic crystals. The approach used is that of the Bloch "approximation of tight binding" in the theory of metals, the exchange energy being treated as a Weiss internal field as in the work of Stoner and Slater, and the spin-orbit coupling being introduced as a perturbation. The anisotropy is shown to appear in the fourth approximation, and to have the correct order of magnitude for iron and nickel. The model also predicts the correct sign of K_1 in nickel and iron, but this prediction is not entirely satisfactory because computational difficulties prevent the inclusion of all the d-wave functions in the calculation. A qualitative discussion of the behavior of iron-nickel alloys is given. The chief weakness of the model is its failure to take account adequately of Russell-Saunders coupling within the atom, and the dependence of many of its predictions on details of the model which are not very well established.

INTRODUCTION

A CONSIDERABLE amount of experimental data has accumulated in recent years on the magnetic anisotropy of ferromagnetic cubic crystals.[1] Most of the observed effects can be interpreted on the assumption that the crystal is composed of a number of magnetized domains,[2] whose energy depends upon the orientation of the magnetic intensity in the domain relative to the crystalline axes. Thus the energy of a domain takes the form

$$E=E_0+f(\alpha_1, \alpha_2, \alpha_3), \tag{1}$$

where $\alpha_1, \alpha_2, \alpha_3$ are the direction cosines of the magnetization. Fortunately the form of the function $f(\alpha_1, \alpha_2, \alpha_3)$ may be deduced from the symmetry class[3] of the crystal without any assumptions as to the mechanism responsible for the anisotropy. In a cubic crystal, for example, it may be shown that the energy must take the form

$$E=E_0+K_1(\alpha_1^2\alpha_2^2+\alpha_2^2\alpha_3^2+\alpha_1^2\alpha_3^2)+K_2(\alpha_1^2\alpha_2^2\alpha_3^2) \tag{2}$$

plus higher degree terms which have never been found necessary in practice. The magnitude and general properties of the coefficients K_1 and K_2 are not, of course, determined by the symmetry, but may be deduced from experiment.[1] The elucidation of the magnitude, sign, and temperature and alloy composition dependence of K_1 and K_2 is a task for the electron theory of metals. The Heisenberg exchange coupling, which accounts so nicely for the existence and general properties of the ferromagnetic state,[4] is of no use in explaining the anisotropy since it depends only on the relative orientations of neighboring spins and not on their absolute orientation with respect to the crystal. The earliest such mechanism proposed was the magnetic dipole interaction between spins. This interaction contains a term depending on the orientation of the spins with respect to the line joining them, and such terms are naturally structure dependent since they depend on the actual positions of the spins in the lattice. In cubic crystals, however, the magnetic interaction vanishes in first approximation because of the symmetrical arrangement of nearest neighbors, and the second approximation of perturbation theory gives much too small a magnitude for the anisotropy constants.[5] Bloch and Gentile[5] suggested instead that the spin-orbit coupling, acting in conjunction with the electrostatic coupling of the orbit to the crystal, would provide an anisotropy of the proper magnitude, and at present this is the generally accepted view. The two models are not dissimilar from the mathematical viewpoint, since, as Van Vleck[6] has

[1] R. M. Bozorth, J. App. Phys. **8**, 575 (1937); E. C. Stoner, *Magnetism and Matter* (Methuen, 1933).
[2] Cf., for example, W. Heisenberg, Zeits. f. Physik **69**, 287 (1931); R. M. Bozorth and E. C. Stoner, reference 1.
[3] F. Bitter, *Introduction to Ferromagnetism* (McGraw-Hill, 1938).
[4] W. Heisenberg, Zeits. f. Physik **49**, 619 (1928).
[5] R. Becker, Zeits. f. Physik **62**, 253 (1930); F. Bloch and G. Gentile, Zeits. f. Physik **70**, 395 (1931).
[6] J. H. Van Vleck, Phys. Rev. **52**, 1178 (1937).

indicated, the mechanism of Bloch and Gentile gives rise to an apparent dipole-dipole as well as quadrupole-quadrupole coupling which is of much greater magnitude than the purely magnetic interaction. Calculations using this somewhat phenomenological substitute for the true mechanism were undertaken from different viewpoints by Van Vleck and van Peype, a pupil of Kramers.[7]

In spite of their success these methods are not entirely satisfactory because of their semiphenomenological approach, and it therefore seems worth while to attempt a calculation with a more explicit model, which gives a more detailed insight into the origin of the coupling terms. Van Vleck's theory is based on the many-electron (Heisenberg) model, which is too complicated for rigorous solution. At Professor Van Vleck's suggestion, accordingly, we have treated ferromagnetic anisotropy from the standpoint of the "itinerant" or "collective" electron model of Bloch, Stoner, and Slater,[8] in which each electron is treated as belonging to the metal as a whole and as moving independently of the other electrons in a self-consistent field determined by the potential of the ions and the "time exposure" field of the other electrons. Although this model is a far poorer approximation for the tightly bound d electrons involved in ferromagnetism than the Heisenberg model, it leads to a secular equation which is reasonably manageable, and which, with the introduction of spin-orbit interaction, gives rise to ferromagnetic anisotropy in a straightforward manner.

Quenching of Orbital Momentum

The whole mechanism of ferromagnetic anisotropy bears an intimate relation to the quenching of the orbital angular momentum in solids. Determinations of the gyromagnetic ratio for the ferromagnetic metals and alloys give a g factor only slightly less than 2, showing that even though the electrons involved in the magnetic properties are d electrons, their orbital angular momentum is not free to orient and precess in an external field. This means that there is a powerful force within the crystal tending to orient the charge cloud around each atom in a definite manner with respect to the crystal axes. The weak magnetic coupling of the spin to the orbit insures that this force will be "felt" slightly by the spin, whose energy is therefore not entirely independent of orientation. The most obvious orienting or "quenching" mechanism would be the crystalline Stark effect,[9] lifting as it does the degeneracy between the various magnetic substates of a given total angular momentum, but unfortunately this is not an adequate mechanism for cubic crystals, where the asymmetry of the electrostatic field is not sufficient completely to destroy the degeneracy with respect to the magnetic quantum number. In a cubic field, as shown by Bethe,[9] an atomic d level subdivides into two levels, forming the representations Γ_3 and Γ_5 of the cubic group. The Γ_3 level is doubly degenerate but magnetically inactive, but the Γ_5 level is triply degenerate and possesses matrix elements of the magnetic moment between its substates. If the level is not completely filled in the solid state, therefore, we should expect contributions to the magnetic moment from the orbit as well as the spin, and a g factor considerably less than 2. In order to remove this discrepancy Sommerfeld and Bethe[10] suggested an additional quenching arising from an antiferromagnetic coupling between orbital angular momenta on different atoms, and this is the sort of quenching postulated by Van Vleck and van Peype. In the itinerant electron picture the quenching arises naturally from the hopping of electrons between adjacent atoms. Even in the tightly bound d band the hopping takes place with sufficient frequency to destroy any orientation in an external magnetic field. In more quantum-mechanical language, the situation may be described as follows. In the Heisenberg model each electron is confined to its own atom, and its energy levels are determined by a field having the symmetry of the point group about a fixed atom. In this field the representations and energy levels are degenerate as described above. In the

[7] W. van Peype, Physica **5**, 465 (1938).

[8] F. Bloch, Zeits. f. Physik **57**, 545 (1929); J. C. Slater, Phys. Rev. **49**, 537 (1936); E. C. Stoner, Proc. Roy. Soc. **A165**, 372 (1938).

[9] H. Bethe, Ann. d. Physik **3**, 137 (1929); Zeits. f. Physik **60**, 218 (1930); H. Kramers, Proc. Amst. Acad. **32**, 1176 (1929); **33**, 959 (1930); W. G. Penney and R. Schlapp, Phys. Rev. **41**, 194 (1932); **42**, 166 (1932); J. H. Van Vleck, *Electric and Magnetic Susceptibilities* (Oxford, 1932), Section 73.

[10] A. Sommerfeld and H. Bethe, *Handbuch der Physik* (second edition, Berlin, 1933), Vol. 24/2, p. 613.

itinerant model, on the other hand, each electron moves in a field whose symmetry is determined by the space group of the whole crystal, including translations as well as rotations. For the majority of wave vectors $\mathbf{k}$ the representations are nondegenerate, the space-group insuring the removal of the degeneracy which may exist under the point group alone. The reality of the resultant nondegenerate wave functions then precludes the existence of diagonal matrix elements of the magnetic moment, and such nondiagonal elements as there may be join states whose energy differences are large compared to the magnetic perturbation.

Approximate Structure of D Bands

In order to put these ideas on a quantitative basis it is necessary to say something about the form of the d bands in cubic crystals. This is a case where the Bloch "approximation of tight binding"[11] is reasonably reliable, since the overlapping of the d shells is small. The energy levels are just those of the single atom subject to the crystalline Stark effect, except that each level is broadened out into a band, arising from the possibility of leakage of electrons between atoms. When the original atomic levels are degenerate, however, the substates give rise to a number of overlapping bands, and considerable care is necessary in choosing the correct linear combinations of wave functions which diagonalize the perturbing energy.

In setting up the secular equation we confine ourselves to the Γ_5 level, although this is a poor assumption, in that there are matrix elements of the magnetic moment between the Γ_3 and Γ_5 levels as well as between the substates of Γ_5. For the purposes of this paper we shall assume that the separation between Γ_3 and Γ_5 is large compared to the broadening of the individual levels. The atomic wave functions of the Γ_5 level are:

$$\phi_1 = yzf(r), \quad \phi_2 = zxf(r), \quad \phi_3 = xyf(r). \tag{3}$$

In the approximation of tight binding we start with the linear combinations:[11]

$$\psi_n(\mathbf{k}) = N^{-\frac{1}{2}} \sum_{\mathbf{l}} \exp\,(ia\mathbf{l}\cdot\mathbf{k})\phi_n(\mathbf{r}-a\mathbf{l}), \tag{4}$$

where a is the lattice constant, N the total number of atoms in a domain, $\mathbf{l}$ a vector representing the lattice points. With these wave functions and a perturbing potential equal to the difference between the crystalline self-consistent field and the potential due to the free ion, the secular equation factors according to $\mathbf{k}$, but for each value of $\mathbf{k}$ there are in general matrix elements of the "hopping" energy (perturbing potential) between states of different n. Thus for each value of $\mathbf{k}$, the wave vector, the energy is obtained as a root of a third-degree secular equation:

$$\begin{vmatrix} H_1-E & H_{12} & H_{13} \\ H_{12} & H_2-E & H_{23} \\ H_{13} & H_{23} & H_3-E \end{vmatrix} = 0, \qquad \begin{aligned} H_1 &= \int \psi_1^*(\mathbf{k}) H \psi_1(\mathbf{k})\, d\tau, \\ H_{12} &= \int \psi_1^*(\mathbf{k}) H \psi_2(\mathbf{k})\, d\tau. \end{aligned} \tag{5}$$

This equation was first obtained by Jones and Mott[12] for the body-centered cubic lattice. In this case the matrix elements are:

$$\begin{aligned} H_1 = H_2 = H_3 &= -8A \cos\xi \cos\eta \cos\zeta, & H_{12} &= 8B \sin\xi \sin\eta \cos\zeta, \\ H_{23} &= 8B \cos\xi \sin\eta \sin\zeta, & H_{13} &= 8B \sin\xi \cos\eta \sin\zeta \end{aligned} \tag{6}$$

[11] F. Bloch, Zeits. f. Physik **52**, 55 (1928); N. F. Mott and H. Jones, *Properties of Metals and Alloys* (Oxford, 1936), Chapter II.

[12] H. Jones and N. F. Mott, Proc. Roy. Soc. **A162**, 49 (1937).

where ξ, η, ζ are defined by $\xi=\frac{1}{2}k_x a$, $\eta=\frac{1}{2}k_y a$, $\zeta=\frac{1}{2}k_z a$ and where

$$\begin{aligned} A &= -\int \phi_1(xyz) H' \phi_1(x+\tfrac{1}{2}a, y+\tfrac{1}{2}a, z+\tfrac{1}{2}a) dV, \\ B &= -\int \phi_1(xyz) H' \phi_2(x+\tfrac{1}{2}a, y+\tfrac{1}{2}a, z+\tfrac{1}{2}a) dV. \end{aligned} \tag{7}$$

Since the perturbing potential is negative, A and B are positive.[13]

For the face-centered cubic the matrix elements are readily obtained. The diagonal elements are:

$$\begin{aligned} H_1 &= 4A_1(\cos\xi\cos\eta+\cos\xi\cos\zeta)-4A_2\cos\eta\cos\zeta, \\ H_2 &= 4A_1(\cos\xi\cos\eta+\cos\eta\cos\zeta)-4A_2\cos\xi\cos\zeta, \\ H_3 &= 4A_1(\cos\xi\cos\zeta+\cos\eta\cos\zeta)-4A_2\cos\xi\cos\eta, \\ A_1 &= \int xyf(r)H'(x+\tfrac{1}{2}a)yf(|(x+\tfrac{1}{2}a)^2+y^2+(z+\tfrac{1}{2}a)^2|^{\frac{1}{2}})dV, \\ A_2 &= -\int xyf(r)H'(x+\tfrac{1}{2}a)(y+\tfrac{1}{2}a)f(|(x+\tfrac{1}{2}a)^2+(y+\tfrac{1}{2}a)^2+z^2|^{\frac{1}{2}})dV. \end{aligned} \tag{8}$$

A simple argument shows that A_1 and A_2 are positive as defined and that $A_2>A_1$.[14]

The off-diagonal elements are

$$H_{12}=-4B\sin\xi\sin\eta, \quad H_{23}=-4B\sin\eta\sin\zeta, \quad H_{13}=-4B\sin\xi\sin\zeta \tag{9}$$

and B as defined is positive.

Solutions of Secular Equation

1. Body-centered cubic

The solution has been obtained in approximate form by Jones and Mott.[12] The result is expressed in terms of a variable $x=(E/8B)+(A/B)\cos\xi\cos\eta\cos\zeta$. For most values of the wave vector the approximate solutions are:

$$x=0, \quad x=\pm\epsilon=\pm(a^2+b^2+c^2)^{\frac{1}{2}}, \tag{10}$$

where

$$a=\sin\xi\sin\eta\cos\zeta, \quad b=\sin\xi\cos\eta\sin\zeta, \quad c=\cos\xi\sin\eta\sin\zeta.$$

With these energies the approximate form of the diagonalizing transformation is:

	ϕ_1	ϕ_2	ϕ_3
0	$-c\epsilon^{-1}$	$b\epsilon^{-1}$	$a\epsilon^{-1}$
+	$\frac{1}{2}\sqrt{2}\tau\epsilon^{-1}$	$\frac{1}{2}\sqrt{2}\tau^{-1}(a+bc\epsilon^{-1})$	$\frac{1}{2}\sqrt{2}\tau^{-1}(b+ac\epsilon^{-1})$
−	$-\frac{1}{2}\sqrt{2}\tau\epsilon^{-1}$	$\frac{1}{2}\sqrt{2}\tau^{-1}(a-bc\epsilon^{-1})$	$\frac{1}{2}\sqrt{2}\tau^{-1}(b-ac\epsilon^{-1})$

(11)

where

$$\tau=(a^2+b^2)^{\frac{1}{2}}, \quad \epsilon=(a^2+b^2+c^2)^{\frac{1}{2}}.$$

This gives the energy correctly except for terms of order abc/ϵ^2, which happens to be small for most values of the wave vector $\mathbf{k}$. Thus the continuum generated by the three Γ_5 functions really consists of three overlapping bands. Each band is referred to an atomic function which is a linear combination of the functions (3), and which is different for each choice of propagation vector.

2. Face-centered cubic

We divide the secular equation through by $4B$ and define

$$x=(E/4B)-(A_1/B)(\cos\xi\cos\eta+\cos\xi\cos\zeta+\cos\eta\cos\zeta), \quad Q=(A_1+A_2)/B. \tag{12}$$

Here it must be remembered that $B<(A_1+A_2)$, and that therefore Q is large compared to unity. This being the case, the secular equation is largely dominated by its diagonal elements, except for the special values of $\mathbf{k}$ for which they become nearly equal. This means that in the face-centered cubic the original ϕ_1, ϕ_2, ϕ_3 are nearly the true atomic wave functions for the three bands of the Γ_5 level.

Similar results apply in the simple cubic lattice, but here it may be shown that the off-diagonal matrix elements vanish altogether so that the functions (3) are just correct.

[13] This follows from the fact that $xyf(r)$, $yzf(r)$, and $zxf(r)$ are even with respect to reflections along the body diagonal.

[14] A_1 is positive since the perturbing potential is negative while x and $x+\frac{1}{2}a$ have opposite signs on nearest neighbors. A_2 is positive because the integrand is positive in the region between nearest neighbors. $A_2>A_1$ because $y\sim 0$, i.e., the wave function has a node in the region of maximum perturbing potential.

Spin-Orbit Interaction

In order to carry on the discussion it is necessary to obtain the matrix elements of the spin-orbit interaction in the system of representation in which the band or "hopping" energy is diagonal. This interaction may be expressed in the form

$$O'=\sum_{\mathbf{l}} \zeta(|\mathbf{r}-a\mathbf{l}|)\mathbf{S}\cdot\mathbf{L}(\mathbf{r}-a\mathbf{l}), \tag{13}$$

where $\mathbf{L}(\mathbf{r}-a\mathbf{l})$ is the angular momentum operator about the atom at lattice position $\mathbf{l}$, and $\zeta(|\mathbf{r}-a\mathbf{l}|)$ is a function falling off as $1/r^3$ at large distances and depending only on the absolute magnitude of the radius vector.[15] O' is an operator which is periodic in the fundamental lattice translations, and hence is rigorously diagonal in $\mathbf{k}$.[16] Its matrix elements between Bloch functions of the same $\mathbf{k}$ and different n are furthermore independent of $\mathbf{k}$ to a first approximation. It is easily shown that

$$(n\mathbf{k}|\zeta(|\mathbf{r}-a\mathbf{l}|)\mathbf{S}\cdot\mathbf{L}(\mathbf{r}-a\mathbf{l})|n'\mathbf{k})=\sum_{\mathbf{l}} \exp(-ia\mathbf{l}\cdot\mathbf{k})\int \phi_{n'}(\mathbf{r}-a\mathbf{l})\zeta(r)\mathbf{S}\cdot\mathbf{L}\phi_n(\mathbf{r})dV. \tag{14}$$

If $\zeta(r)$ falls off sufficiently rapidly the integral in (14) will be inappreciable unless $\mathbf{l}=0$.[17] Thus we see that the matrix elements of the spin-orbit interaction with respect to Bloch functions are practically the same as between the corresponding atomic functions, that is

$$\int \psi_{n'}(\mathbf{k})O'\psi_n(\mathbf{k})dV=A(n'm_s'|\mathbf{S}\cdot\mathbf{L}|nm_s). \tag{15}$$

In this equation A is the ordinary spin-orbit interaction parameter for free atoms. It is the interaction for an individual electron, corresponding to the small a_i in Goudsmit's[18] notation, and must not be confused with the spin-orbit interaction parameter for the atom as a whole. The point is that we are here assuming the "hopping" energy sufficient completely to destroy the Russell-Saunders coupling within the atom, so that there is no question of the individual electronic angular momenta combining to form a resultant $\mathbf{L}$ and $\mathbf{S}$. This is a poor approximation since, owing to the tight binding of the d shell, there must be a rather high degree of internal coupling, but so far no way has been developed of taking it into account in the itinerant electron model, where the electrons are treated as essentially independent. We assume that the secular equation for the Γ_5 bands is diagonalized by a set of real transformation coefficients $a(\tau, n)$. In terms of this diagonal representation (labeled by the index τ), we find for the matrix elements of the spin-orbit interaction

$$\begin{aligned}(\tau m_s|\mathbf{S}\cdot\mathbf{L}|\tau'm_s')&=\sum a(\tau, n)(nm_s|\mathbf{S}\cdot\mathbf{L}|n'm_s')a(\tau', n')\\ &=\sum_{n<n'}\{a(\tau, n)a(\tau', n')-a(\tau', n)a(\tau, n')\}(nm_s|\mathbf{S}\cdot\mathbf{L}|n'm_s'),\end{aligned} \tag{16}$$

where the index n refers to the original set of atomic wave functions [Eq. (3)]. In this representation the spin is quantized along the z axis. In practice, however, the spin must be quantized parallel to the external field. In this new system of representation the matrix elements are as follows:

$$\begin{aligned}&(\tau_1, \tfrac{1}{2}|\mathbf{S}\cdot\mathbf{L}|\tau_2, \tfrac{1}{2})=-i\cos\theta', \qquad (\tau_1, \tfrac{1}{2}|\mathbf{S}\cdot\mathbf{L}|\tau_3, \tfrac{1}{2})=i\sin\theta'\sin\phi',\\ &(\tau_2, \tfrac{1}{2}|\mathbf{S}\cdot\mathbf{L}|\tau_3, \tfrac{1}{2})=-i\sin\theta'\cos\phi', \quad (\tau_1, \tfrac{1}{2}|\mathbf{S}\cdot\mathbf{L}|\tau_2, -\tfrac{1}{2})=\exp(-i\phi')[-i\sin\theta'],\\ &(\tau_1, \tfrac{1}{2}|\mathbf{S}\cdot\mathbf{L}|\tau_3, -\tfrac{1}{2})=\exp(-i\phi')[-\cos\phi'-i\cos\theta'\sin\phi'],\\ &(\tau_2, \tfrac{1}{2}|\mathbf{S}\cdot\mathbf{L}|\tau_3, -\tfrac{1}{2})=\exp(-i\phi')[-\sin\phi'+i\cos\theta'\cos\phi'].\end{aligned} \tag{17}$$

The angles θ', ϕ' are measured not with respect to the x, y, z axes but with respect to a new set of axes determined by the unit vectors $\mathbf{i}'$, $\mathbf{j}'$, $\mathbf{k}'$, which are defined in terms of the transformation coefficients as follows:

$$\mathbf{i}'=[a(\tau_1, 1), a(\tau_1, 2), a(\tau_1, 3)], \quad \mathbf{j}'=[a(\tau_2, 1), a(\tau_2, 2), a(\tau_2, 3)], \quad \mathbf{k}'=[a(\tau_3, 1), a(\tau_3, 2), a(\tau_3, 3)]. \tag{18}$$

[15] E. U. Condon and G. Shortley, *Theory of Atomic Spectra* (Cambridge, 1936), p. 120.
[16] N. F. Mott and H. Jones, reference 11, p. 59.
[17] A more detailed analysis of the spin-orbit effects would necessitate inclusion of the spin-other-orbit interaction. For atoms distant from the one in question this would tend to cancel out almost exactly the $1/r^3$ term arising from the ions, and so in effect $\zeta(r)$ would probably fall off exponentially rather than as $1/r^3$.
[18] S. Goudsmit, Phys. Rev. **31**, 946 (1928).

TABLE I. *Secular equation for ferromagnetic anisotropy, including spin-orbit interaction. Angles measured with respect to special skew axes determined by transformation coefficients, as shown in Eq. (18).*

	$\tau_1, \frac{1}{2}$	$\tau_2, \frac{1}{2}$	$\tau_3, \frac{1}{2}$	$\tau_1, -\frac{1}{2}$	$\tau_2, -\frac{1}{2}$	$\tau_3, -\frac{1}{2}$
$\tau_1, \frac{1}{2}$	$E_1+\delta-E$	$-iA\cos\theta'$	$iA\sin\theta'\sin\phi'$	0	$-iA\sin\theta'$	$-A\cos\phi'-iA\cos\theta'\sin\phi'$
$\tau_2, \frac{1}{2}$	$iA\cos\theta'$	$E_2+\delta-E$	$-iA\sin\theta'\cos\phi'$	$iA\sin\theta'$	0	$-A\sin\phi'+iA\cos\theta'\cos\phi'$
$\tau_3, \frac{1}{2}$	$-iA\sin\theta'\sin\phi'$	$iA\sin\theta'\cos\phi'$	$E_3+\delta-E$	$A\cos\phi'+iA\cos\theta'\sin\phi'$	$A\sin\phi'-iA\cos\theta'\cos\phi'$	0
$\tau_1, -\frac{1}{2}$	0	$-iA\sin\theta'$	$A\cos\phi'-iA\cos\theta'\sin\phi'$	$E_1-\delta-E$	$iA\cos\theta'$	$-iA\sin\theta'\sin\phi'$
$\tau_2, -\frac{1}{2}$	$iA\sin\theta'$	0	$A\sin\phi'+iA\cos\theta'\cos\phi'$	$-iA\cos\theta'$	$E_2-\delta-E$	$iA\sin\theta'\cos\phi'$
$\tau_3, -\frac{1}{2}$	$-A\cos\phi'+iA\cos\theta'\sin\phi'$	$-A\sin\phi'-iA\cos\theta'\cos\phi'$	0	$+iA\sin\theta'\sin\phi'$	$-iA\sin\theta'\cos\phi'$	$E_3-\delta-E$

Because of the unitary property of the transformation matrix the vectors $\mathbf{i}'$, $\mathbf{j}'$, $\mathbf{k}'$ form an orthogonal unit set, and θ', ϕ' are the polar angles of the magnetic field vector measured with respect to this set.

The complete secular problem, including the spin-orbit interaction, is of the sixth order, corresponding to the three overlapping bands of the Γ_5 level, and the two possible orientations of the spin. The secular determinant is shown in Table I. E_1, E_2, and E_3 are the energies of the three bands, and are, of course, functions of the wave vector $\mathbf{k}$. In this problem we have made the usual approximation of replacing the exchange energy by an internal "molecular" field $\delta=k\tau'\lambda$. Here λ is the fractional magnetization I/I_0, where I_0 is the saturation intensity, and $k\tau'$ is n_BJ, where n_B is the number of free spins per atom (electrons or holes) corresponding to the saturation magnetization; also J is the atomic exchange integral,[19] that is, the exchange integral between electronic wave functions normalized per unit cell rather than for the whole crystal. In the system of representation we have chosen, the energy matrix is diagonal in everything except the spin-orbit interaction, which may be considered as small compared to the difference between diagonal elements in Table I. Thus the solutions of the secular problem may readily be expanded in powers of the spin-orbit parameter A, the successive powers being obtained in the successive orders of perturbation theory.

DETAILED DERIVATION OF G FACTOR

We have already seen that the removal of the degeneracy of the cubic levels under the space group accounts for the almost complete quenching of the orbital angular momentum. There is, however, a secondary effect which allows the g factor to differ slightly from 2. Owing to the spin-orbit interaction there is in effect a small internal field tending to orient the orbital angular momentum, in addition to the large field acting on the spins and arising from exchange. The result of this field is always to make the g factor slightly less than 2. From the secular equation we obtain the first-order correction to the wave-functions by the usual perturbation method:

$$\psi=\phi_3^+-\frac{iA\sin\theta'\sin\phi'}{\epsilon_1}\phi_1^+-\frac{iA\sin\theta'\cos\phi'}{\epsilon_2}\phi_2^+ -\frac{A\cos\phi'+iA\cos\theta'\sin\phi'}{\epsilon_1+2\delta}\phi_1^- -\frac{A\sin\phi'-iA\cos\theta'\cos\phi'}{\epsilon_2+2\delta}\phi_2^-, \quad (19)$$

$$\epsilon_1=E_3-E_1, \quad \epsilon_2=E_3-E_2,$$

where ϕ_1, ϕ_2, ϕ_3 are the wave functions for the three bands and the indices $+$, $-$ stand for the spin directions. We must find the mean of the magnetic energy with respect to these wave functions. Unfortunately, since it is linear in the coordinates, the vector potential cannot be treated as a small perturbation throughout the crystal. This difficulty may be obviated by a method of gauge transformations due to Peierls and F. London,[20] in such a way that the magnetic energy for Bloch functions is the same as for the corresponding atomic functions.[21] The correction to the energy arising in this way is

$$\Delta E=-2\mu HA(\alpha_2'^2\epsilon_1^{-1}+\alpha_1'^2\epsilon_2^{-1})+O(A^2). \quad (20)$$

Here α_1', α_2' are direction cosines with respect to the skew axes defined by (18). Equation (20) gives the energy correction for one electron. To obtain the magnetic energy for the crystal as a whole we must sum over the occupied electronic states of the Fermi distribution, taking proper account of the symmetry properties of the energy

[19] J. C. Slater, E. C. Stoner, reference 8.

[20] R. Peierls, Zeits. f. Physik **80**, 763 (1933); F. London, J. de phys. et rad. **8**, 397 (1937).

[21] One naturally neglects diamagnetic effects arising from the migration of electrons among many atoms.

surfaces.[22] Finally dividing by the total angular momentum leads to a g factor

$$g=2+\tfrac{2}{3}A\langle\epsilon_1^{-1}+\epsilon_2^{-1}\rangle_{Av}. \quad (21)$$

The average is taken over all the occupied states for both directions of spin. Since the second term of (21) averages to zero when all the d levels are fully occupied, we may replace the average over the occupied states by the negative of the average over unoccupied states or "holes" of the distribution. In nickel and iron the band is nearly full, and most of the holes are in the highest of the three energy bands so that the energy differences $\epsilon_1(=E_3-E_1)$ and $\epsilon_2(=E_3-E_2)$ are positive for the overwhelming majority of the states involved in the averaging processes. Thus the second term of (21) is always negative, and the g factor is slightly less than 2, since A is positive for single electrons. This is in agreement with observation, and means simply that there is a slight tendency for the orbit to aline itself parallel to the orienting fields (external and internal). Assuming a spin-orbit parameter of about 500 cm^{-1}, and a mean band width of about 20,000 cm^{-1}, we obtain a g factor in the neighborhood of 1.97. Experimentally the departures from 2 range between 0.1 given by Barnett[23] to 0.004 obtained by Sucksmith and Bates for Ni.[24] Our calculated departure of 0.03 is thus of the correct order of magnitude.

Calculation of Anisotropy Constant

The calculation of the anisotropy constant K_1 is made by applying fourth-order perturbation theory to the secular equation shown in Table I. The energy corrections arising from lower orders of perturbation theory are easily shown to possess no angular dependence when the summation is carried out over all the occupied states. This result follows from the symmetry properties of the energy surfaces and is analogous to the argument usually employed to fix the form of the angular dependence in cubic crystals.[25] In carrying out the fourth-order calculation, we need include only terms whose angular dependence is of the form $\alpha_i'^2\alpha_j'^2$.[26] In this way we obtain for the fourth-order energy an expression

$$A_{12}\alpha_1'^2\alpha_2'^2+A_{23}\alpha_2'^2\alpha_3'^2+A_{13}\alpha_1'^2\alpha_3'^2 \quad (22)$$

in which α_1', α_2', α_3' are the direction cosines of the magnetic field with respect to the skew axes defined by (18), and A_{12}, A_{13}, A_{23} are given by the following expressions:

$$A_{12}=\frac{A^4}{2\delta}\left\{\frac{1}{\epsilon_1}-\frac{1}{\epsilon_2}-\frac{1}{\epsilon_1+2\delta}+\frac{1}{\epsilon_2+2\delta}\right\}^2+A^4\left\{\frac{1}{\epsilon_1}-\frac{1}{\epsilon_2}-\frac{1}{\epsilon_1+2\delta}+\frac{1}{\epsilon_2+2\delta}\right\}\left\{\frac{1}{\epsilon_1^2}-\frac{1}{\epsilon_2^2}-\frac{1}{(\epsilon_1+2\delta)^2}+\frac{1}{(\epsilon_2+2\delta)^2}\right\},$$

$$A_{23}=A^4\left\{\frac{1}{\epsilon_2}-\frac{1}{\epsilon_2+2\delta}+\frac{1}{2\delta}+\frac{1}{\epsilon_1}+\frac{1}{\epsilon_1+2\delta}\right\}\left\{\frac{1}{\epsilon_1}-\frac{1}{\epsilon_1+2\delta}\right\}^2, \quad (23)$$

$$A_{13}=A^4\left\{\frac{1}{\epsilon_1}-\frac{1}{\epsilon_1+2\delta}+\frac{1}{2\delta}+\frac{1}{\epsilon_2}+\frac{1}{\epsilon_2+2\delta}\right\}\left\{\frac{1}{\epsilon_2}-\frac{1}{\epsilon_2+2\delta}\right\}^2,$$

where now $\epsilon_1=E_3-E_1$, $\epsilon_2=E_3-E_2$, $\delta=n_BJI/I_0$.

In Eq. (22) we must expand the primed direction cosines in terms of the unprimed ones, using the definition of the primed axes: $\alpha_\tau'=\sum_n a(\tau,n)\alpha_n$, where the α_n are defined so that $\alpha_1=\alpha_x$, $\alpha_2=\alpha_y$, $\alpha_3=\alpha_z$. Substituting into Eq. (22), and using the symmetry argument once again, as well as the unitary property of the transformation coefficients, we obtain a relatively simple formula for the anisotropy constant K_1, namely

$$K_1=\tfrac{1}{3}\sum_{\mu<\nu}A_{\mu\nu}[1-5J_{\mu\nu}]\times\{\alpha_x^2\alpha_y^2+\alpha_x^2\alpha_z^2+\alpha_y^2\alpha_z^2\}, \quad (24)$$

[22] Brouckaert, Wigner and Smoluchowski, Phys. Rev. **50**, 58 (1936); Conyers Herring, Phys. Rev. **52**, 365 (1937). Cf. particularly Manning and Chodorow, Phys. Rev. **56**, 787 (1939), discussion in fine print at end of paper.

[23] S. J. Barnett, Rev. Mod. Phys. **7**, 129 (1935).

[24] W. Sucksmith and L. F. Bates, Proc. Roy. Soc. **A104**, 499 (1923); L. F. Bates, *Modern Magnetism* (Cambridge, 1939).

[25] Details of this argument, which is really quite obvious physically, are included in the author's thesis, Harvard (1940).

[26] It is to be understood, however, that all terms in the fourth power of the direction cosines such as $\alpha_1'^4$ are to be expressed as: $\alpha_1'^2(1-\alpha_2'^2-\alpha_3'^2)$.

where the $J_{\mu\nu}$ are defined by a biquadratic expression in the transformation coefficients:

$$J_{\mu\nu}=\sum_j [a(\mu,j)]^2[a(\nu,j)]^2. \qquad (25)$$

On account of the terms in $J_{\mu\nu}$ the anisotropy bears a very close relation to the structure of the energy bands. If the original wave functions $xyf(r)$, $yzf(r)$, $zxf(r)$ are a good set of atomic functions for setting up the Bloch waves which diagonalize the band energy, then the $J_{\mu\nu}$ will be small and the anisotropy, as will be shown, is negative. But if the bands are not well described by the functions $xyf(r)$, etc., but rather by linear combinations such as $\psi_\tau=\sum_n a(\tau, n)\phi_n$, then the $J_{\mu\nu}$ may become important, and the anisotropy may even change sign and become positive as we shall show to be the case for iron. This effect has no counterpart in the theories of Van Vleck and van Peype, but seems to be characteristic of the particular model we have adopted.

Nickel

The above discussion is well illustrated by the two common ferromagnetics nickel and iron. As can be seen by reference to the section on the structure of the d bands, nickel is a good example of the case where the functions $xyf(r)$, etc., are a good approximation and the $J_{\mu\nu}$ are small. To simplify the discussion we shall consider only the case of magnetic saturation, i.e., very low temperatures. The expressions for the $A_{\mu\nu}$ in Eq. (23) must be summed over all the occupied states in the three bands. The summation is carried out most readily by expressing each of the $A_{\mu\nu}$ as a sum $f_1(\delta)+f_2(\delta)$ of an even function of δ plus an odd function of δ, respectively ($f_1(\delta)=f_1(-\delta)$, $f_2(\delta)=-f_2(-\delta)$). Here δ, it must be remembered, is a quantity proportional to the exchange energy, whose sign is negative for spins parallel to the external field and positive for spins antiparallel to this field. The terms in the summation of the odd function cancel out in pairs for all states which are occupied by both directions of spin, so that we are left with a summation over only those states which contribute directly to the magnetic moment, whose spins are parallel to the external field. On the other hand, the summation for the even function must be carried out over all occupied states since the function has the same sign for both spin directions. However, $\sum f_1(\delta)$ vanishes when taken over all states, unoccupied and occupied alike, as follows by application of the diagonal sum rule to the matrix of Table I. Thus the sum over occupied states may be replaced by the negative of the sum over unoccupied states, and since the sign of δ is immaterial for the function $f_1(\delta)$, the summation may be carried out over exactly the same states as f_2, namely, those contributing directly to the magnetic moment. Thus we have the result: K_1 = sum over all occupied states of $(A_{12}+A_{23}+A_{13})$ = sum over states of unpaired spin of $-f_1(\delta)+f_2(-\delta)=-[f_1(\delta)+f_2(\delta)]$. The last is just the negative of Eqs. (23) summed over all the magnetic states, but with δ treated as a positive quantity. Since we are dealing with a band which is well over half full, most of the unpaired spins lie in the uppermost of the three Γ_5 bands, so that both the quantities ϵ_1 and ϵ_2 are positive. With these facts it is readily shown that $A_{\mu\nu}$ in Eq. (23) are all positive, irrespective of the numerical magnitudes of ϵ_1, ϵ_2, and δ. Thus the sign of K_1 in nickel is proved to be negative under quite general conditions.

The most recent results on the anisotropy of iron and nickel are due, for nickel, to Bozorth and Williams[27] who find $K_1=8\times10^5$ ergs/cc by extrapolation to absolute zero; for iron to L. P. Tarasov[28] who gives $K_1=5.3\times10^5$ ergs/cc at room temperature. The latter value would probably not be increased by a factor of more than 2 on extrapolation to absolute zero. It is of course impossible to reproduce these values to within better than a factor of 10 by means of the theory, but with this accuracy the theory predicts the correct order of magnitude. In his paper on ferromagnetism Slater[29] has given curves showing the distribution of states in the d band for copper, which he assumes to be similar to that of nickel. The six highest energy electrons, which presumably correspond to those occupying the states of the Γ_5 level in our model, occupy an energy range of about 50,000 cm^{-1}. Thus we

[27] H. J. Williams and R. M. Bozorth, Phys. Rev. **56**, 837 (1939).
[28] L. P. Tarasov, Phys. Rev. **56**, 1231 (1939).
[29] J. C. Slater, Phys. Rev. **49**, 537 (1936).

should not be far off in taking as a mean value for the separation of levels of the same $\mathbf{k}$, (i.e., the quantities ϵ_1 and ϵ_2 in Eq. (23)), a value of 10,000 cm^{-1}. Slater has also estimated the value of the exchange integral δ, assuming that it arises from intra-atomic exchange. On the face of it, this seems highly unlikely, but the work of Stoner,[30] on the other hand, certainly indicates that the exchange energy cannot be much less than the band spread if ferromagnetism is to occur at all. We should probably not be far off in taking 2δ equal to 8000 cm^{-1} for nickel. Estimates of the spin-orbit parameter A have been made for the transition elements by Goudsmit.[18] Again these estimates cannot be taken too seriously in the solid state, not only because of the uncertainty arising from the incomplete destruction of Russell-Saunders coupling, but also because of the entirely altered screening effect of the conduction electrons in the solid phase.[31] With Goudsmit's estimate of $A=630$ cm^{-1} for nickel, we obtain a value of K_1 between 10^5 and 10^6 ergs/cc, which is the correct order of magnitude. The screening effect of the conduction electrons would tend to reduce the estimate of the spin-orbit parameter somewhat, and provide worse agreement with experiment. For iron Goudsmit estimates $A=390$ cm^{-1}, which would give an anisotropy for iron less than $\frac{1}{8}$ that of nickel, other factors being equal. However, the order of magnitude is still correct, and most of the discrepancy can be accounted for by the greater exchange energy in iron, and the greater number of spins per cc.

Sign of K_1—Iron

Iron is a good example of the case where the $J_{\mu\nu}$ of Eqs. (24) and (25) are not negligible. This arises from the fact in the body-centered cubic the diagonal elements of the secular equation for the "hopping" energy are all the same. For the highest of the three Γ_8 bands, namely the band corresponding to $x=+\epsilon$ in Eq. (10), the $J_{\mu\nu}$ may be obtained from the transformation matrix (11) by means of (25), and are as follows:

$$J_{12}=R, \quad J_{23}=R, \quad J_{13}=\tfrac{1}{2}(1-R),$$
$$R=(a^2b^2+a^2c^2+b^2c^2)/\epsilon^4, \tag{26}$$
$$\epsilon=(a^2+b^2+c^2)^{\frac{1}{2}}.$$

a, b, c are defined in terms of the components of the wave vector, as shown in Eq. (10). The maximum value of R is $\frac{1}{3}$.

With these values of $J_{\mu\nu}$, the anisotropy constant follows from Eq. (24). The exact expression is very complicated, but it may be very closely approximated by the formula:

$$K_1=\frac{4\delta^2}{\epsilon^2(\epsilon+2\delta)^2}\left[\frac{1}{6\delta}+\frac{2}{3\epsilon}\right]. \tag{27}$$

This expression applies only to the uppermost of the three bands, in which most of the electrons will lie in practice. The expression is easily seen to be positive for all positive values of ϵ and δ, in agreement with the observed positive sign of K_1 in iron.

The theory is very attractive in that it makes a satisfactory unambiguous prediction of the correct sign of K_1 in nickel and iron. When we come to examine the data on alloys, however, some difficulties begin to appear. The theory suggests, for example, that the sign of the anisotropy is to be correlated with the crystal structure, the difference between iron and nickel arising from the difference in the form of the energy bands between the face-centered and the body-centered lattices. Yet the observations on the Fe-Ni alloy system[32] show no marked discontinuity in the anisotropy as we pass from the face-centered to the body-centered phase. In fact the change in sign of K_1 takes place well within the γ-phase (face-centered) at a composition corresponding to one free spin per atom. All the alloy data suggest a much closer correlation of the anisotropy with the number of free spins per atom than with the crystal structure. In spite of this it is possible to devise a crude qualitative explanation of the alloy data, based on the itinerant electron model, somewhat as follows. In our discussion of the band structure of nickel we assumed that the off-diagonal matrix elements of

[30] E. C. Stoner, Proc. Roy. Soc. **A165**, 372 (1938).
[31] This effect is discussed in detail by M. F. Manning and M. I. Chodorov, Phys. Rev. **56**, 787 (1939).
[32] R. M. Bozorth, reference 1.

the "hopping" energy could be neglected. This is true in the approximation of very tight binding, but at the lattice spacing which actually obtains in nickel it is probably a very poor assumption except in portions of the Brillouin Zone in which $\sin \xi$, $\sin \eta$, and $\sin \zeta$ are very small, where, as a consequence, the off-diagonal matrix elements are negligible. The electrons or holes in the highest energy states occupy just such a portion of **k**-space. Now, nickel has only 0.6 free spin per atom, and most of these lie in states very near the maximum. We should therefore expect the anisotropy of nickel to be negative, since small off-diagonal elements of the "hopping" energy imply small $J_{\mu\nu}$ in Eq. (24) and hence negative K_1. As iron is added the number of free spins per atom increases rapidly. The additional holes are forced into parts of **k**-space where the off-diagonal "hopping" integrals are large, and these holes will therefore tend to have positive K_1, opposing the effect of holes higher in the band, until finally the interior holes predominate and cause the K_1 for the whole crystal to change sign. For the body-centered phase a somewhat similar explanation applies in reverse. Here the experiments indicate a gradual falling off of K_1 with increasing percentage of nickel. In our model of the body-centered structure we have neglected the effect of next nearest neighbors. This effect will indeed be small except when the off-diagonal elements of the hopping energy are small, namely, near the top of the band. In this case the secular equation for the hopping energy takes a form similar to that for the simple cubic, since the next nearest neighbors lie in the same relative positions as the nearest neighbors in the simple cubic. Thus holes very near the top of the band in iron may be expected to make a negative contribution to K_1, since K_1 for a simple cubic may easily be shown to be negative in our model. Now the addition of nickel to iron decreases the number of free holes, and so increases the relative number of states of negative anisotropy, as these lie closest to the top of the band and so tend to hang on to the bitter end, as it were. There will thus be a gradual decrease of the positive anisotropy of iron with increasing percentage of nickel, in agreement with experiment.

This explanation of the alloy data is very rough, and an attempt at quantitative verification of it with the present model did not prove successful. Nevertheless, the effects calculated were in the right direction, if not of sufficient magnitude to substantiate the qualitative discussion. This is hardly surprising in view of the very approximate nature of our treatment of the band structure.

It would be desirable to obtain some idea of the temperature variation of K_1. Unfortunately, this would involve integration over the distribution with a Fermi distribution function, a task in which the labor involved is hardly commensurate with the results obtainable from so crude a picture of the band structure. It was at first believed that the temperature variation could be represented by a formula such as (27), the anisotropy being expressed as a function of magnetization as in Van Vleck's theory. The variation obtained from this formula, however, is much too slow, being of the order of the square of the magnetization instead of the tenth power as observed experimentally for iron.[33] The agreement with experiment in this respect is considerably worse than in Van Vleck's theory. Probably most of the discrepancy can be taken care of under the assumption of variations of the $J_{\mu\nu}$ in Eq. (24) arising from thermal excitation of the band electrons.

In conclusion I should like to express my thanks to Professor Van Vleck for suggesting the problem and for many helpful discussions and suggestions during the course of the work.

[33] N. Akulov, Zeits. f. Physik **100**, 197 (1936).

The Thermodynamics of Irreversible Processes

III. Relativistic Theory of the Simple Fluid

CARL ECKART
Ryerson Physical Laboratory, University of Chicago, Chicago, Illinois
(Received September 26, 1940)

The considerations of the first paper of this series are modified so as to be consistent with the special theory of relativity. It is shown that the inertia of energy does not obviate the necessity for assuming the conservation of matter. *Matter* is to be interpreted as number of molecules, therefore, and not as inertia. Its velocity vector serves to define local proper-time axes, and the energy momentum tensor is resolved into proper-time and -space components. It is shown that the first law of thermodynamics is a scalar equation, and not the fourth component of the energy-momentum principle. Temperature and entropy also prove to be scalars. Simple relativistic generalizations of Fourier's law of heat conduction, and of the laws of viscosity are obtained from the requirements of the second law. The same considerations lead directly to the accepted relativistic form of Ohm's law.

INTRODUCTION

IN the second paper of this series,[1] the theory of ϵ-substitutions was outlined, and it was shown that this device can be used to simplify the derivation of some thermodynamic formulae. However, the author was reluctant to use it in the derivation of any fundamental formulae because the ϵ-substitution depends on the fact that the internal energy contains an arbitrary additive constant, while the principle of the equivalence of mass and energy appears to give an absolute meaning to the energy content of any portion of matter. Thus it seemed possible that in a relativistic theory of thermodynamics, ϵ-substitutions might be inadmissible. The considerations which follow show that this is not the case. To establish this result, it was necessary to develop a complete relativistically invariant theory of the simple fluid—a project which is of interest in itself, even though the departures of such a theory from a classical theory must be negligible in most cases.

In I, four general principles were used: (a) The conservation of matter; (b) the conservation of momentum; (c) the conservation of energy; and (d) Kelvin's hypothesis concerning the thermodynamic temperature. It might seem as though the equivalence of mass and energy would make (a) superfluous in a relativistic theory. This is not the case, as becomes clear if *matter* is interpreted as number of molecules rather than inertia. The principles (b) and (c) combine into a single tensor equation, as is well known. This is somewhat disconcerting, for the first law of thermodynamics is a scalar equation; its relation to the energy-momentum principle must be discovered. Moreover, the correct form of the energy-momentum tensor is still a matter of discussion, and some assumption must be made before the theory can be completed. Finally, Kelvin's hypothesis involves Fourier's law of heat conduction, and the relativistic generalization of this presents a difficulty, arising from the fact that in the classical theory there is a three-vector that represents the flow of heat, but no density of heat to combine with it to form a four-vector. A somewhat similar difficulty arises in connection with the stress-tensor.[2] It will be shown that all of these problems can be solved in a systematic manner if one defines proper-time and proper-space in terms of the velocity of matter.

MATTER, PROPER-TIME, AND PROPER-SPACE

A Galilean coordinate system ($x^0=ct$, x^1, x^2, x^3) will be assumed, in which the metric tensor is

$$g^{\alpha\beta}=\begin{matrix}-1 & 0 & 0 & 0\\ 0 & 1 & 0 & 0\\ 0 & 0 & 1 & 0\\ 0 & 0 & 0 & 1\end{matrix} \qquad (1)$$

[1] C. Eckart, Phys. Rev. **58**, 267, 269 (1940); hereafter cited as I and II, respectively.

[2] R. C. Tolman has solved this problem for the stresses; see his *Theory of the Relativity of Motion* (University of California Press, 1918), Chap. X, and *Relativity, Thermodynamics and Cosmology* (Oxford, 1934), Chap. III.

and this tensor will be used to raise and lower indices in the usual manner. Matter will be represented by a four-vector, m^α, which has the units g/cm^3, and depends only on the molecular weight and on the motion of the molecules. The inertia and internal energy of the molecules will be introduced later, so that the molecular weight is to be considered only as a convenient conversion factor. The conservation of matter is expressed by the equation

$$\partial m^\alpha/\partial x^\alpha = 0. \tag{2}$$

It is to be assumed that $m^0 > 0$, and that the invariant density

$$m = (-g_{\alpha\beta} m^\alpha m^\beta)^{\frac{1}{2}} \tag{3}$$

is real and positive. The (dimensionless) velocity of matter is

$$u^\alpha = m^\alpha/m, \tag{4}$$

so that

$$u_\alpha u^\alpha = -1 \tag{5}$$

and

$$u^\alpha(\partial u_\alpha/\partial x^\beta) = u_\alpha(\partial u^\alpha/\partial x^\beta) = 0. \tag{6}$$

The vector u^α will be a function of the coordinates, and will determine a direction at each point of four-space—the local axis of proper-time. Three directions orthogonal to this are the local axes of proper space. Any vector F^α, then gives rise to a scalar and a vector by means of the equations

$$f = -u_\alpha F^\alpha, \tag{7}$$

$$f^\alpha = s_\beta{}^\alpha F^\beta, \tag{8}$$

$$s_\beta{}^\alpha = \delta_\beta{}^\alpha + u^\alpha u_\beta. \tag{9}$$

The scalar f is the projection of F^α on the axis of proper-time, and f^α is the projection of F^α into proper-space. It is easily seen that

$$F^\alpha = fu^\alpha + f^\alpha$$

and that

$$u_\alpha s_\beta{}^\alpha = 0, \quad u^\beta s_\beta{}^\alpha = 0. \tag{10}$$

Covariant vectors can be resolved into proper components in an analogous manner.

The tensor $s_\beta{}^\alpha$ has several important properties: it is easily seen that

$$s_\beta{}^\alpha s_\gamma{}^\beta = s_\gamma{}^\alpha \tag{11}$$

and

$$\begin{aligned} s^{\alpha\beta} &= s_\gamma{}^\alpha g^{\gamma\beta} \\ &= g^{\alpha\beta} + u^\alpha u^\beta \end{aligned} \tag{12}$$

is a symmetric tensor. A simple calculation shows that

$$s^{\alpha\beta} = s^{\alpha\gamma} s_\gamma{}^\beta = s_\delta{}^\alpha g^{\delta\gamma} s_\gamma{}^\beta, \tag{13}$$

so that, because of Eq. (5),

$$s^{\alpha\beta} F_\alpha F_\beta = g^{\gamma\delta} f_\gamma f_\delta \geqslant 0, \tag{14}$$

the equality holding only when $F_\alpha = fu_\alpha$.

This resolution of vectors into time and space components is quite consistent with Einstein's theory of simultaneity, since there is no reference to separated points of four-space. This becomes clearer on defining the proper-rate of change of a quantity:

$$D\phi = u^\alpha(\partial\phi/\partial x^\alpha). \tag{15}$$

This may be called the derivative of ϕ with respect to proper-time. However, proper-time itself has not yet been defined; one may try to define it by the equation

$$D\tau = 1$$

but this does not determine a unique function τ. To make τ unique, it is necessary to specify one surface in four-space on which $\tau = 0$, i.e., one locus of simultaneous events. The essence of Einstein's theory is that this locus cannot be specified in a physically unique manner, so that τ remains somewhat arbitrary. The differential operator D is unique, however, and corresponds closely to the classical operator D/Dt.

The Eq. (2) is readily transformed into

$$\partial u^\alpha/\partial x^\alpha = -vDm = mDv, \tag{16}$$

where $v = 1/m$ is the invariant specific volume (cf. I, Eq. (2)). Equation (6) yields

$$u^\alpha Du_\alpha = u_\alpha Du^\alpha = 0. \tag{17}$$

Resolution of the Energy-Momentum Tensor into Proper Components

The energy-momentum principle will be assumed in the usual relativistic form,

$$\partial W^{\alpha\beta}/\partial x^\alpha = 0, \quad W^{\alpha\beta} = W^{\beta\alpha}, \tag{18}$$

the units of W being erg/cm^3.

The equation obtained by setting $\beta = 0$ in Eq. (18) is variously called the equation of conservation of matter, of mass or inertia, and of energy. It seems to the author that, while each of these designations can be justified in

special cases, the first two are misleading in general. He would prefer to retain only the third, and refer to the equation $W^{\alpha 0}=W^{0\alpha}$ as the principle of the inertia of energy. Even the third is misleading unless a distinction is made between the principle of conservation of energy and the first law of thermodynamics, the two being identical only when matter is at rest (see below).

For the moment, no assumption will be made concerning the form of $W^{\alpha\beta}$, but it will be used in defining other quantities, such as the internal energy and heat flow. Assumptions concerning the form of these quantities will be made below.

The tensor W may be resolved into proper-components: if

$$w=W^{\alpha\beta}u_\alpha u_\beta, \tag{19}$$

$$w^\alpha=-s_\beta{}^\alpha W^{\beta\gamma}u_\gamma, \tag{20}$$

$$w^{\alpha\beta}=s_\gamma{}^\alpha s_\delta{}^\beta W^{\gamma\delta}, \tag{21}$$

then

$$W^{\alpha\beta}=wu^\alpha u^\beta+w^\alpha u^\beta+w^\beta u^\alpha+w^{\alpha\beta}. \tag{22}$$

It will appear that each of these components has an important physical interpretation. Thus, w is the invariant density of energy (erg/cm³). The internal energy, ϵ (erg/g=cm²/sec.²), is appropriately defined by

$$m(\epsilon+a)=w, \tag{23}$$

a being an arbitrary constant. It will appear that a does not enter into the first law of thermodynamics. The vector

$$q^\alpha=cw^\alpha \tag{24}$$

is the heat flow in erg/cm² sec.; the equation

$$u_\alpha q^\alpha=0, \tag{25}$$

which follows from Eq. (10) and (20), corresponds to the absence of a density of heat in the classical theory. The symmetric tensor $-w^{\alpha\beta}$ is the stress tensor (dynes/cm²); the equation

$$u_\alpha w^{\alpha\beta}=0 \tag{26}$$

reduces the number of its independent components to six, as in the classical theory.

The First Law of Thermodynamics

The first law of thermodynamics can be derived from Eq. (18) and the definitions just adopted. Multiplying Eq. (18) scalarly by $-u_\beta$ and rearranging, we have

$$-(\partial/\partial x^\alpha)(u_\beta W^{\alpha\beta})+W^{\alpha\beta}(\partial u_\beta/\partial x^\alpha)=0; \tag{27}$$

because of Eqs. (19), (20), (22)

$$\begin{aligned}-u_\beta W^{\alpha\beta}&=wu^\alpha+w^\alpha\\&=m(\epsilon+a)u^\alpha+q^\alpha/c.\end{aligned}$$

Since $mu^\alpha=m^\alpha$, Eq. (2) results in the disappearance of a from the equation:[3]

$$\begin{aligned}-(\partial/\partial x^\alpha)(u_\beta W^{\alpha\beta})&=(\partial/\partial x^\alpha)(m\epsilon u^\alpha+q^\alpha/c)\\&=mD\epsilon+(1/c)(\partial q^\alpha/\partial x^\alpha).\end{aligned}$$

Equations (6) and (22) result in

$$W^{\alpha\beta}(\partial u_\beta/\partial x^\alpha)=w^\beta Du_\beta+w^{\alpha\beta}(\partial u_\beta/\partial x^\alpha),$$

so that finally Eq. (27) becomes

$$\begin{aligned}mD\epsilon+(1/c)[(\partial q^\alpha/\partial x^\alpha)+q^\alpha Du_\alpha]\\+w^{\alpha\beta}(\partial u_\beta/\partial x^\alpha)=0.\end{aligned} \tag{28}$$

This is to be compared with the classical form of the first law (cf. I, Eq. (7))

$$m(D\epsilon/Dt)+\nabla\cdot\mathbf{q}-(\mathfrak{p}\cdot\nabla)\cdot\mathbf{V}=0,$$

$\mathbf{q}$ being the heat flow, $\mathbf{V}$ the velocity and $\mathfrak{p}$ the total stress. The terms of the two equations are in an obvious correspondence, except that the term $(1/c)q^\alpha Du_\alpha$ does not appear in the classical case. This term is very small in all ordinary cases, and may be interpreted as the work done by a flow of heat through accelerated matter—a phenomenon not envisaged by the classical theory.

---

[3] It will be noted that, up to this point, the introduction of the matter vector, m^α, served no purpose except to define the density and velocity of matter, m and u^α. Tolman, reference 2, and others avoid introducing m^α, but cannot avoid introducing u^α. At this place in the considerations, however, it becomes important that matter be conserved (Eq. (2)). If this were not the case, the constant a would enter into the first law of thermodynamics, Eq. (28), in the form of a term $a(\partial m^\alpha/\partial x^\alpha)$. In other words, the creation or annihilation of matter requires energy absorption or release. This is as it should be, and indicates that the theory of ϵ-substitutions may be used even in relativistic considerations, except when matter is being created or destroyed. The theory of such nuclear processes is beyond the scope of the present paper, particularly insofar as electric charges and radiation are involved. Insofar as only heavy particles are involved, the device of using mass numbers (integers) in the definition of m^α (and thus including the packing-fraction energy in ϵ) will insure the validity of Eq. (2).

The Simple Fluid and the Second Law of Thermodynamics

The theory of the simple fluid is of considerable importance, since in this case it is possible to prove the existence of temperature and entropy (cf. I, Eq. (9) *et seq.*). The appropriate definition of the hydrostatic pressure is

$$p=\tfrac{1}{3}w_\alpha{}^\alpha \tag{29}$$

and it is to be assumed that the viscous stress tensor,

$$P^{\alpha\beta}=-w^{\alpha\beta}+ps^{\alpha\beta} \tag{30}$$

is a linear function of $(\partial u_\gamma/\partial x^\delta)$ and proportional to the scalar coefficient of viscosity, λ. This together with the equations

$$u_\alpha P^{\alpha\beta}=0, \quad P_\alpha{}^\alpha=0, \tag{31}$$

which follow from Eqs. (29) and (30), restricts the form of P very materially. The equation

$$P^{\alpha\beta}=\lambda c\{s^{\alpha\gamma}s^{\beta\delta}[(\partial u_\gamma/\partial x^\delta)+(\partial u_\delta/\partial x^\gamma)] -\tfrac{2}{3}s^{\alpha\beta}s^{\gamma\delta}(\partial u_\gamma/\partial x^\delta)\} \tag{32}$$

is very strongly indicated, if not uniquely determined. At any rate, this expression for P satisfies Eq. (31), and differs from the classical expression only by terms that are ordinarily negligible (see below).

Since

$$s^{\alpha\beta}(\partial u_\beta/\partial x^\alpha)=(\partial u^\alpha/\partial x^\alpha)=mDv$$

by Eqs. (6), (12), and (16), the Eq. (28) becomes

$$m(D\epsilon+pDv)+(1/c)[(\partial q^\alpha/\partial x^\alpha)+q^\alpha Du_\alpha] -P^{\alpha\beta}(\partial u_\beta/\partial x^\alpha)=0. \tag{33}$$

For the simple fluid, ϵ is a function of p and v only, so that there are two functions θ and η such that

$$D\epsilon+pDv=\theta D\eta; \tag{34}$$

the proof is identical with that given in I. Since ϵ, p and v are scalars, θ and η will also be scalars.[4] Substituting in Eq. (33) and rearranging, we obtain

$$mD\eta+(\partial/\partial x^\alpha)(q^\alpha/c\theta)=-(1/c\theta^2)q^\alpha[(\partial\theta/\partial x^\alpha) +\theta Du^\alpha]+(1/\theta)P^{\alpha\beta}(\partial u_\beta/\partial x^\alpha). \tag{35}$$

[4] The scalar character of η appears to be generally accepted (cf. Tolman, *Relativity of Motion*, Chap. XI). However, M. Planck introduced a nonscalar quantity, T, which he identified with temperature, and which appears to be related to the present θ by the equation $T=\theta u^0$. Tolman introduces a quantity T° which appears to be identical with θ.

The inequality

$$mD\eta+(\partial/\partial x^\alpha)(q^\alpha/c\theta)\geqslant 0 \tag{36}$$

cannot be proved without some assumption concerning the relativistic form of Fourier's law and Kelvin's hypothesis. The simplest assumption leading to Eq. (36) is that

$$q^\alpha=-ks^{\alpha\beta}[(\partial\theta/\partial x^\beta)+\theta Du_\beta], \tag{37}$$

which satisfies Eq. (25) and reduces to the classical Fourier's law when ordinarily negligible terms are canceled (see below). The scalar $k(\geqslant 0)$ is the thermal conductivity of the fluid. The term $s^{\alpha\beta}(\partial\theta/\partial x^\beta)$ is obviously the relativistic temperature gradient. The term $-\theta Du_\beta$ has no classical analog, and implies an isothermal flow of heat in accelerated matter, in the direction opposite to the acceleration. It is ordinarily small, and may be explained as due to the inertia of energy. Equation (37) shows that $q^\alpha=0$ when the vector $\partial\theta/\partial x^\beta+\theta Du_\beta$ is parallel to the proper-time axis. This seems strange at first, but on reflection, it is seen to correspond to the fact that, in the classical theory, there will be no flow of heat if $\nabla\theta=0$ even though $\partial\theta/\partial t\neq 0$—i.e., that there are adiabatic changes of temperature.

As was discussed in I, Eq. (34) does not determine θ and η uniquely; however, if it be assumed that Eq. (37) holds for two of the possible functions θ, θ_0 and all possible values of

$$s^{\alpha\beta}(\partial v/\partial x^\beta), \quad s^{\alpha\beta}(\partial p/\partial x^\beta), \quad s^{\alpha\beta}Du_\beta,$$

then it can be shown as in I that

$$\theta/\theta_0=\text{const.}$$

Thus Eq. (37) fixes the definition of the temperature except for a choice of unit.

From Eqs. (14) and (37), it follows at once that

$$-(1/c\theta^2)q^\alpha[(\partial\theta/\partial x^\alpha)+\theta Du_\alpha]\geqslant 0. \tag{38}$$

It therefore remains to show that

$$P^{\alpha\beta}(\partial u_\beta/\partial x^\alpha)\geqslant 0, \tag{39}$$

the positiveness of λ and θ being assumed. For this purpose, the attention may be fixed on a single arbitrary point, A, in four-space. If the time-axis of the Galilean coordinate system is chosen parallel to the proper-time axis at A,

then at this point,

$$u^\alpha = 1, 0, 0, 0, \qquad u_\alpha = -1, 0, 0, 0, \tag{40}$$

and

$$s^{\alpha\beta} = \begin{matrix} 0 & 0 & 0 & 0 \\ 0 & 1 & 0 & 0 \\ 0 & 0 & 1 & 0 \\ 0 & 0 & 0 & 1. \end{matrix} \tag{41}$$

Substitution into Eq. (32) shows that

$$P^{00} = P^{01} = \cdots = 0,$$

while

$$P^{11} = \tfrac{2}{3}\lambda c\{[(\partial u_1/\partial x^1) - (\partial u_2/\partial x^2)] + [(\partial u_1/\partial x^1) - (\partial u_3/\partial x^3)]\}, \tag{42}$$

$$P^{12} = \lambda c[(\partial u_1/\partial x^2) + (\partial u_2/\partial x^1)], \text{ etc.},$$

which are the classical expressions for the viscous stresses. It then follows, as in I, that Eq. (39) is true at the point A, and thus everywhere in four-space.

The Momentum of Heat

The general principle of the inertia of energy leads one to expect that a flow of heat q will be associated with a momentum q/c^2. This result can be read out of the form of the energy-momentum tensor (Eqs. (22) and (24)), but it is interesting to consider the question in somewhat more detail. It will be supposed that the fluid is at rest in the Galilean system x^α, so that Eqs. (40) and (41) are valid at all points of four-space and $P^{\alpha\beta} = 0$. Then Eq. (37) yields

$$q^0 = 0$$
$$q^\kappa = -k\partial\theta/\partial x^\kappa, \quad \kappa = 1, 2, 3,$$

while Eq. (2) becomes

$$\partial m/\partial t = 0$$

so that m and v are functions of x^1, x^2, x^3 only. The components of the energy-momentum tensor are

$$W^{00} = m(\epsilon + a),$$
$$W^{0\kappa} = q^\kappa/c = W^{\kappa 0},$$
$$W^{\kappa\mu} = p\delta^{\kappa\mu}.$$

The Eqs. (18) become

$$m(\partial\epsilon/\partial t) + (\partial q^\kappa/\partial x^\kappa) = 0 \tag{43}$$

and

$$(\partial/\partial t)(q^\kappa/c^2) + (\partial p/\partial x^\kappa) = 0. \tag{44}$$

Equation (43) is the equation of conservation of energy, and is (in this case only!) identical with the first law, Eq. (33). The Eqs. (44) are the momentum equations, and it is immediately seen that q^κ/c^2 is a momentum, since its time rate of increase is equal to the negative gradient of the pressure.

Ohm's Law

The general problem of thermoelectromagnetic phenomena is too complex for brief discussion, but it is of interest to indicate how these phenomena may be included in the present theory. Consider an ideal fluid whose internal energy is independent of the electromagnetic quantities, but which is an electric conductor. A molten metal approximates such a fluid, but shows thermoelectric effects, etc., which indicate a slight dependence of its internal energy on the electromagnetic variables.

Let j^α be the electric current density in e.m.u./cm² sec. = e.s.u./cm³, and

$$F^{\alpha\beta} = \begin{matrix} 0 & -E_x & -E_y & -E_z \\ E_x & 0 & -B_z & B_y \\ E_y & B_z & 0 & -B_x \\ E_z & -B_y & B_x & 0 \end{matrix} \tag{45}$$

be the field tensor, the E's being the electric field in e.s.u., the B's the magnetic induction in e.m.u. The energy-momentum principle is now to be formulated as

$$\partial W^{\alpha\beta}/\partial x^\alpha = j_\alpha F^{\alpha\beta}. \tag{46}$$

The tensor W can be resolved into components as before, and the first law becomes

$$-(\partial/\partial x^\alpha)(u_\beta W^{\alpha\beta}) + W^{\alpha\beta}(\partial u_\beta/\partial x^\alpha) = -j_\alpha u_\beta F^{\alpha\beta}. \tag{47}$$

This may be transformed into an equation similar to Eq. (33), except that the right side is not zero, but the same as that of Eq. (47).

The entropy and temperature may be introduced in exactly the same manner as above, and an equation, differing from Eq. (35) only by the additional term

$$-(1/\theta)j_\alpha u_\beta F^{\alpha\beta}$$

can be deduced. The Eq. (36) requires this

term to be positive for all possible values of j_α and u_β; this will certainly be the case if (with $\sigma>0$ and ρ a scalar)

$$j^\alpha=\rho u^\alpha-\sigma F^{\alpha\beta}u_\beta, \tag{48}$$

since $F^{\alpha\beta}u_\beta$ is a vector in proper-space. However, Eq. (48) is precisely the well-known invariant form of Ohm's law;[5] in the case of stationary matter it reduces to the classical form:

$$j^\alpha=\rho,\ \sigma E_x,\ \sigma E_y,\ \sigma E_z.$$

Thus ρ is the charge density and σ the electrical conductivity.

The ease with which this law can be incorporated into the equations lends strong support to the theory developed above. It will be noted that Maxwell's equations have not entered this discussion. However, the Eqs. (47) and (48) are too few to determine all the variables, and the Maxwell equations are needed to complete the theory.

[5] See Tolman, *Relativity, Thermodynamics and Cosmology*, p. 114.

Conclusion

It has been shown that the classical considerations of I can readily be extended so that they are consistent with the special theory of relativity. The further extension into the general theory should offer no special difficulties.

One result has appeared clearly: It is necessary to introduce the current-density of matter separately from the energy-momentum tensor. This is also apparent from other treatments of energy and matter, but has rarely been emphasized. From the macroscopic standpoint, therefore, matter cannot be considered a form of energy, even though inertia is a property of energy rather than of matter. Matter has inertia because it has energy, but is not a form of energy. This same conclusion can be reached from a consideration of recent attempts to construct microscopic theories of the ultimate particles.

Correction: The Thermodynamics of Irreversible Processes. II.

(Phys. Rev. **58**, 269 (1940))

Carl Eckart

Ryerson Physical Laboratory, University of Chicago, Chicago, Illinois

On page 274 of the above paper, the sentence beginning "It is not easy to see . . ." should be replaced by the following:

It can be shown that

$$\sum_i \Gamma_i(-\Delta_i/\theta)\geqslant 0$$

for all values of Δ_i. Let

$$x_s'=\sum_k \nu_{ks}'\Delta_k/R\theta,$$
$$x_s''=\sum_k \nu_{ks}''\Delta_k/R\theta,$$

so that this sum may be written

$$R\sum_s a_s[x_s'-x_s'']\left[\exp(x_s')-\exp(x_s'')\right].$$

Since the exponentials are monotonically increasing positive functions of their arguments, it follows that both brackets in the above expression always have the same sign. Since $a_s\geqslant 0$, the required inequality follows at once.

LETTERS TO THE EDITOR

Prompt publication of brief reports of important discoveries in physics may be secured by addressing them to this department. Closing dates for this department are, for the first issue of the month, the eighteenth of the preceding month, for the second issue, the third of the month. Because of the late closing dates for the section no proof can be shown to authors. The Board of Editors does not hold itself responsible for the opinions expressed by the correspondents.

Communications should not in general exceed 600 words in length.

Hyperfine Structure of Ionized Mercury Lines

In connection with his investigations on the isotope shift in the band spectra of ionized mercury hydride, it has become necessary for Mrozowski to investigate the hyperfine structure of certain ionized mercury lines. He has recently reported his results[1] regarding the analysis and the interpretation of the structure of some ionized mercury lines. Reference has been made by him to a short note in which the structure of λ3984A had just been mentioned by Venkatesachar and myself;[2] but it is unfortunate that Mrozowski seems to be quite unaware of our subsequent detailed paper[3] on the "Hyperfine structure of some HgII lines," in which the structures of λλ3984, 2848 and 2262A had been investigated as early as in 1934. Mrozowski's results in regard to the structure as well as the scheme of hyperfine levels of the line λ3984A agree with our earlier findings. Mrozowski, just like ourselves, has been unable to confirm the satellite at $+1.950$ cm^{-1} reported by Murakawa[4] earlier, and it is now certain that no such satellite exists. The total spin separations of the two levels $6\,^2P_{3/2}$ and $5d^9\,6s^2\,^2D_{5/2}$ given by Mrozowski agree with those previously determined by us and are consistent with theoretical expectations based on Goudsmit's formulae.[5] The scheme of hyperfine levels worked out by us for explaining the observed structure of the line is identical with the scheme proposed by Mrozowski; the agreement in the nuclear spin separations of the upper and lower levels is shown in Table I.

In the case of λ2848A, the analysis of the line has been rendered incomplete for want of sufficient resolving power. But it is certain that the line exhibits no even isotope shift and has, in agreement with theoretical expectations, a few close components arising from the odd isotopes of mercury. Large isotope shifts of the order of 0.680 cm^{-1} between successive even isotopes have been observed by us in the level $5d^9\,6s\,6p\,^2\bar{D}_{5/2}$ as shown from the analysis of λ2262A ($^2D_{5/2}-{}^2\bar{D}_{5/2}$).

TABLE I. *Nuclear spin separations of the upper and lower levels in mercury isotopes.*

	Hg 199		Hg 201	
AUTHOR	$\Delta 6^2P_{3/2}$	$\Delta^2D_{5/2}$	$\Delta 6^2P_{3/2}$	$\Delta^2D_{5/2}$
V. and S. Mrozowski	0.050 0.049	0.127 0.118	0.060 0.054	0.135 0.131

It is abundantly clear that Mrozowski, who has analyzed λ3894A completely unaware of our earlier work, has lent valuable support to our conclusions.

L. SIBAIYA

University of Mysore,
Central College,
Bangalore, India,
August 20, 1940.

[1] S. Mrozowski, Phys. Rev. **57**, 207 (1940).
[2] B. Venkatesachar and L. Sibaiya, Naturwiss. **52**, 1041 (1931).
[3] B. Venkatesachar and L. Sibaiya, Proc. Ind. Acad. Sci. **1**, 8 (1934).
[4] K. Murakawa, Sci. Papers of Inst. of Phys. and Chem. Research, Tokyo **18**, 299 (1932).
[5] S. Goudsmit, Phys. Rev. **43**, 636 (1933).

On the Nuclear Gyromagnetic Ratios of the Chlorine Isotopes*

The nuclear gyromagnetic ratios of the chlorine isotopes have already been determined[1] by the molecular-beam magnetic-resonance method. On the basis of the depths of the resonance minima the observed g value of 0.546 was assigned to the Cl^{35} nucleus and that of 0.454 to Cl^{37}. Although this assignment seemed reasonably certain it was thought worth while to eliminate any possible doubt on this point by experimenting with a molecular beam of an alkali chloride containing an enriched proportion of Cl^{37}.

One of us (E.F.S.) has obtained,[2] by the use of the thermal diffusion method, a sample of HCl in which the abundance of Cl^{37} was raised from the normal 24 percent to about 50 percent. A portion of this sample was used to prepare about 20 mg of LiCl.

Two resonance minima, corresponding to the g values previously reported for chlorine, were again observed. The ratio of the depth of the 0.546 resonance minimum to that of the 0.454 minimum was found to be 1.2 for the enriched sample instead of 3.1 to 3.4 previously reported for normal samples. This constitutes conclusive evidence that the assignment has been correctly made.

A recent determination[2] of the spin of Cl^{37} by the observation of alternating intensities of lines in bands due to $Cl^{37}Cl^{37}$ yields 5/2 as the most probable value of the spin of Cl^{37}. If we assume this value of the spin the moment of Cl^{37} is 1.135 nuclear magnetons.

E. F. SHRADER

Yale University, New Haven, Connecticut

S. MILLMAN

Columbia University and City College, New York, New York

P. KUSCH

Columbia University, New York, New York
October 25, 1940.

* Publication assisted by the Ernest Kempton Adams Fund for Physical Research of Columbia University.

[1] P. Kusch and S. Millman, Phys. Rev. **56**, 527 (1939).
[2] E. F. Shrader, Phys. Rev. **58**, 475 (1940).

Identification of Two Radioactive Xenons from Uranium Fission

The observation of two long-life radioactive xenons growing out of radioactive iodine from uranium fission has been reported by us[1] and confirmed by Dodson and Fowler.[2] Recently some samples of cesium and barium were placed immediately behind a beryllium target bombarded by 16-Mev deuterons. After the bombardment the active cesium or barium was dissolved in water and the radioactive gas was then extracted into an ionization chamber. In the case of cesium only one radioactivity was observed which decayed with a half-life of 5 days, but in the case of barium, both 9.4-hr. and 5-day periods were present. The identity of the periods and of the absorption curves of these 9.4-hr. and 5-day radioactive gases from cesium and barium with those of radioactive xenon from uranium and thorium fission proves that they are the same substances.

Cesium has only one stable isotope with a mass number of 133, and since its bombardment gives only one radioactive xenon, we assume that the 5-day xenon is produced by the following reaction

$$_{55}Cs^{133}(n, p)_{54}Xe^{133}$$

and assign to it the mass number 133.

Although barium has seven known isotopes (130, 132, 134, 135, 136, 137 and 138), only three of them would be able to produce radioactive xenon (except for isomers of stable nuclei) by $a(n, \alpha)$ reaction. These are 130, 136, and 138. We have seen that Ba gives by $a(n, \alpha)$ reaction the 5-day xenon and we interpret this as

$$_{56}Ba^{136}(n, \alpha)_{54}Xe^{133}.$$

Since the abundance of Ba^{130} is only 1/700 of that of Ba^{138}, it is very likely that the barium of mass number 138 is responsible for the formation of the 9.4-hour xenon according to the reaction

$$_{56}Ba^{138}(n, \alpha)_{54}Xe^{135}.$$

Based on these results, the two chains found in uranium and thorium fission may be identified as

$$_{52}Te^{133}\ 60\ \text{min.} \rightarrow {}_{53}I^{133}\ 22\ \text{hr.} \rightarrow {}_{54}Xe^{133}\ 5\ \text{days} \rightarrow {}_{55}Cs^{133}$$

and

$$_{52}Te^{135} \sim 10\ \text{min.} \rightarrow {}_{53}I^{135}\ 6.6\ \text{hr.} \rightarrow {}_{54}Xe^{135}\ 9.4\ \text{hr.} \rightarrow {}_{55}Cs^{135}?.$$

Iodine was also separated from the fast-neutron-activated cesium sample. The separated iodine decayed with a single period of 12.6 hr. This confirms the assignment[3] of 12.6-hr. iodine to $_{53}I^{130}$ resulting from a reaction

$$_{55}Cs^{133}(n, \alpha)_{53}I^{130}.$$

The author wishes to thank Professor E. O. Lawrence for his interest in this work and Dr. E. Segrè for his helpful suggestions and criticisms.

C. S. Wu

Radiation Laboratory,
University of California,
Berkeley, California,
October 17, 1940.

[1] E. Segrè and C. S. Wu, Phys. Rev. 57, 552 (1940).
[2] R. W. Dodson and R. D. Fowler, Phys. Rev. 57, 966 (1940).
[3] J. J. Livingood and G. T. Seaborg, Phys. Rev. 54, 775 (1938).

Vibration Analysis of the Chlorine Dioxide Absorption Spectrum

The electronic band system appearing in the absorption spectrum of chlorine dioxide between 2600A and 5225A has been measured by several investigators[1-4] and vibration analyses have been attempted. The author offers evidence in support of a new analysis. Urey and Johnston were the first to attempt a detailed analysis of this system. However, none of their frequencies for the ground state agreed with the two infra-red frequencies found later by Bailey and Cassie;[5] namely, 945 cm^{-1} and 1109 cm^{-1}. For the third fundamental frequency of the ground state Bailey and Cassie accepted 528 cm^{-1} which appeared as a constant difference in two pairs of strong progressions in Urey and Johnston's analysis. Later Ku made more accurate and more complete measurements on the bands and attempted an analysis using the above frequencies but did not use the selection rules of Herzberg and Teller.[6]

Using the data of Ku, one finds that the 528 frequency comes out to be either 528 cm^{-1} or 524 cm^{-1} depending on which pair of progressions is used in determining its value. This disagreement is greater than experimental error. The author proposes to replace the fundamental frequency of 528 cm^{-1} by 447 cm^{-1} which appears as a constant difference in three separate pairs of progressions.

Photographs taken by the writer with the absorbing gas at dry ice temperature give clear evidence in support of this change.

From electron diffraction experiments, Brockway[7] finds that the apex angle of ClO_2 is 137°±15°. On this basis one must make the following assignment to the fundamental frequencies of the lower state:

$$\nu_1'' = 447\ cm^{-1},$$
$$\nu_2'' = 945\ cm^{-1},$$
$$\nu_3'' = 1109\ cm^{-1},$$

where ν_1'' designates the frequency of the bending vibration, ν_2'' that of the breathing vibration, and ν_3'' that of the antisymmetrical vibration. The apex angle of the lower state of ClO_2 calculated from these frequencies on the basis of the valence force model is approximately 122°.

As for the symmetrical frequencies of the upper state, the author essentially agrees with Urey and Johnston as well as Ku. These are:

$$\left.\begin{matrix}\nu_1' \\ \nu_2'\end{matrix}\right\} \begin{cases}290\ cm^{-1}, \\ 708\ cm^{-1}.\end{cases}$$

The bands have been photographed by the writer in the second order of the 30-ft. 30,000-line per inch grating at the University of Chicago. Each band is made up of sub-bands, some of which show clearly defined rotational series. This rotational structure is now in process of analysis. The sub-bands, like the bands themselves, degrade to the red. This is sufficient to show that both dimensions of the molecule increase as it passes to the upper state.

Further, the 708 frequency is excited up to 20 quanta or more, while no more than two quanta of the 290 frequency are excited with enough intensity to be observed. If qualitative use is made of the Franck-Condon principle,

the foregoing facts require the assignment

$$\nu_1' = 290 \text{ cm}^{-1},$$
$$\nu_2' = 708 \text{ cm}^{-1}.$$

In addition, if use is made of two series in which it appears that ν_3' changes by two quanta, the present analysis gives

$$\nu_3' = 790 \text{ cm}^{-1}.$$

On the basis of these approximate frequencies, the angle for the upper state is found to be about 114° compared to 122° in the lower state. This small change is consistent with the already mentioned fact that only ν_2' progressions are appreciably excited. The numerical value of each frequency given above corresponds to a one-quantum jump from the 0, 0, 0 state of vibration.

All distinct bands excluding isotope bands are now grouped into twelve progressions. All other reported bands can be classed as sub-bands, or are in the violet region of the spectrum where predissociation causes confusion. In the notation $(v_1'v_2'v_3')\leftarrow(v_1''v_2''v_3'')$ these progressions are:

Strong	Medium
(0 v_2' 0)←(0 0 0)	(0 v_2' 0)←(0 1 0)
(1 v_2' 0)	(1 v_2' 0)
(0 v_2' 2)	
(1 v_2' 2)	Weak
	(0 v_2' 0)←(0 2 0)
Medium	(1 v_2' 0)
(0 v_2' 0)←(1 0 0)	
(1 v_2' 0)	Weak
(2 v_2' 0)	(0 v_1' 0)←(1 1 0)

The (0 0 0)←(0 0 0) band, contrary to previous analysis, is the 21,016 cm^{-1} band.

The fact that (0 v_2' 2)←(0 0 0) and (0 v_2' 0)←(0 1 0), as well as (0 v_2' 0)←(0 2 0) are stronger than would ordinarily be expected is consistent with the qualitative picture of the Franck-Condon principle, taking into consideration the change in shape of the molecule.

The author wishes to thank Professor R. S. Mulliken for suggesting the problem and for generous interest and advice throughout the work. The author is also indebted to Dr. H. G. Beutler for helpful experimental suggestions.

J. B. Coon

Chicago University,
Chicago, Illinois,
October 25, 1940.

[1] C. F. Goodeve and C. P. Stein, Trans. Faraday Soc. **25**, 738 (1929).
[2] H. C. Urey and H. Johnston, Phys. Rev. **38**, 2131 (1931).
[3] W. Finkelnburg and H. J. Schumacher, Zeits f. physik. Chemie Bodenstein-Festband, 704 (1931).
[4] Z. W. Ku, Phys. Rev. **44**, 378 (1933).
[5] C. R. Bailey and A. B. D. Cassie, Proc. Roy. Soc. **A137**, 622 (1932).
[6] G. Herzberg and E. Teller, Zeits. f. physik. Chemie **B21–22**, 410 (1932).
[7] L. O. Brockway, Rev. Mod. Phys. **8**, 231 (1936).

Remarks on the Temperature Dependence of the Work Function of Tungsten

A few remarks in criticism of the paper by J. G. Potter[1] on "Temperature dependence of the work function of tungsten . . ." are called for, since in my opinion Dr. Potter has overestimated the reliability of the interpretation of his work when he writes: "The coefficient obtained resolves the discrepancy between the experimental value of A in the Richardson equation and the theoretical factor of 120 without the introduction of a reflection coefficient."

The so-called "experimental" value of A is taken as 60 amp. per sq. cm per degree squared. Its determination depended on the assumption that the entire area of the filament studied had a constant work function and that this could be obtained by measuring the emission with a strong accelerating field and then extrapolating back according to the Schottky theory to zero in order to evaluate the "theoretical" emission which should obtain at zero field.

Experiments by Johnson and Shockley,[2] Martin,[3] and Nichols[4] demonstrate beyond any doubt that the emission from a tungsten wire is far from uniform and, in fact, probably over 95 percent of all of the emission comes from less than 50 percent of the surface. Although no theoretical investigation has as yet shown that an appreciable reflection effect is to be expected when very slow electrons pass over a potential barrier, *all* experiments designed to investigate the energy distribution of electrons emitted thermionically or photoelectrically show a very considerable deficiency in the number of slow electrons. The experimental fact is that the order of 50 percent or more of the electrons normally expected are apparently reflected at the surface and do not contribute to the observed emission. Either the effect of the non-uniform emission or the reflection effect alone would be capable of "resolving" the discrepancy between the "experimental" value of $A=60$ and the theoretical value of $A=120$. A positive temperature coefficient of the work function as reported by Dr. Potter makes matters worse when all of the recognized experimental results are considered.

The negative temperature coefficient of the work-function as determined by Langmuir[5] has been shown[6] to be capable of resolving the difficulty and yet it is necessary to stress the fact that this problem cannot be said to be "resolved" until every step in the argument has been checked and cross-checked by independent experiments since the experimental difficulties are known to be so great.

Dr. Potter leads the reader to think that Langmuir attributed his observed negative temperature to "effects resulting from imperfect vacuum conditions." A careful reading of Langmuir's paper shows that the more likely source of error was to be attributed to possible alterations in the exact relative positions of his tube elements as the temperature was changed. As a result of a recently completed investigation of field emission by J. H. Daniel,[7] it has been possible to demonstrate that even under the most favorable vacuum conditions, which can be obtained only with sealed-off and properly "gettered" tubes, a surface of tungsten cannot be maintained at temperatures below 900°K more than a very few minutes without considerable alteration of the work function because of the adsorption of gas. Most experimenters in this field know that serious adsorption takes place many times more rapidly when the experimental tube is *not* sealed off from the pumping system even though the pressure as measured by an ionization gauge is of the order of 5×10^{-9} mm. Therefore it is not surprising that Dr. Potter experienced so much difficulty in this respect. At this pressure a monolayer could be formed in about five minutes and only a fraction of a monolayer is needed to make a very considerable alteration in the work function. This would confuse any measurements

made on the temperature coefficient of the work function of tungsten over the range of temperature below 900°K, where the effect sought amounts to only 0.04 volt.

W. B. NOTTINGHAM

George Eastman Laboratory of Physics,
Massachusetts Institute of Technology,
Cambridge, Massachusetts,
October 18, 1940.

[1] J. G. Potter, Phys. Rev. **58**, 623 (1940).
[2] R. P. Johnson and W. Shockley, Phys. Rev. **49**, 436 (1936).
[3] S. T. Martin, Phys. Rev. **56**, 947 (1939).
[4] M. H. Nichols, Phys. Rev. **57**, 297 (1939).
[5] D. B. Langmuir, Phys. Rev. **49**, 428 (1936).
[6] W. B. Nottingham, Phys. Rev. **49**, 78 (1936).
[7] J. H. Daniel, M. I. T. Doctor's Thesis (to be published).

Reply to Remarks on the Temperature Dependence of the Work Function of Tungsten

In the paper[1] criticized in the letter of W. B. Nottingham[2] the statement, that the positive temperature coefficient obtained for the work function of tungsten "resolves the discrepancy between the experimental value of A in the Richardson equation and the theoretical factor of 120 without the introduction of a reflection coefficient," does not imply that the coefficient is *uniquely* capable of resolving the discrepancy. As cited by Dr. Nottingham, interpretations of thermionic emission phenomena are possible on the basis of several other lines of experimental evidence, and more research will be necessary before a decision can be made in favor of any one interpretation.

In the paper criticized, the effects of adsorbed gas were taken into account, whereas in the paper by Langmuir,[3] in which it was stated that the vacuum was not "unimpeachable," no criterion was established for distinguishing between true temperature effects and contamination effects.

JAMES G. POTTER

Department of Physics,
South Dakota State School of Mines,
Rapid City, South Dakota,
October 28, 1940.

[1] J. G. Potter, Phys. Rev. **58**, 623 (1940).
[2] W. B. Nottingham, preceding letter.
[3] D. B. Langmuir, Phys. Rev. **49**, 428 (1936).